UNIVERSITÄT ZU LÜBECK

From the Institute of Experimental Endocrinology of the

University of Lübeck

Director: Prof. Dr. rer. nat. Jens Mittag.

"Thyroid Hormone Receptor Beta in MASH: A Wizard Without a Wand?"

Dissertation for Fulfillment

of Requirements for the

Doctoral Degree

of the University of Lübeck

Submitted by

Nuria López Alcántara

from Madrid

Lübeck 2024

First referee: Prof. Dr. Jens Mittag

Second referee: Prof. Dr. Henrik Oster

Date oral examination: 10/10/2024

Approved for printing: 6/11/2024

Eigenständigkeitserklärung

Ich bestätige hiermit, dass ich diese Dissertation eigenständig verfasst und dabei keine anderen Hilfsmittel als die angegebenen benutzt habe. Ich habe weder vorher noch gleichzeitig bei einer anderen Institution einen Antrag auf Zulassung gestellt oder diese Dissertation eingereicht. Ebenso habe ich mich bisher an keinem anderen Promotionsverfahren beteiligt.

_____

Nuria López Alcántara

Lübeck, den

List of publications

Sections of this thesis were previously submitted to or published in peer-reviewed journals due to priority considerations:

1. **Lopez-Alcantara N**, Oelkrug R, Sentis SC, Kirchner H, Mittag J. Lack of thyroid hormone receptor beta is not detrimental for non-alcoholic steatohepatitis progression. iScience. 2023 Oct;26(10):108064.

Publications that are not part of this thesis:

1. Dore R, Sentis SC, Johann K, **Lopez-Alcantara N**, Resch J, Chandrasekar A, et al. Partial resistance to thyroid hormone-induced tachycardia and cardiac hypertrophy in mice lacking thyroid hormone receptor β. Thyroid®. 2024 Mar 25; thy.2023.0638.
2. Dore R, Watson L, Hollidge S, Krause C, Sentis S.C, Oelkrug R, Geißler C, Johann K, Pedaran M, Lyons, G, **Lopez-Alcantara N**, et al. Resistance to thyroid hormone induced tachycardia in RTHα syndrome. Nat Commun. 2023 Jun 7;14(1):3312.
3. Britsemmer JH, Krause C, Taege N, Geißler C, **Lopez-Alcantara N**, Schmidtke L, et al. Fatty Acid Induced Hypermethylation in the Slc2a4 Gene in Visceral Adipose Tissue Is Associated to Insulin-Resistance and Obesity. IJMS. 2023 Mar 29;24(7):6417.
4. Villanueva-Paz M, Morán L, **López-Alcántara N**, Freixo C, Andrade RJ, Lucena MI, et al. Oxidative Stress in Drug-Induced Liver Injury (DILI): From Mechanisms to Biomarkers for Use in Clinical Practice. Antioxidants. 2021 Mar 5;10(3):390.
5. Benedé-Ubieto R, Estévez-Vázquez O, Guo F, Chen C, Singh Y, Nakaya HI, Gómez del Moral M, Lamas-Paz A, Morán L, **López-Alcántara N** et al. An Experimental DUAL Model of Advanced Liver Damage. Hepatol Commun. 2021 Jun;5(6):1051–68.
6. Lamas-Paz A, Morán L, Peng J, Salinas B, **López-Alcántara N**, Sydor S, et al. Intestinal Epithelial Cell-Derived Extracellular Vesicles Modulate Hepatic Injury via the Gut-Liver Axis During Acute Alcohol Injury. Front Pharmacol. 2020 Dec 21; 11:603771.

Table of Contents

List of figures

List of tables

Appendix tables

List of abbreviations

AAV	Associated adenovirus
ACC	Acetyl CoA carboxylase Alpha
AHDS	Allan-Herndon-Dudley syndrome
ALP	Alkaline phosphatase
ALT	Alanine aminotransferase
AST	Aspartate aminotransferase
BAT	Brown adipose tissue
BMI	Body mass index
BMR	Basal metabolic rate
cAMP	Cyclic AMP
CCl4	Carbon tetrachloride
CD	Choline-deficient diet
CD-HFD	Choline-deficient high-fat diet
ChoRE	Carbohydrate response elements
CPT1α	Carnitine palmitoyl transferase 1 alpha
CV	Central vein
CVD	Cardiovascular disease
CYP7A1	Cytochrome P450 family 7 subfamily A member 1
DEE	Daily energy expenditure
DIO	Iodothyronine deiodinase
DIO3	Deiodinase type 3
DIT	Diiodotyrosine
DNL	De novo lipogenesis
ELISA	Enzyme-linked immunosorbent assay
FA	Fatty acids
FFA	Free fatty acids
FLI	Fatty liver index
FT3	Free T3
FT4	Free T4
GTH	Gemeinsame Tierhaltung
GTT	Glucose tolerance test
GWAS	Genome-wide analysis
H&E	Haematoxylin and eosin staining
HCC	Hepatocellular carcinoma
HDAC3	Histone deacetylase 3
HDL	High-density lipoprotein
HFD	High-fat diet
HL	Hepatic lipase
HMG-CoA	β-hydroxy-β-methylglutaryl-CoA reductase
HPT	Hypothalamic-pituitary-thyroid
HSC	Hepatic stellate cells

IL-1β	Interleukin 1β
IL-6	Interleukin 6
ITT	Insulin tolerance test
LAT	L-type amino acid transporters
LDL-C	Low-density lipoprotein cholesterol
LDLR	Low-density lipoprotein receptor
LFD	Low fat diet
LST-1	Liver-specific transporter 1
MASH	Metabolic Dysfunction-Associated Steatohepatitis
MASLD	Metabolic Dysfunction-Associated Steatotic Liver Disease
MCDD	Methionine- choline- deficient diet
MCT	Monocarboxylate transporter
ME	Malic enzyme
miRNA	microRNA
MIT	Monoiodotyrosine
NAFLD	Non-alcoholic fatty liver disease
NASH	Non-alcoholic steatohepatitis
NCoR	Nuclear receptor corepressor
NMR	Nuclear magnetic resonance
OATP	Organic anion transporters
ORO	Oil Red O staining
PFA	Paraformaldehyde
PMH	Primary mouse hepatocytes
PTU	6-n-propyl-2 thiouracil
PV	Portal vein
PVN	Paraventricular nucleus of hypothalamus
qPCR	real-time qPCR
RMR	Resting metabolic rate
RQ	Respiratory quotient
rT3	Reverse T3
RTHβ	Thyroid hormone resistant β
RXR	Retinoid X receptor
SERBP-2	Sterol regulatory element-binding protein-2
SMRT	Silencing mediator of retinoid
SR	Sirius Red staining
SRC	Steroid receptor coactivator
T2DM	Type 2 diabetes mellitus
T3	3,3’,5-Triiodo-L-thyronine
T4	Thyroxine
TBG	Thyroxine-binding globulin
TG	Thyroglobulin
TGA	Triglyceride
TH	Thyroid hormone
TPO	Thyroid peroxidase

TR	Thyroid hormone receptor
TRE	Thyroid hormone response elements
TRH	Thyrotropin-releasing hormone
TRβ	Thyroid hormone beta receptor
TSH	Thyroid-stimulating hormone
tT3	Total T3
tT4	Total T4
VLDL	Very-low density lipoprotein
WT	Wild type

Abstract

Metabolic dysfunction-associated steatotic liver disease (MASLD) and steatohepatitis (MASH) are widespread diseases influenced by thyroid hormone (TH). Hypothyroidism promotes hyperlipidemia, obesity, and insulin resistance, while TH replacement therapy and thyromimetics show promising results in improving disease progression. However, recent studies indicate that is not the systemic levels but the local hepatic TH metabolism that plays a crucial role. This is primarily controlled in the liver by the TH beta receptor (TRβ) and TH-activating deiodinase type I (DIO1). In humans, the severity of MASH correlates with reduced hepatic TRβ expression, indicating developing TH resistance, which could therapeutically diminish the efficacy of thyromimetics.

This dissertation investigates the role of hepatic TRβ and DIO1 during MASH development. Using TRβ knockout mice and viral overexpression of TRβ, the influence of receptor levels on MASH progression is examined. The experimental approach also included the development of a novel MASH mouse model by combining a choline-deficient high-fat diet with optimized methionine concentration and thermoneutral housing, reflecting important human characteristics such as a reduction in TRβ during disease progression. Additionally, *in vitro* studies with primary mouse hepatocytes were conducted to identify specific factors that can selectively modulate deiodinase type 1 or TRβ to find new therapeutic approaches for improving local TH availability.

The main results showed that thermoneutrality not only mitigates the usual hyperthyroidism of TRβ knockout mice, allowing the study of TRβ without confounding effects, but also that such a mouse model better reflects the human situation compared to studies at room temperature. The lack of TRβ in the animals led to increased fat mass but improved fibrosis and less inflammation, while TRβ overexpression had no effect. Increased Dio1 mRNA after MASH induction indicated a protective compensatory mechanism. The findings clearly demonstrate that a reduction in the TRβ signaling pathway can be beneficial for certain disease pathologies, thus questioning the use of thyromimetics in later stages of fibrosis.

Zusammenfassung

Metabolische Dysfunktion-assoziierte Steatose der Leber (MASLD) und Steatohepatitis (MASH) sind weltweit verbreitete Krankheiten, die durch Schilddrüsenhormone (TH) beeinflusst werden. Hypothyreose fördert Hyperlipidämie, Fettleibigkeit und Insulinresistenz, während eine TH-Ersatztherapie und Thyromimetika vielversprechende Ergebnisse bei der Verbesserung des Krankheitsverlaufs zeigen. Neuere Studien zeigen allerdings, dass nicht die systemischen Spiegel, sondern der lokale hepatische TH-Stoffwechsels hier die tragende Rolle einnimmt. Dieser wird in der Leber primär durch den TH Rezeptor Beta (TRβ) und die TH aktivierende Deiodinase Typ I (DIO1) kontrolliert. Beim Menschen korreliert der MASH Schweregrad mit einer verringerte hepatische TRβ-Expression, was auf eine sich entwickelnde TH Resistenz hinweist, und therapeutisch vor allem die Wirksamkeit der Thyromimetika abschwächen könnte.

Diese Dissertation untersucht nun die Rolle des hepatischem TRβ und der DIO1 während der MASH Entwicklung. Durch den Einsatz von TRβ-Knockout-Mäusen und einer viralen Überexpression von TRβ wird der Einfluss des Rezeptorsspiegels auf den MASH Fortschritt untersucht. Der experimentelle Ansatz umfasste auch die Entwicklung eines neuartigen MASH-Mausmodells durch die Kombination einer cholinarmen fettreichen Diät mit optimierter Methioninkonzentration und thermoneutraler Haltung, welcher wichtige humane Merkmale abbildet, wie eine Reduktion des TRβ im Krankheitsverlauf. Zusätzlich wurden in vitro Studien mit primären Maus-Hepatozyten durchgeführt, um spezifische Faktoren zu identfizieren, die gezielt Deiodinase Typ 1 oder TRβ modulieren können, um neue therapeutische Ansätze zur Verbesserung der lokalen TH Verfügbarkeit zu finden.

Die wichtigsten Ergebnisse zeigten, dass Thermoneutralität nicht nur die übliche Hyperthyreose von TRβ-Knockout-Mäusen mildert, was die Untersuchung von TRβ ohne störende Effekte ermöglicht, sondern ein solches Mausmodell die humane Situation auch besser abbilden kann als Studien bei Raumtemperatur. Der Mangel an TRβ führte in den Tieren zu einer erhöhten Fettmasse, aber verbesserter Fibrose und weniger Entzündung, während die Überexpression von TRβ keinen Einfluss hatte. Erhöhte Dio1-mRNA nach MASH Induktion deutete auf einen protektiven Kompensationsmechanismus hin. Die Ergebnisse zeigen eindeutig, dass eine Reduktion des TRβ Signalwegs für gewisse Krankheitspathologien durchaus

vorteilhaft sein kann, und stellen daher den Einsatz von Thyromimetika in späteren Fibrose-stadien in Frage.

1. INTRODUCTION

Thyroid hormones (TH) are crucial for a wide range of physiological processes including development, growth, pregnancy, and the proper functioning of the cardiovascular system, brain, and metabolism. Impaired thyroid hormone regulation has been associated with the development and progression of liver diseases. Hypothyroidism and subclinical hypothyroidism are linked to higher risk of Metabolic Dysfunction-Associated Steatotic Liver Disease (MASLD) and Metabolic Dysfunction-Associated Steatohepatitis (MASH) (1–3) by contributing to hyperlipidemia, obesity, insulin resistance, diminishing autophagy and mitochondrial metabolism (4–9). Recent research highlighted the greater significance of local hepatic TH metabolism as compared to systemic circulating levels for the pathogenesis of these steatotic liver diseases. Local control of THs is achieved by the differential expression of TH transporters, deiodinases (DIOs), and TH receptors (TRs). A small cohort study using human liver biopsies of patients with MASLD revealed increased activation of the TH deactivating enzyme deiodinase type 3 (DIO3) (10), while a comprehensive study involving a large cross-section of MASH patients found decreased expression of thyroid hormone beta receptor (TRβ) in the liver (11). Taken together these studies suggest that in the course of disease progression, the human hepatic TH metabolism might be reduced, and its restoration could be beneficial for MASLD and MASH, which is supported by observations in patients treated with THs or thyromimetics, in particular liver-specific agonist for TRβ (12–15).

1.1. MASLD and MASH

The common nomenclature for non-alcoholic fatty liver disease (NAFLD) has been changed to MASLD, and non-alcoholic steatohepatitis (NASH) to MASH, as it captures better the metabolic risk factors associated to each condition without exclusionary confounder terms or stigmatising language (16). Despite the new terminology varies on several diagnosis criteria (Table S2), numerous studies have conducted comparisons in diagnosed patients, revealing that 99% of individuals diagnosed with NAFLD meet MASLD classification criteria (17–19). Henceforth, the new terminology MASLD and MASH will be employed throughout this document indistinctively when referring to NAFLD and NASH respectively.

MASLD is the most common chronic liver disease worldwide. It comprehends a spectrum of liver affections ranging from isolated hepatic steatosis without inflammation and involving a minimum of one out of five cardiometabolic risk factors, to steatohepatitis along with hepatic injury, with or without fibrosis, commonly known as MASH (Figure 1). MASLD global prevalence is 25-38% of all adults with an increased prevalence rate of 50.4% in the past 3 decades (20,21). Of those, 60% of biopsied patients progressed to MASH (22). Importantly, MASH is considered the most rapidly increasing contributor for chronic liver diseases such as cirrhosis and hepatocellular carcinoma (HCC) (23,24).

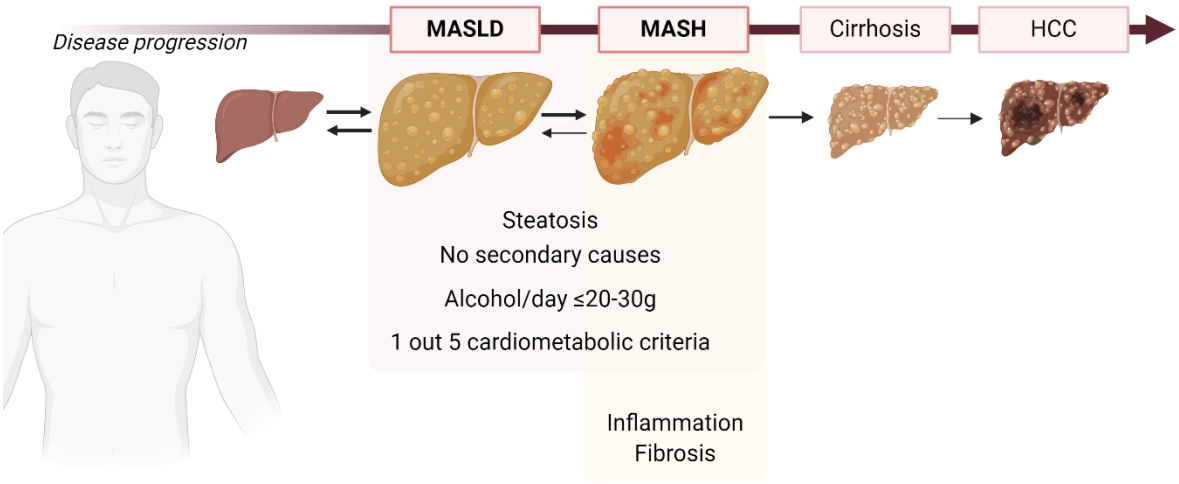

Figure 1 – MASLD disease severity progression and diagnostic criteria. Excess liver fat accumulation >5% (steatosis) disrupts hepatic metabolism overtime, often leading to inflammation and potentially to increased fibrogenesis, resulting in MASH. Progressive fibrosis may advance to cirrhosis and eventually to hepatocellular carcinoma (HCC). Diagnostic criteria of MASLD and MASH exclude secondary underlying causes of fat accumulation, require restricted alcohol intake, and presence of at least one cardiovascular risks factor such as BMI ≥25 kg/m², insulin resistance, hypertension, plasma hypertriglyceridemia, or plasma hyperlipidaemia. Figure created with BioRender.

Common disorders related to MASDL and MASH

MASLD in patients is tightly associated with comorbid diseases that affect not only the liver, but adipose tissue, heart, kidney, muscle, and other extrahepatic disorders, further driving MASLD prevalence and severity.

Obesity

Although MASLD is often observed in patients with obesity, it is unclear whether it is the cause or a consequence of the metabolic dysfunction. A systematic review in 2020 revealed that within the MASLD population, 19.2% of patients were lean and 40.8% were non-obese (body mass index (BMI) <25kg/m^2), representing a 5.1% and 12.1% of the global prevalence (25). However, within the obese population, the incidence of MASLD is approximately 75% with one fifth diagnosed as MASH (26). Both diseases are known to increase free fatty acids (FFA) and *de novo* lipogenesis (DNL) in the liver, leading to lipid metabolism dysfunction and steatosis. Lipotoxicity, oxidative stress, mitochondrial dysfunction, and endoplasmic reticulum stress would further contribute to cell injury and death, leading to inflammation, and eventually fibrosis. Hence, is not a surprise that the incidence of these diseases is tightly correlated, but the nature of the pathology remains different, especially on the severity of insulin resistance, degree of dyslipidaemia and fat distribution.

Type 2 diabetes mellitus

MASLD and type 2 diabetes mellitus (T2DM) are known to coexist and synergistically act to increase the risk of adverse clinical outcomes. T2DM and liver steatosis share common pathophysiological features and mechanisms where one can lead to the other (27). For this reason, experts decided to include T2DM as one of the metabolic risk conditions in the new nomenclature for MASLD diagnosis (16). Importantly, although strongly linked, the global prevalence of T2DM in patients with MASLD is 34.1% whereas the prevalence of MASLD in T2DM patients is 55.5% (22,28). Insulin resistance increases hepatic glucose production and stimulates lipolysis in adipocytes resulting in the release of FFA in excess and glycerol into the bloodstream, predisposing the liver, as well as other tissues, to lipotoxicity, further impairing insulin secretion (27). Moreover, the release of pro-inflammatory adipokines (*e.g.,* MCP-1, TNF-α, TGF-β, IL6) from the adipose tissue, along with the excess of FFA, activate pro-inflammatory pathways in the liver like the activation of hepatic stellate cells (HSC) resulting in increased fibrogenesis (29,30).

Cardiovascular disease

Cardiovascular disease (CVD) supersedes liver-related death as the leading cause of mortality of MASLD patients without advanced fibrosis (31). CVDs share many common risk factors with

MASLD (obesity, insulin resistance, T2DM, and dyslipidaemia) but there is increasing evidence suggesting that MASLD directly impacts CVD risk. Individuals with fatty liver have more than 2-fold greater risk of suffering non-fatal cardiovascular events, which increases to 4-fold when fibrosis is present (32,33). Recent studies on patients diagnosed with non-obese MASLD (BMI <25kg/m^2) by ultrasound or fatty liver index (FLI) have also shown a heightened likelihood of non-fatal cardiovascular event which was greater with the increasing fibrosis score (33,34). Notably, MASLD patients with diabetes exhibited the higher risk for CVD, followed by overweight and lean patients diagnosed with MASLD with metabolic disorder. However, the precise mechanisms linking MASLD, and CVDs remain unclear due to insufficient clinical and biochemical parameters.

Hypertension, a well-established risk factor for CVDs has been suggested as one potential connecting factor. Studies suggest a bidirectional relationship between MASLD and hypertension. Hypertension is reported to increase the risk of developing MASLD in 1.63-fold and is present in 40% of the patients. Conversely, MASLD patients exhibit a 1.55 times higher risk of developing hypertension (35). One proposed mechanism involves insulin resistance. Hypertension diminishes blood circulation to peripheral tissues, thereby reducing insulin access and promoting compensatory hyperinsulinemia. Elevated insulin levels may further contribute to the proliferation of smooth muscle cells and vascular fibroblasts, resulting in narrowing of the vascular lumen together with the release of fatty acids from adipose tissue, thus exacerbating hepatic steatosis (36,37). Moreover, liver lipid metabolism disruption leads to the release of proinflammatory and profibrogenic cytokines and hepatokines, further contributing to the endothelial dysfunction (38). Given these findings, further research is crucial to better understand the cardiovascular implications of MASLD. Nonetheless, the importance of comprehensive cardiovascular assessments for MASLD patients cannot be overstated.

Other extrahepatic disorders

A meta-analysis including 9 observational studies with a total of 96,595 adult patients concluded that MASLD increased the risk of chronic kidney disease cases by 40%, which was also related to greater MASLD severity (39). Additionally, it is further supported by large cohort cross-sectional studies (40,41).

Hepatocellular carcinoma

HCC ranks as the sixth most frequently diagnosed cancer globally and holds third leading cause of cancer-related mortality (42). It represents the primary form of liver cancer accounting for 70-85% of all liver cancer cases (43). In the United States, death rates from HCC have increased by 43% between 2000 and 2016 (44). The relationship between HCC and MASH was initially described in the early 1990s through a 5-years follow-up study, which demonstrated a correlation between MASH severity with the development of cirrhosis (45). Classically, HCC prevalence has been associated to underlying liver disease such as hepatitis B, C, or alcohol abuse, relegating MASLD to a secondary position in terms of risk association. However, the contribution of MASLD to HCC has seen a significant increase, rising 7.7-fold from 2002 to 2016 while the rates for hepatitis or alcohol abuse remained stable. Thus, currently MASLD represents the second leading etiology of HCC (46). Furthermore, the incidence of MASH is expected to rise in the future and consequently the increase of HCCs.

Dyslipidaemia

Dyslipidaemia is characterized by an imbalance of lipids such as cholesterol, low-density lipoprotein cholesterol (LDL-C), triglycerides (TGAs), and high-density lipoprotein (HDL) in serum or tissues (47). The liver plays a critical role in cholesterol synthesis and clearance, as well as storage and clearance of fatty acids (FA) and bile production. Alterations on any of these pathways can impair hepatic function, potentially leading to steatosis. In the context of MASLD, patients often present with hypertriglyceridemia, elevated LDL-C and low HDL (47). These lipid abnormalities are of great importance as they not only contribute to the progression of MASLD and MASH but increase the risk of developing other comorbidities, (e.g., CVD).

Hypothyroidism

Hypothyroidism is a condition characterized by low thyroid hormone levels in serum. Symptoms include fatigue, weight gain, cold intolerance, slow heart rate and reduced metabolism. Hypothyroidism is associated with low energy expenditure, increased cholesterol levels, and reduced lipolysis and gluconeogenesis (48). A cross-sectional study including 4648 participants, half of whom with hypothyroidism, established a correlation between hypothyroidism and subclinical hypothyroidism with MASLD in a severity-dependent manner (2). This finding was supported by a prospective cohort study from the Netherlands including 9419

participants (49). Additionally, biopsies of 246 MASLD diagnosed patients revealed that hypothyroidism is more frequently among MASLD patients (50). Low levels of free 3,3',5-Triiodo-L-thyronine (T3), has also been associated with advanced fibrosis in MASLD patients, indicating a higher risk towards MASH progression (51). Furthermore, hypothyroid patients with over ten years of thyroid dysfunction show significantly increased likelihood of developing HCC, a common condition derived from MASH (23,46). Consistently, treatment of hypothyroidism by THs replacement or hyperthyroidism has been shown to improve MASH (12,52,53). Patients with hypothyroidism are often co-presented with dyslipidaemia which itself represents an important risk factor for MASLD by contributing to intrahepatic lipid accumulation.

1.2. Thyroid hormone action in hepatic lipid metabolism linked to MASDL and MASH

In the liver, TH regulates metabolism at different levels, including cholesterol, FA and DNL pathways, thus directly affecting MASLD and MASH.

Cholesterol metabolism

T3 regulates cholesterol biosynthesis by modulating *SERBP-2* (sterol regulatory element-binding protein-*2*) expression, which in turn influences the β-hydroxy-β-methylglutaryl-CoA (HMG-CoA) reductase, the rate-limiting enzyme in cholesterol synthesis (54,55). T3 also enhances cholesterol clearance from the blood by increasing the expression of low-density lipoprotein receptor (LDLR) through SERBP-2, promoting cholesterol endocytosis in the hepatocytes (54,55). Although seemingly contradictory, T3 promotes cholesterol production as well as cholesterol influx in the liver, but also facilitates their excretion into bile acids. Here, T3 induces cytochrome P450 family 7 subfamily A member 1 (*CYP7A1),* a key enzyme in bile acid synthesis, facilitating the conversion of cholesterol and subsequent excretion (48,56,57). Additionally, the excretion of bile acids is also enhanced by T3 through the ATP binding cassette subfamily G member 5, and 8 (*Abcg5*, *Abcg8*) expression and activity (58). Therefore, in states of reduced T3 levels, such as hypothyroidism, there is a decline of SREBP-2, followed by LDLR. This reduction hampers the liver cholesterol uptake, contributing to hypercholesterolemia in serum, a common finding in hypothyroid patients (59). Thus, THs are critical regulators of both cholesterol synthesis and clearance, ultimately influencing cholesterol levels and metabolism in the body, which is a major risk of MASLD and MASH.

Fatty acids β-oxidation

The release of FA from adipose tissue occurs through lipolysis, resulting in their release into the bloodstream as FFA. In the liver, the excess of FA undergoes esterification into neutral fats like TGAs and cholesterol ester, a process essential for clearing FFAs from the bloodstream. THs regulate the hepatic uptake of FAs through transcriptional regulation of the transporters for FA (60). Depending on the energy requirements, β-oxidation within the mitochondria is upregulated, allowing the breaking down of FAs to produce energy. THs levels are directly associated with levels of hepatic lipase (HL) activity, which is important for releasing FA from TGAs (61). Clinical interventions using levothyroxine as replacement therapy in hypothyroid patients, resulted in elevated HL along with reduced TGAs and cholesterol (62). The transport of the FAs from the cytosol to the mitochondria is mediated by carnitine palmitoyltransferase 1 alpha (CPT1α), the rate-limiting enzyme in β-oxidation. The activity of CPT1α is strongly positively regulated by THs in the liver, underscoring the significant role THs in β-oxidation, as demonstrated in multiple studies (63–65).

De novo lipogenesis

Endogenous FA synthesis in the liver is done via DNL using carbohydrates and acetate as initial substrate (66). T3 directly influences DNL by enhancing the first step of this pathway through modulating the transcription of acetyl CoA carboxylase alpha (ACC), which catalyses the conversion of acetyl CoA to malonyl CoA (67). Similarly, T3 is known to increase fatty acid synthetase (*Fasn*) and TH-responsive Spot14 (*Thrsp*), both of which are essential for DNL. Beyond this direct effect, T3 also impacts DNL indirectly by boosting the expression of malic enzyme (*ME)*, important for NADPH production, the main reducing power source of DNL (68). Importantly, all these genes have identified thyroid hormone responsive elements (TREs) located within the promoter region (67,69–71). Subsequently, these FAs are esterified to form TAGs, which are either stored in lipid droplets or released as very low-density lipoprotein (VLDL).

Thus, THs are crucial in managing hepatic lipid balance, a regulation that is critically important in the context of MASDL and MASH, where dysregulation of lipid metabolism leads to hepatic steatosis.

The only effective therapeutic approaches for MASLD and MASH until now included combining dietary restrictions and physical activity. The Food and Drug Administration (FDA) have approved at the beginning of 2024 the first treatment drug for MASH, resmetirom, now under the name Rezdiffra™ (72). Resmetirom is a hepatocyte-specific thyromimetic, highlighting once more the relevance of TH metabolism in MASLD and MASH.

1.3. Thyroid hormones

The term THs is commonly used to refer to the less active precursor thyroxine (T4) and the active hormone 3,3',5-T3. These hormones are crucial mediators of physiological processes in all the tissues of the body as well as their development. Consequently, the regulation of THs levels in serum is tightly regulated by the hypothalamic-pituitary-thyroid (HPT) axis, and locally in the target tissues by the differential expression of TH transporters, TH converting enzymes known as DIOs, and TRs.

Thyroid hormone regulation

Starting from the hypothalamus, the thyrotropin-releasing hormone (TRH) is synthesized in the paraventricular nucleus and then is transported to the anterior pituitary gland (73). Consequently, the pituitary releases the thyroid-stimulating hormone (TSH) which binds to the thyrotropin receptor on the thyrocytes at the thyroid gland leading to the release of T4 and small amounts of T3 into the bloodstream. Circulating THs can be found as free hormones, free T4 (fT4) and free T3 (fT3) or bound to protein transporters (74,75). In both cases, THs reach the tissues entering the cells via TH transporters. Circulating THs negatively exerts a feedback effect on the secretion of TRH and TSH, thus maintaining the balance of the HPT axis (76). In peripheral tissues, THs can be modulated locally by the action of DIOs which mediates their conversion by catalysing the removal of iodine atoms in their outer or inner ring. Finally, T3 binds to the TRs and modulates the expression of TH-responsive genes (Figure 2).

Thyroid hormone metabolism in the liver and its role in MASLD and MASH

THs availability in peripheral tissues depends not only on serum levels of the hormones but also on THs transporters, DIOs, and receptors, which are differently expressed depending on the tissue.

Transporters

TH transporters mediate the cellular uptake and efflux of THs. There are 5 families of TH transporters, highly conserved between rodents and humans, including the organic anion transporters (OATPs, SLC10, and SLC17), monocarboxylate transporter (MCTs), L-type amino acid transporters (LATs) and the bile acid transporter family. Among them only MCT8, OATP1B1, NPT5 and NTCP are highly expressed in the human and mouse liver (77).

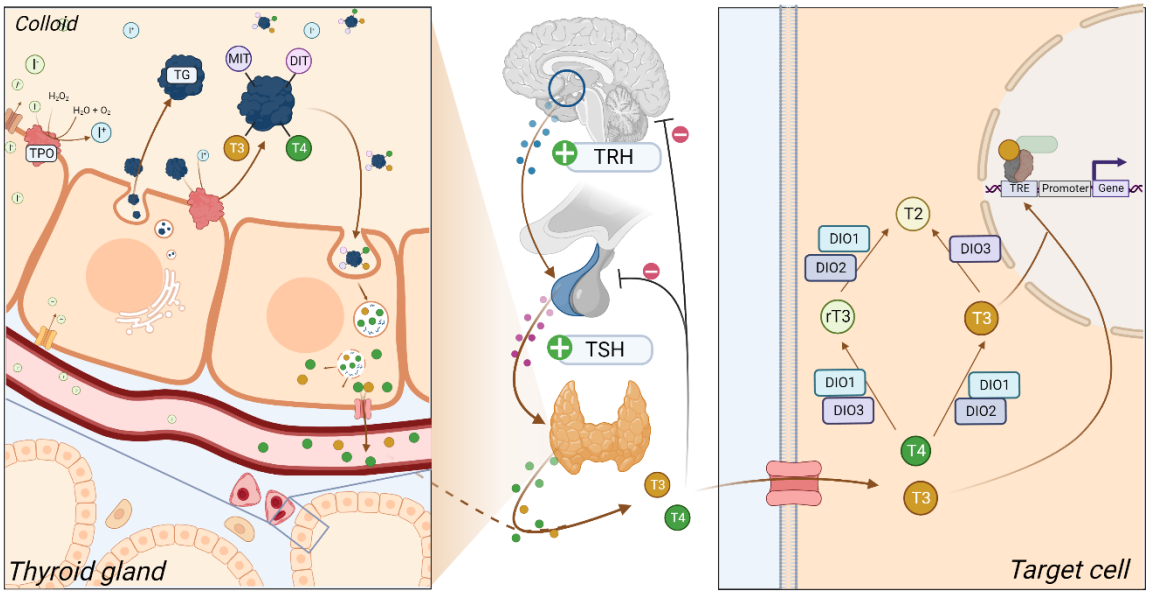

Figure 2 – Thyroid hormone synthesis. "Iodine is transported into the thyroid gland, oxidized by thyroid peroxidase (TPO), and incorporated into thyroglobulin (TG) to form monoiodotyrosine (MIT) and diiodotyrosine (DIT), which are stored in thyroid follicles. MIT and DIT couple to form T3 and T4. Upon TSH stimulation, TG is endocytosed and degraded by lysosomal proteases, releasing T3 and T4 into the bloodstream. This process is regulated by the hypothalamic-pituitary-thyroid axis. TRH from the hypothalamus triggers TSH release, stimulating T3 and T4 synthesis and secretion. In peripheral tissues, THs are converted by DIOs, and T3 binds to TRs to regulate gene expression. Circulating THs provide negative feedback to control TRH and TSH secretion. Figure created with Biorender.

MTC8 encoded by *SLC16A2*, is highly expressed in the brain and liver, playing a pivotal role in brain development (78,79). Mutations in MCT8 are linked to Allan-Herndon-Dudley syndrome (AHDS), characterized by elevated T3, reduced T4, and variable TSH levels in serum (80), along with hepatic thyrotoxic profile with elevated T3 (81). *Mct8* knockout mice display 2.3-fold increase on T3 content in the liver accompanied by elevated DIO1 expression and

activity, indicating that other transporters continue to facilitate TH influx, compensating for the absence of MCT8 (82). In MASLD, MCT8 expression showed to be increased at early stages of the disease in both humans and mice (83,84).

OATP1B1, also referred as liver-specific transporter 1 (LST-1) is encoded by *SLCO1B1* in humans and *Slco1b2* in mice (78,79). While its role in TH transport remains underexplored, OATP1B1 has been extensively studied in hepatocyte-specific drug delivery, and its role in unconjugated bilirubin uptake (85–88). In the context of MASLD, OATP1B1 has recently been proposed as the hepatocyte-specific transporter for the thyromimetic MGL-3196 (Resmetirom), highlighting the importance of TH regulation in the progression of MASLD (89). More details about resmetirom and thyromimetic will be discussed in the chapter of thyromimetics.

A recent studied using genome-wide analysis (GWAS) in humans identified NPT5 as a novel TH transporter (78). NPT5 is encoded by *SLC17A4* and is abundantly expressed in liver, kidney, and gastrointestinal tract (79,90). Its expression is elevated in MASLD mouse models using db/db mice, or wild-type (WT) receiving a high-sucrose/high fat diet. Further studies on inactivating mutations or knockout models are necessary to understand the physiological role of this novel TH transporter in TH homeostasis.

Lastly, NTCP is exclusively expressed in the basolateral membrane of mammalian hepatocytes, it belongs to the solute carrier transporter family and is encoded by *SLC10A1* (78,79,91). Besides THs, NTCP primarily transports bile salts and sulphated compounds in a Na^+ dependent manner, underscoring its importance on bile acid homeostasis and enterohepatic circulation (92,93). Inhibition of NTCP in animal models does not affect hepatic T4 uptake (94). Despite MASLD and MASH patients sometimes are presented with high bile acids levels in blood, partly explained by reduced NTCP activity (95,96), there is no epidemiological evidence correlating these two pathologies. Hence, NTCP acts as a general hepatic anion transporter rather than specific TH transporter where the extent of its involvement in TH clearance remains uncertain.

In summary, despite TH transporters play roles in hepatic TH homeostasis, their individual contributions are unlikely to promote the hypothyroid state of the liver during MASLD and MASH.

Deiodinases

Classically, it is believed that most of the circulating T3 is produced in peripheral tissues mediated by iodothyronine deiodinases (DIO) in humans and mice. Moreover, DIOs are key modulators of intracellular T3 levels by controlling the activation and deactivation of THs (Figure 2). In this process, iodothyronines enter the target cells via specific transporters where DIO catalyse the removal of iodine atoms in their outer or inner ring. Three DIOs have been described, DIO1, DIO2 and DIO3. They are dimeric integral membrane proteins belonging to the group of selenoenzymes (97,98). Despite their sequence similarity and the presence of an amino acid selenocysteine (SeCys) in their active centre, they are encoded by different genes (*DIO1, DIO2, DIO3)* located in different chromosomes, indicating a possible origin in common (97,99). Moreover, they display differential expression depending on tissue or stage of development, as well as different affinity for substrate, and subcellular location (100–102). In the adult liver, there is abundant expression and activity of DIO1 and at significantly lower levels of DIO3 whereas DIO2 is restricted to liver development.

DIO1 serves as the primary deiodinase in both humans and mice liver, but it is also expressed in kidney, thyroid, and pituitary (103) . DIO1 is abundant in hepatocytes and is able to catalyse the deiodination of the outer and inner ring of T4 to obtain T3 and reverse T3 (rT3) respectively, as well as the outer ring of rT3 to obtain T2 (104). The substrate preference of the enzyme is rT3> T4> T3, with *Km* values in sequential order of 0.2-1µM, 2µM, 8-10µM (104). In humans, *DIO1* is located on chromosome 1p32.3 and contains two identified TRE in the first 2.5 kbp of the 5' flanking region (105). Interestingly, despite no TREs have been clearly pinpointed in mice *Dio1* so far, prior studies showed similar induction of *Dio1* by T3 in both mice and humans (106,107). Moreover, mice studies showed that while induction of *Dio1* was T3-dependent, it was more pronounced in WT mice compared to TRβ knockout mice, with the latter still showing higher *Dio1* expression compared to untreated mice, suggesting a compensatory effect involving TRα and supporting the presence of TREs in mice *Dio1* (107,108). Hence, DIO1 modulates local hepatic T3 availability while itself its modulated by T3 levels. However, the exact contribution of DIO1 in systemic TH levels, and especially the contribution of hepatic DIO1, is still under debate.

On one hand, results from hyperthyroid patients showed elevated levels of DIO1 expression and activity, resulting in increased T3 levels in plasma which decreased patients after

inhibition of DIO1 by 6-n-propyl-2 thiouracil (PTU) treatment in greater degree on hyperthyroid compared to euthyroid individuals (99). Furthermore, polymorphisms associated with increased DIO1 activity in humans resulted in increased serum T3 concentrations (109,110). Interestingly, genetically modified mouse models overexpressing human *DIO1* did not show significant changes in serum TH levels compared to control mice (111). These discrepancies between human and mouse TH levels in response to increased DIO1 activity are believed to be attributed to the 80% in humans and 60% in rodents contribution of peripheral tissues in T3 production (112).

In contrast, loss-of-function mutations on *DIO1* in humans lead to a two to three-fold reduced enzymatic substrate affinity and resulted in increased serum levels of rT3 and rT3/T3 ratio with normal T3 and T4 (113). Similarly, CH3 mice and whole body *Dio1*-deficient mice, showed increased rT3, T4 and rT3/T3 ratio in serum, with normal T3 levels (114). Importantly, *Dio1* knockout mice treated with T3 reduce significantly the excretion of TH in feces and urine, indicating that although contributing to increase the T3 levels in hyperthyroidism, DIO1 also enhances T3 clearance.

These observations highlight the likely differential catalytic activity of the enzyme depending on the cell, tissue, or hormonal status of the organism. While in euthyroid mice DIO1 might act as a modulator of T3 availability, maintaining the delicate balance of THs, in cases where the TH status is compromised, DIO1 might present itself as a key player for TH metabolism.

DIO2 is encoded by *DIO2* on chromosome 14q24.3 in humans. It is located in the endoplasmic reticulum (ER) with the catalytic domain towards the cytosol (101). Studies on DIO2 kinetics revealed T4>rT3 as preferable substrate with *Km* values of 1-3nM and 3-30nM respectively (103). Although important during development, DIO2 is not detectable in adult liver and there is no data pointing to the involvement of DIO2 in MASLD or MASH development and progression. Nevertheless, results of *Dio2* inactivation *in vivo* showed that perinatal *Dio2* is highly important for hepatocytes susceptibility to liver steatosis and obesity in adult mice, probably due to modulating epigenetics, underscoring the importance of THs during development and metabolism (115).

Lastly, DIO3 is an inactivating deiodinase catalysing the conversion of T4 and T3 to rT3 or T2 respectively. It is located on chromosome 14q32.31 in humans. DIO3 is very important during embryogenesis where it controls THs bioavailability by limiting the cellular exposure to T3 (116). *DIO3* expression is elevated during fetal and neonatal stages in most of the tissues, also in placenta and uterus during pregnancy. After birth *DIO3* expression declines and expression of *DIO1* and *DIO2* increases (116). Mice knockout for *DIO3* presented with growth impairment, perinatal mortality and impaired fertility accompanied with elevated T3 levels in serum (117).

Receptors

TRs belong to a nuclear receptor family that acts as a ligand-dependent transcription factor. There are two major TRs isoforms encoding by two different genes, α (*THR*α) and β (*THR*β), similar in humans and mice. The TRs are expressed in most of the tissues but following a differential distribution throughout the body and cell type (118). TRs forms homo- and heterodimers with retinoid X receptor (RXR) (119) and binds to the TREs of target genes to modulate their transcription levels. Classically, in the absence of ligand, co-repressors including the nuclear receptor corepressor 1 and 2 (NCoR1, NCoR2), the silencing mediator of retinoid and thyroid hormone receptors (SMRT) are recruited resulting in histone deacetylation by histone deacetylase 3 (HDAC3), repressing gene transcription. Upon ligand binding, co-repressors are released, and co-activators consisting of the steroids receptor coactivator (SRC) family, CBP/300 and other transcriptional activator with acetyltransferase activity are recruited to promote gene transcription (120).

TRα, also known as c-erbA-alpha, *THRA* is located on chromosome 17 in humans and 11 in mice. TRα is the main isoform in the heart and brain (121). As a result of alternative splicing on the initial mRNA, TRα results in two proteins: TRα1 and TRα2. The latter, although it can bind to TREs, it lacks the TH-binding site important for T3 binding and therefore cannot transactivate TH-responsive genes, suggesting its role as repressor (89). In the liver, TRα is expressed predominantly in hepatic stellate cells (HSCs), the main cell type involved in collagen production, while TRβ is the main isoform in hepatocytes (122). Recent research showed contribution of TRα in HSCs during chronic liver disease (122).

There are two *THR*β isoforms, *THR*β1 is abundant in liver, kidney, brain, and pituitary whereas *THR*β2 is found mostly in central nervous system, hypothalamus, pituitary (123), retina (124) and cochlea (125). Both isoforms bind to TREs and to TH with high affinity, hence they regulate TH-mediated transcription. In early MASLD *THR*β is upregulated but it declines at more severe stages of the disease, whereas in MASH, *THR*β is reduced, and its expression levels correlate with the MASH score (11).

Forrest et al, developed a global *Thrb* knockout ($Thrb^{-/-}$) and demonstrated that TRβ action in the hypothalamus and pituitary cannot be compensated by TRα, identifying TRβ as the primary regulator of the HPT axis. Additionally, they found that the endocrine disorder of $Thrb^{-/-}$ mice resemble the one of RTHβ, though the overall phenotype was milder (126–128). This difference in phenotype may partially result from interactions between the mutant receptor with its WT dimeric partners in RTH, which is absent in $Thrb^{-/-}$. Consequently, the lack of TRβ eliminates the negative effect of a mutated receptor, providing a better study of Thrb's role. However, it remains unclear whether TRα can compensate for TRβ in the liver, as findings in the literature are contradictory (129,130). Nevertheless, studies have shown that despite the co-expression of TRs in most tissues, they often regulate independent process where the phenotype resulting from the absence of one isoform cannot be fully compensated by the other (126,131,132). This observation suggest that a similar mechanism may exist in the liver. $Thrb^{-/-}$ mice are presented with elevated TSH and THs levels in serum, enlarged and hyperplastic thyroid gland, and cochlear defects.

Given the plethora of results indicating the importance of TH action and TRβ in the development and progression of MASLD and MASH, and the rising interest in therapeutic strategies targeting this receptor, TRβ emerges as a promising focal point for future treatments.

Thyromimetics for MASLD/MASH treatment

Given the importance of THs in metabolism homeostasis, and more importantly, the benefits observed in patients using TH replacement treatment in fatty liver disease (12,52,53), it is reasonable to assume that THs might represent a potential therapy for MASLD and MASH. However, T3 treatment has been demonstrated to induce undesired effects in other organs, for example tachycardia and cardiac hypertrophy (131). In the liver, T3 treatment has shown

to lower hepatic fat content and improve the disease, but also helped reducing the risk of developing fibrosis (133). THs action depends in great extent on the TRs, which show tissue- and cell- specificity across the body. In the liver, TRβ is the predominant isoform. Compounds that agonistically target TRβ, and hence mimic the action of T3 have been proposed as potential therapeutic strategy for the treatment of MASLD and MASH. These compounds are known as thyromimetics and include KB2115 (Eprotirome), GC-1 (Sobetirome), GC-24, KB-141, and the recent FDA approved MGL-3196 (Resmetirom). Among those, only Eprotirome, Sobetirome, and Resmetirom were subjected to clinical trial.

KB2115 or Eprotirome, has high affinity for TRβ in the liver. Treatment with Eprotirome showed to reduce cholesterol, stimulate synthesis of bile acids in humans and rodents, and prevented hepatic steatosis in rats fed with HFD (134–136). Moreover, in MASLD patients, it reduced cholesterol and TGAs. However, increased fasting blood insulin was observed (134). Notably, Eprotirome was not detectable in the heart (135), but adverse findings on dog's cartilage led to its direct termination in phase III of clinical trials (137).

GC-1, known as Sobetirome, is a synthetic thyromimetic developed in 1998 that showed potential to bind to both TRs but with 10-fold higher affinity to TRβ (138). GC-1 selectivity to TRβ is confirmed in many studies. Hypothyroid rodents and primates treated with GC-1 displayed reduced TGAs and cholesterol, without affecting the heart rate (60,139,140). In MASLD treatment, GC-1 proved to reduce hepatic TGAs, decrease lipoperoxidations and prevented the occurrence of liver steatosis (60). Among other benefits of GC-1 usage include increased hepatocyte proliferation in pre-damaged tissues (141) whereas it also inhibits HCC progression (142). Additionally, GC-24, a second-generation of TR-selective agonists derived from GC-1 with 40-fold higher affinity for TRβ demonstrated that despite improving key metabolic parameters it failed to improve hypercholesterolemia (143). Side effects reported of GC-1 include pancreatic proliferation (141) and insulin resistance in rats (134). Its discontinuation from clinical trials was a result of the observed side effects on dogs' cartilage of Eprotirome, which questioned the use of thyromimetics for MASLD treatment.

MGL-3196, more commonly known as Resmetirom, it has been recently approved by the FDA (72). Resmetirom is 28 times more selective for TRβ compared to TRα and is specifically taken up by the liver showing poor penetration to other tissues (15). The liver-specificity of Resmetirom is achieved by the liver-specific transporter OATP1B1 (89). The evaluation of

Resmetirom as treatment for MASLD in the phase III of clinical trials provided significant insight into its potential benefits and limitations (15). The double-blind, placebo-controlled trail set up included 966 participants, where 95% presented fibrosis in stage 2 to 3, and the mean BMI was 36 kg/m^2. Results from the trial indicated a significant reduction on steatosis levels from baseline and improved fibrosis without affecting heart rate, bone density, or insulin sensitivity in animal or human studies. Moreover, the clinical trial of Resmetirom included participants with comorbidities associated to MASH such type 2 diabetes, hypertension, obesity, and high cardiovascular risk patient (15).

These studies provide insights on how important the study of thyroid hormone metabolism in the liver is for MASLD and MASH managing. Focusing on the liver-specific pathways and receptors such as TRβ may provide valuable insights into minimizing disease progression while avoiding systemic side effects, highlighting the importance of targeted research in this area. Unfortunately, no molecular data on TH metabolism in humans subjected to these thyromimetics is currently available.

1.4. Animal models for MASLD and MASH

Mouse models are indispensable for the study of MASLD and MASH given the complexity of these diseases, and the inherent challenges of studying these conditions *in vitro*. Moreover, animal models offer a dynamic system to investigate the pathophysiological mechanisms and the potential therapeutic targets facilitating a more comprehensive understanding of MASLD and MASH.

Current limitations in mouse models of MASLD and MASH include the long periods of dietary intervention required, the use of genetic modified mouse lines, the necessary addition of fibrogenic drugs, and the incomplete pathophysiological profile of advanced MASH compared to humans, such as hepatocyte ballooning, fibrosis or weight loss, and sex-based differences. A summary is included in Table 11.

Commonly, obesogenic diets for the development of MASH mouse models include the use of high carbohydrates (HCD) or high fat diets (HFD). These models mostly reproduce the metabolic and pathological features of MASLD in addition to insulin resistance and obesity, which are common comorbidities of MASLD. However, these models require extensive periods of time to fully develop and even then, failed to induce advance fibrosis and to progress to

MASH. A combination of high-fat and high-carbohydrate diet is a successful model that mimic the Western Diet (WD) in humans. Although WD-fed mouse model is described as the best to recapitulate the features of MASLD in terms of pathogenesis and transcriptomic signature (144,145), it fails to progress to full MASH without adding carbon tetrachloride (CCl4) or other fibrogenic drugs (145–148).

Other animal models like methionine- choline- deficient diet (MCDD), choline-deficient diet (CD), or a combination between HFD and pharmacological intervention (e.g., CCl4) result in steatohepatitis accompanied with fibrosis in short time, resembling features of MASH. However, these diets lead to pronounced weight loss and do not fully reproduce the natural development of MASLD and MASH in humans. A more recent mouse model combining choline-deficient with high fat diet (CD-HFD) revoked the weight loss, allowing to study the different stages of the disease, from MASLD to MASH and HCC (149,150). Notably, CD-HFD combined with sufficient methionine (>0.1%), showed insulin resistance in mice models (151).

Unfortunately, up to date there are no mouse models that mimic all the spectrum of features, metabolic and molecular alterations observed in humans. Given that MASLD and MASH are characterized by high heterogeneity regarding comorbid diseases, the animal models should be carefully chosen depending on the focus of the study.

1.5. Aim of this project

THs play a pivotal role in a wide range of physiological processes. Dysregulation of TH has been linked to various metabolic diseases including MASLD and MASH (1–3). These conditions are associated with hypothyroidism, which contributes to metabolic dysfunction by promoting hyperlipidaemia, obesity, and insulin resistance, thus exacerbating the liver pathology (4–9). Conversely, hyperthyroidism, TH supplement therapy, or the use of thyromimetics ameliorates MASLD and MASH (12,15,52,53). Recent research highlights the importance of local hepatic TH metabolism over systemic levels in the pathogenesis of MASLD and MASH.

Among the key components of the local control of TH metabolism in the liver, TRβ has gained significant attention after the results of a comprehensive study involving MASH patients revealing a notable decrease in TRβ expression in the liver, which also correlated with worsen MASH score (11). This reduction suggests that the liver might become less TH

responsive, potentially exacerbating disease progression, which might also be extended to the liver response to thyromimetics.

Given these observations, this dissertation aims to investigate TH metabolism during MASLD and MASH progression with special focus on TRβ and other regulators of local hepatic TH action (Figure 3). First, by stablishing an animal model of MASH combined with TRβ knock-out or genetically engineered overexpressing TRβ mice, to explore the role of TRβ in hepatic TH metabolism and its impact in MASLD and MASH progression. Second, by using primary mouse hepatocytes (PMH) to determine single factors affecting hepatic TH metabolism. And third, by employing *Dio1* overexpressing mice to study the role of other TH regulators, this thesis will address the following questions:

1. Establish a MASH animal model that replicates the observed decline in TRβ expression in humans.
2. Is TRβ declining expression during MASH detrimental for disease progression?
3. Can the restoration of TRβ expression in the liver have beneficial effects on MASH?
4. Are other regulators of local TH action, such as DIO1, involved in the pathogenesis of MASH?

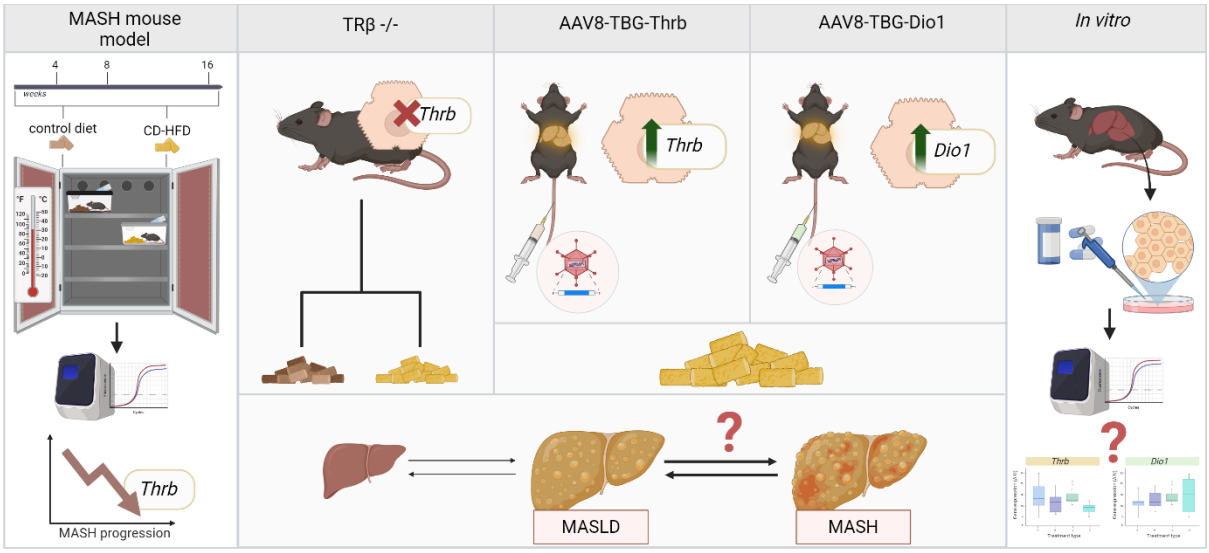

Figure 3 – Aims of the study. From left to right. Establishment of MASH mouse that replicates the TRβ decline observed in humans using control or CD-HFD at thermoneutrality. Is TRβ decline in MASH promoting disease progression? Can the restoration of TRβ improve MASH? What is the role of DIO1 in hepatic TH action during MASH? What are the individual factors affecting hepatic *Thrb* and *Dio1* gene expression? Figure created with BioRender.

2. MATERIAL AND METHODS

In the following sections are included all the materials and methods used in this study.

2.1. Materials

Antibodies, chemicals, and reagents

The following antibodies, chemicals and reagents listed in Table 1 were used during the experiments.

Table 1| Antibodies, chemicals, and reagents used for experiments.

Item	*#Catalog*	*Source*
2-Propanol	CP41.3	Carl Roth GmbH + Co. KG, Germany
3,3',5-Triiodo-L-Thyronine sodium salt (T3)	T6397	Sigma Aldrich Chemie GmbH, Germany
Acetic acid	3738.4	Carl Roth GmbH + Co. KG, Germany
Alexa Fluor 594TM antibody	A-11058	Invitrogen, Thermo Fisher Scientific Inc., Germany
Anti-mCherry antibody	AB0040	OriGene, Germany
BSA-Palmitate Saturated Fatty Acid Complex (5 mM)	29558	Cayman Chemical, USA
Chloroform	C2432	Sigma Aldrich Chemie GmbH, Germany
Collagen type I from rat tail	C3867	Sigma Aldrich Chemie GmbH, Germany
Collagenase type IA (Clostridium histolyticum)	C9891	Sigma Aldrich Chemie GmbH, Germany
cOmplete Protease Inhibitor Cocktail	5892970001	Roche Diagnostics GmbH, Germany
Corticosterone	C2505	Sigma Aldrich Chemie GmbH, Germany
D-(+)-Glucose	G7021	Sigma Aldrich Chemie GmbH, Germany
D(+)-Saccharose (C12H22O11)	4621.1	Carl Roth GmbH + Co. KG, Germany
DEPC-treated Water	AM9906	Thermo Fisher Scientific Inc., Germany
Dexamethasone	D4902	Sigma Aldrich Chemie GmbH, Germany
Dimethyl sulfoxide (DMSO)	A3672	AppliChem GmbH, Germany
Direct Red 80	365548	Sigma Aldrich Chemie GmbH, Germany
di-Sodium hydrogen phosphate dihydrate (Na2HPO4*2H2O)	1.0658	Supelco, Inc., USA
EGTA	E3889	Sigma-Aldrich Chemie GmbH, Germany
Eosin G-solution 0.5% water	X883.2	Carl Roth GmbH + Co. KG, Germany
Ethanol ≥70%	T913.2	Carl Roth GmbH + Co. KG, Germany
Ethanol ≥99,8%	K928.4	Carl Roth GmbH + Co. KG, Germany
Ethanol absolute for analysis	UN1170	Sigma Aldrich Chemie GmbH, Germany
Fetal Bovine Serum	10270106	Thermo Fisher Scientific Inc., Germany

Item	*#Catalog*	*Source*
Fetal Bovine Serum, charcoal stripped	12676029	Thermo Fisher Scientific Inc., Germany
GibcoTM Dulbecco's modified eagle medium (DMEM/F-12)	31331028	Thermo Fisher Scientific Inc., Germany
HBSS w/o Ca2+, Mg2+, phenol red	L2045	Biochrom GmbH, Germany
Heparin	H3393-50KU	Sigma Aldrich Chemie GmbH, Germany
HEPES 1M	H0887	Sigma Aldrich Chemie GmbH, Germany
Histoplast Paraffin Wax	6774060	Thermo Fisher Scientific Inc., Germany
Hydrochloric acid (HCl; 37 %)	9277.1	Carl Roth GmbH + Co. KG, Germany
Insulin (NovoRapid Penfill 100E/ml)	558713	Novo Nordisk, Denmark
Isoflurane	TU 061219	Zoetis Inc., USA
L-glutamine	A2916801	Thermo Fisher Scientific Inc., Germany
Mayer's hemaium solution	1.09249.1000	Sigma Aldrich Chemie GmbH, Germany
Metformin (1,1-Dimethylbiguanide hydrochloride)	D150959	Sigma-Aldrich Chemie GmbH, Germany
Micromount Mounting Medium	3801731	Leica Biosystems Richmond, Inc., USA
Mounting medium, Aqueous, BioAssay	M4679-01	USBiological, USA
Normal donkey serum	END9010-10	BIOZOL Diagnostics, Germany
Nuclease-Free Water	P119E	Promega GmbH, Germany
Oil Red O	O0625	Sigma Aldrich Chemie GmbH, Germany
Paraformaldehyde solution (4 % in PBS)	J19943-K2	Thermo Fisher Scientific Inc., Germany
Penicillin-Streptomycin (10000 U/mL)	15140122	Thermo Fisher Scientific Inc., Germany
Picric aqueous solution 1.2%	A2520	AppliChem GmbH
Potassium chloride (KCl)	P017.1	Carl Roth GmbH + Co. KG, Germany
Potassium dihydrogen phosphatee (KH2PO4)	P018.2	Carl Roth GmbH + Co. KG, Germany
ProLong Diamond Antifade Mountant with DAPI	P36971	Life Technologies, USA
QIAzol	79306	QIAGEN GmbH, Germany
RNaseZAP TM	AM9780	Th. Geyer GmbH, Germany
RNeasy® Fibrous Tissue Mini Kit	74704	QIAGEN GmbH, Germany
Simvastatin	S6196	Sigma Aldrich Chemie GmbH, Germany
Sobetirome (GC-1)	SML1900	Sigma Aldrich Chemie GmbH, Germany
Sodium Chloride (NaCl)	9265.2	Carl Roth GmbH + Co. KG, Germany
Sodium chloride (NaCl; 0.9 % sterile)	6605514	Fresenius Kabi Deutschland GmbH, Germany
Sodium hydroxide (NaOH)	1310-73-2	Carl Roth GmbH + Co. KG, Germany
Sodium pyruvate 100mM	L0642	Sigma Aldrich Chemie GmbH, Germany
Tissue-Tek® O.C.T.TM Compound	4583	Sakura Finetek USA, Inc. USA
TritonTMX-100	X100	Sigma Aldrich Chemie GmbH, Germany
Trypan Blue 0.4%	15250-061	Thermo Fisher Scientific Inc., Germany
Vaseline	771055	Balea; dm-Drogeriemarkt GmbH + Co. KG, Germany

Item	*#Catalog*	*Source*
Williams E media	12551032	Thermo Fisher Scientific Inc., Germany
Xylol	360.25	Th. Geyer GmbH, Germany
β-mercaptoethanol	M6250	Sigma Aldrich Chemie GmbH, Germany

Commercial kits

The following available commercial kits listed in Table 2 were used in this study.

Table 2| Commercial kits used for experiments.

Item	*#Catalog*	*Source*
Alanine Aminotransferase (ALT) Activity Assay	MAK052	Sigma Aldrich Chemie GmbH, Germany
Aspartate Aminotransferase (AST) Activity Assay	MAK055	Sigma Aldrich Chemie GmbH, Germany
Glycogen assay kit	MAK016	Sigma Aldrich Chemie GmbH, Germany
GoTaq® qPCR Mastermix	A6002	Promega GmbH, Germany
MILLIPLEX® Mouse Pituitary Magnetic Bead Panel (TSH)	MPTMAG-49K	Merck Millipore
miRNeasy® Mini Kit	1038703	QIAGEN GmbH, Germany
NucleoType™ Mouse PCR	743200	Marcherey-Nagel GmbH & Co. KG, Germany
Rat/Mouse C-Peptide 2 ELISA	EZRMCP2-21K	Sigma Aldrich Chemie GmbH, Germany
RevertAid First Strand cDNA Synthesis kit	K1622	Thermo Fisher Scientific Inc., Germany
RNase-Free Dnase Set	79256	QIAGEN GmbH, Germany
RNeasy® Fibrous Tissue Mini Kit	74704	QIAGEN GmbH, Germany
RNeasy® Lipid Tissue Mini kit	1023539	QIAGEN GmbH, Germany
RNeasy® Mini kit	74106	QIAGEN GmbH, Germany
TaqMan™ Fast Advance Master Mix	4444557	Thermo Fisher Scientific Inc., Germany
TaqMan™ Advanced miRNA cDNA Synthese-Kit	A28007	Thermo Fisher Scientific Inc., Germany
Total T3 ELISA	DNOV053	NovaTec Immundiagnostica GmbH, Germany
Total T4 ELISA	EIA-1781	DRG Instruments GmbH, Germany
Triglyceride Quantification Kit	MAK266	Sigma Aldrich Chemie GmbH, Germany

Consumables and devices

Table 3 lists the consumables and devices used during the experiments.

Table 3| Consumables and devices used for experiments.

Item	*#Catalog*	*Source*
23U-Series Color Industrial Camera	n.a.	The Imaging Source Europe GmbH, Germany

Item	*#Catalog*	*Source*
96-PCR plate	72.1979.102	Sarstedt AG & Co., Germany
Accu-Check Aviva test strips	64553970003	Roche Diabetes care GmbH, Germany
Acculab ATL-224-I Atilon Analytical Balance 220g x 0.0001	n.a.	Sartorius Stedim Biotech GmbH, Germany
Acquity UPLC Xevo TQ-S	n.a.	Waters GmbH, Germany
Adhesive clear PCR seal sheets	600208	BiozymScientific GmbH, Germany
Alcohol pads	9160612	B. Braun SE, Germany
BD Microlance™ 3, 26G x 1/2" (0,45x13mm)	303800	Becton Dickinson GmbH, Germany
BD Neoflon™ I.V. Cannula 26G (0.6 x 19mm)	391349	Becton Dickinson GmbH, Germany
Biosphere® Plus (20 µL, 100 µL, 200µL, 1000 µL)	70.3020.305, 70.3030.305, 70.3060.100	Sarstedt AG & Co., Germany
Biosphere® Plus Filter tips (20 µL, 100 µL, 200µL, 1000 µL)	70.3020.355, 70.3020.385, 70.760.212, 70.760.211, 70.3060.355	Sarstedt AG & Co., Germany
Bright field microscope Axiovert 40 CFL	n.a.	Carl Zeiss AG, Germany
Cell scraper M (sterile)	83.3951	Sarstedt AG & Co., Germany
Cell strainer (70 µm)	542070	Greiner Bio-One International GmbH, Germany
Centrifuge 5430, 5430 R, and multifuge 3 S-R	n.a.	Eppendorf AG, Germany
Centrifuge Mikro 22R	n.a.	Andreas Hettich GmbH & Co. KG, Germany
Ceramic beads (1.4 mm, 325g)	432-0356	VWR International, USA
Combitips advanced ® (0.2, 0.5, 2.5, 5, 10mL)	2030-06-28, 2027-10-28, 2027-11-28, 2030-03-28, 2028-08-28	Eppendorf AG, Germany
Corning® Cell lifter sterile	3008	Corning Incorporated GmbH, Germany
Cotton swaps	974116	Nobamed, Germany
Cover glasses	6701212	Th. Geyer GmbH, Germany
Cryostat CM3050 S	n.a.	Leica Biosystems, Germany
Dräger Isoflurane Vapor® 19.3	n.a.	Drägerwerk AG & Co. KGaA, Germany
EVOS® FL Auto Imaging System	AMAFD1000	Thermo Fisher Scientific Inc., Germany
Feather disposable scalpel	02.001.30.010	Feather Safety Razor Co.,Ltd., Japan
Filtropur S 0.2 (Syringe filters 0.2 µm)	83.1826.001	Sarstedt AG & Co., Germany
FisherbrandTM Homogenizer Bead Mill 24	n.a.	Fisher Scientific GmbH, Germany
Flatfilter 595 1/2 Ø125 mm	10311644	Schleicher & Schuell MicroScience GmbH, Germany
Glucometer (Accu Chek Aviva®)	n.a.	Roche Diagnostics, Germany
Green Line Sealsafe Plus	GM500	Tecniplast S.p.A, Italy

Item	*#Catalog*	*Source*
Heating pad Thermolux®	n.a.	Witte + Sutor GmbH, Germany
Hybridization oven	n.a.	Hybaid GmbH, Germany
Incubator HERA Cell	n.a.	Thermo Fisher Scientific Inc., Germany
Infrared camera T335	n.a.	FLIR Systems Termisk Systemteknik, Sweden
Inject®-FLuerSolo	9166017V	B. Braun SE, Germany
Magnetic Hotplate Stirrer VMS-C4	n.a.	VWR International, Germany
Magnetic stirrer (Rct basic)	n.a.	IKA®-Werke GmbH & Co. KG, Germany
Microscope slides Superfrost ® Plus	P018.2	Thermo Fisher Scientific Inc., Germany
Microtest plate transparent, flat bottom, 96 well	821581001	Sarstedt AG & Co., Germany
Microtome Blade MB35 Premier	3050835	Epredia Netherlands B.V., Netherlands
Minispec BCA Mice Analyzer LF110	n.a.	Bruker Corporation, Germany
Multipette 8-channel (0.5-10µL)	3125000010	Eppendorf AG, Germany
Multipipette® E3	4987000010	Eppendorf AG, Germany
NanoDrop™ One C	ND-ONE-W	Thermo Fisher Scientific Inc., Germany
Parafilm	P7793	Sigma Aldrich Chemie GmbH, Germany
PCR strip of 8 200µL	72.991.992	Sarstedt AG & Co., Germany
Peristaltic pump P-3	n.a.	Pharmacia, Germany
Pestle	7694947	Th. Geyer GmbH, Germany
pH-meter (PB-11)	n.a.	Sartorius Lab Instruments GmbH & Co. KG, Germany
Pipette Research ® Plus (0.5-10µL, 2-20µL, 10-100µL, 20-200µL, 100-1000µL)	3123000020, 3123000039, 3123000047, 3123000055, 3123000063	Eppendorf AG, Germany
Pipetus® red dot	500975	Hirschmann Laborgeräte GmbH & Co. KG, Germany
Precision balance	ECN 611-2605	VWR International, Germany
PV-1 Grantbio	n.a.	Grant Instruments Ltd, UK
QuantStudio Applied Biosystems real-time PCR system	n.a.	Thermo Fisher Scientific Inc., Germany
Rectal thermometer probe BAT-12	n.a.	Physitemp Inc., USA
Rotary microtome Microm HM 340E	n.a.	Thermo Fisher Scientific Inc., Germany
SafeSeal tube (1.5; 2; 5mL)	72.706.400; 72.695.400; 72.701.400	Sarstedt AG & Co., Germany
Screw cap micro tube 2mL	72.694.406	Sarstedt AG & Co., Germany
Serological Pipette (5, 10, 25, 50mL)	86.1253.001; 86.1254.001; 86.1685.001; 86.1256.001	Sarstedt AG & Co., Germany
SONOREX SUPER RK 100 H	n.a.	Bandelin electronic, Germany
SPECTROstar Nano Microplate Reader	n.a.	BMG Labtech, Germany
Staining jar	073.05.001	Isolab Laborgeräte GmbH, Germany

Item	*#Catalog*	*Source*
Stereo microscope VWR® VisiScope ® SZB250	n.a.	VWR International, Germany
Sterican® Safety Needle 30G x 1/2" (0,30x13mm)	4670002S-01	B. Braun SE, Germany
TC dish 100, standard	83.3902	Sarstedt AG & Co., Germany
TC plate, 6 well, standard F	83.3920	Sarstedt AG & Co., Germany
Thermo Scientific™ Safe 2020 Class II Microbiological Safety Cabinet	n.a.	Thermo Fisher Scientific Inc., Germany
Thermocycler PTC-200	n.a.	Biozym Scientific GmbH, Germany
Thermomixer 5436	n.a.	Eppendorf AG, Germany
Tissue-Tek ® Cryomold (25x20x5mm; 15x15x5mm)	4557; 4566	Sakura Finetek USA, Inc., USA
Titramax 100	544-11200-00-3	Heidolph Instruments, Germany
TSE PhenoMaster	n.a.	TSE Systems, Germany
Tubes (15 mL, 50 mL)	62.554.502; 62.547.254	Sarstedt AG & Co., Germany
UNIPROTECT NG cabinet	n.a.	Zoonlab GmbH, Germany
Water bath (OLS 200)	n.a.	Grant Instruments Ltd, UK
Water bath GFL 1052	n.a.	GFL Gesellschaft für Labortechnik mbH, Germany
Weighing pans neoLab®	1-1130	neoLab Migge GmbH, Germany

Diet

The following commercially available diets are listed in table 4 and were used during the experiments.

Table 4| Diets used in the experiments.

Item	*Composition*	*%Kcal*	*#Catalog*	*Source*
Choline-deficient high fat diet (CD-HFD)	Carbohydrates Fat Protein Methionine*	31% 60% 9% 0.4%	S0585-E010	ssniff Spezialdiäten GmbH, Germany
CSAA Control (Control)	Carbohydrates Fat Protein Methionine*	72% 16% 12% 0.4%	E15668-043	ssniff Spezialdiäten GmbH, Germany
High fat diet (HFD)	Carbohydrates Fat Protein	20% 60% 20%	D12492	Research Diets, Inc., USA
Standard chow diet (Chow)	Carbohydrates Fat Protein	59% 14% 27%	1314	Altromin, Germany

*Weight content %.

Software

Table 5| List of software and purpose of use in this study.

Item	*Purpose*	*Source*
FLIR Tools Infrared picture analysis	Infrared picture analysis	FLIR Systems Termisk Systemteknik, Sweden
GraphPad PRISM 9	Statistical analysis	GraphPad Software Inc., USA
MARS Datenanalyse-Software	Microplate reader software	BMG Labtech, Germany
MassLynx ® 4.1	Liquid chromatography mass spectrometry data analysis	Waters GmbH
Microsoft Office Excel	Data processing	Microsoft, USA
OpenLynx ™	Liquid chromatography mass spectrometry data acquisition	Waters GmbH
QuatStudio™ Design & Analysis v1.5.1	qPCR analysis	Thermo Fisher Scientific Inc., Germany
TSE PhenoMaster Software V6.5.3	Indirect calorimetry data acquisition and analysis	TSE Systems, German

2.2. Methods

Animal husbandry and experimental design

All animal experiments were carried out according to EU guideline regulations (210/63/EU) and approved by the MEKUN Schleswig-Holstein (Germany).

Wild-type and TRβ knockout (126) male mice were bred on the C57Bl/6NCrl background in the Gemeinsame Tierhaltung (GTH) University of Lübeck. Mice were single housed at 4-6 months age and placed at thermoneutrality (30 ± 2°C) in a climate chamber (Zoonlab GmbH, Germany) with free access to food and water in a constant 12:12 hour light/dark cycle. After three weeks of acclimation on standard chow diet (#1314, Altromin), mice were randomized into a control group receiving control diet (#E15668-043; Ssniff Spezialdiäten GmbH, Germany) or CD-HFD (#S0585-E010; Ssniff Spezialdiäten GmbH, Germany). An extra group of liver samples from mice fed with standard chow diet for 4 weeks at thermoneutrality was included in the study as baseline for normalization. To improve data visualization, the bar representing this group was omitted on the graphs.

Liver samples from C57BL/6N mice fed with chow or HFD for 1 to 18 weeks were kindly provided by Prof. Dr. Henriette Kirchner (152).

Associated adenovirus (AAV) gene therapy

Male C57Bl/6NCrl mice (4-7 months) were purchased from Charles River Laboratories (Charles Rivers, Germany) and single housed at 30°C under a 12:12 hour light/dark with food and water access *ad libitum*. After one week of acclimation period on a standard chow diet (#1314, Altromin), animals were changed to CD-HFD (#S0585-E010; Ssniff Spezialdiäten GmbH, Germany).

For hepatocyte-specific AAV-mediated studies, serotype 8 combined with the human TBG promotor was used (153,154). After two weeks on CD-HFD, body weight-matched mice were randomly assigned to the different experimental groups. Animals were tail injected with the virus, see table 6 (VectorBuilder GmbH, Germany). Before the intervention, mice were anesthetized with isoflurane, and during the intervention were kept on a homeothermic monitoring system to maintain core body temperature. Body composition was measured by nuclear magnetic resonance (NMR) (minispec LF110, Bruker Corporation, Germany).

Table 6| Viral constructs used in this study.

Item	***Catalog name***	***p.f.u./mouse***	***Source***
AAV8-TBG-Dio1+SECIS	VB210902-1136zrd	$5.73x10^{11}$	VectorBuilder GmbH
AAV8-TBG-mCherry	VB220215-1039 yuh	$1.33x10^{11}$	
AAV8-TBG-miR34aSponge	VB221120-1262dhg	$3.98x10^{11}$	
AAV8-TBG-mSoc3	VB230116-1056vxn	$3.32x10^{11}$	
AAV8-TBG-mThrb	VB211123-1086ztk	$3.44x10^{11}$	

In vivo methods

Glucose and insulin tolerance test

Animals were fasted for 6 hours with free access to water prior to receive an intraperitoneal injection of D-(+)-Glucose (Sigma-Aldrich, Germany) 1.5 g/kg body weight dissolved in sterile 0.9% saline. Glucose levels were measured in blood drawn from the tail before and 15-, 30-, 60-, and 120- minutes post injection using a glucometer (AccuCheck, Aviva). After two days of recovery, mice followed the same fasting protocol described and received an intraperitoneal injection of insulin (NovoRapid Penfill 100E/mL, Novo Nordisk) of 0.75 U/kg body weight. For insulin tolerance recording, blood glucose was measured before and 15-, 30-, 60-, 90-, and 120- minutes post injection as described above.

Indirect calorimetry

Oxygen consumption (VO_2) and carbon dioxide production (VCO_2) in mice were assessed employing indirect calorimetry using an open respirometry system (TSE PhenoMaster, TSE Systems) connected to a climate-controlled chamber maintained at 30 ± 0.5°C. The animals had *ad libitum* access to food and water. Measurements of VO_2, VCO_2, energy expenditure, food, and water intake, were conducted at 20 minutes intervals. The respiratory quotient (RQ) was calculated as RQ = VCO_2/VO_2 and it serves as an indication of the type of macronutrients being metabolized as different energy pathways. If the metabolism consists of mostly lipids, the RQ ≈ 0.7, for proteins RQ ≈ 0.8, and carbohydrates RQ ≈ 1.0. The daily energy expenditure (DEE, kJ/day) was obtained using the RQ and the caloric equivalents given by Heldmaier et al., and heat production (HP, mW = (4.44 + 1.43 * RQ) * VO2(mL O_2/h)) for a 24-hour period (155). Additional calculations for resting metabolic rate (RMR) and basal metabolic rate (BMR) were performed, focusing on periods of inactivity and lowest mean oxygen consumption, respectively. BMR assessment was done during a 6-hour fasting period. Subsequent analysis was done with Microsoft Office Excel and TSE PhenoMaster software V6.5.3 (TSE Systems, Germany).

Infrared thermography

To assess differences in thermoregulation, pictures of brown adipose tissue (BAT), inner ear, tail, and lower back, were taken using T335 infrared camera (FLIR Systems Termisk Systemteknik, Sweden) at 30°C. To ensure reproducibility, all the pictures were taken at the same interval of time in the morning and the animals were brushed on their interscapular area with a cotton swab with Vaseline before the procedure (156). The infrared pictures of the mentioned areas were taken in random order within 3 minutes of taking the animal out of the cage. Assessment of the maximum temperature for each area was determine using the FLIR tools software and normalized to back temperature or inner ear to obtain the relative temperature.

Sacrifice and organ collection

All animals were sacrificed at the same interval of time in the morning. After sacrifice, a longitudinal incision was preformed to open the mice abdominal cavity. Blood was immediately drawn from the caudal vena cava, transferred to a 1.5mL tube allowing it to clot for 5 minutes

at room temperature and then 20 minutes on ice. Following, the blood was centrifuged twice at 4°C and 2000 rfc, the supernatant was transferred to a new tube in each step and stored at -20°C until further use. The tissues of interest were collected, snap-frozen, and store at -80°C. Liver was extracted, weighted, and rinsed with cold PBS to remove the excess of blood. Next, to ensure uniformity and comparability, the livers were excised from identical regions across all subjects and experimental conditions. One fraction underwent dehydration in 30% sucrose followed by embedding in optimal cutting temperature compound (O.C.T compound) (Sakura Finetek Germany GmbH, Germany) and storage at -80°C until sectioning on the cryostat for staining. A second part was placed in a cassette into 4% paraformaldehyde (PFA) for 48h before proceeding with the paraffin embedding protocol. The remaining tissue was snap-frozen and stored at -80°C.

In vitro methods

Primary mouse hepatocytes

PMH were isolated from WT mice livers and cultivated as follows. First, the peristaltic pump was cleaned with ethanol (EtOH) 70%, following by 20mL of prewarmed perfusion buffer (Table 7) at 37°C to remove the excess of alcohol. The animal was sacrificed using CO_2 without cervical dislocation and the abdominal cavity was opened, exposing the liver, caudal vena cava and portal vein. While the perfusion buffer was running at a low flow (3mL/minute) a 26G butterfly cannula was inserted in a flat angle into the caudal vena cava, minimizing the risk of bubbles. After few seconds, immediately upon the appearance of white spots or portal vein swelling, the portal vein was cut to allow draining. At this point, the liver should turn yellow-white indicative of clearance of blood. Afterward, the flow speed was increased and maintained in a constant 6mL/min while the portal vein was clamped for 10-14s and released, allowing the liver to swell. This step was repeated no more than 5 times in intervals of 30 seconds approximately. The perfusion buffer allows the chelate of calcium, facilitating the disruption cell-cell and cell-matrix interaction and to clean the blood from the liver. Following the infusion of 45mL of perfusion buffer into the liver, the pump was stopped, and the warm collagenase buffer (Table 7) was then connected to the pump to proceed with the collagen digestion of the extracellular matrix. As previously, the flow rate was adjusted to a constant 6mL/min, and the portal vein was clamped to ensure even distribution of the buffer throughout the liver, but no more than 3-4 times in intervals of 30 seconds approximately. The

effectiveness of the collagenase digestion was confirmed by observing the lack of relaxation upon clamping the portal vein. After 45mL of collagenase buffer infusion into the liver, the pump was stopped, the cannula removed, and the liver was dissected carefully in one piece and transferred into a tube with 10-15mL of cold attachment media (Table 7), ensuring the liver was fully submerged.

The next steps were carried out under sterile and cold conditions using only 25mL serological pipettes to avoid bubble formation, which will reduce hepatocyte viability. First, the liver was transferred to a culture dish, the gall bladder was removed, and the liver sack ruptured using forceps. The cells were released gently using a cell lifter. The cell suspension was filter through a 70µm cell strainer and centrifuged at 50 x g for 5 minutes with low acceleration and low break. The supernatant was discarded, and the pellet containing the hepatocytes was resuspended in 20mL of fresh attachment media by softly inverting the tube prior to cell counting using Trypan Blue (1:1). Only the cells round, bright and with clear nucleus were considered as viable hepatocytes.

Finally, the cells were plated in a 6-well collagen-coated plates at a density of 4 x 10^5 cells/well with attachment medium and placed in a humidified CO_2 incubator at 37°C. After 3-4h, the cells acquire a spherical shape with one or two nuclei visible, indicator of a successful attachment to the plate. Then, the hepatocytes were changed to a warm maintenance medium (Table 7) containing the different treatment conditions. After 24h, the cells were harvested or in case of prolonged treatment, the media was refreshed according to the treatment condition, and harvested after 48h. For the treatment with insulin, after the attachment period concluded, an additional period of starvation of 4h preceded by a wash of the cells in warm PBS was done. Finally, after the starvation, the cells were washed in warm PBS and exchanged to warm maintenance medium with the desired concentrations of insulin. For the treatment with T3, the fetal bovine serum (FBS) was substituted for charcoal FBS.

Table 7| Buffers and culture media preparations used during primary mouse hepatocytes isolation.

Solution	***Reagent***	
Perfusion buffer	HBSS w/o Ca^{2+}, Mg^{2+}, phenol red	-
	HEPES	10 mM
	EGTA	0.5 mM
	Heparin*	4U/mL

Solution	*Reagent*	
Digestion buffer	Williams E Media	-
	HEPES	10mM
	Collagenase type I*	0.3mg/mL
Attachment media	DMEM/F-12 Media	-
	HEPES	20mM
	Sodium pyruvate	2mM
	Inactive FBS	10%
	Penicillin-streptomycin	1%
	Insulin*	1µM
	Dexamethasone*	1µM
Maintenance Media	Williams E Media	-
	HEPES	20mM
	L-glutamine	2mM
	Inactive FBS/Charcoal FBS	10%
	Penicillin-streptomycin	1%
	Insulin*	1nM
	Dexamethasone*	0.1µM
Collagen coated dishes	PBS	-
	Collagen type I	0.2µg/mL

*Added fresh before use.

Molecular methods

Histology

Tissues were fixed in 4% PFA for 48h, followed by a dehydration process using increasing concentrations of ethanol and xylol before being embedded in paraffin. For cryosections, tissues were either directly frozen in O.C.T (Sakura Finetek Germany GmbH, Germany) or, for fatty tissues, initially fixed in 4% PFA overnight and then subjected to cryoprotection in 30% sucrose for 48 hours. Paraffin embedded sections of 5 µm thickness were stained for Haematoxylin and Eosin (H&E) using Mayer's hemalum solution (Sigma-Aldrich, Germany) and eosin Y solution 0.5% aqueous (Carl Roth GmbH&Co KG, Germany) according to manufacturer's instructions (X883.1, Carl Roth GmbH&Co KG, Germany). Sirius red staining (SR) was done in 5 µm paraffin cuts. Prior to staining, slides were rehydrated and then immersed in Picrosirius solution for 60 min, consisting of 0.1% of Direct Red 80 (Sigma-Aldrich, Germany) in picric aqueous solution 1.2% (AppliChem GmbH, Germany), and then washed for 4 min in 0.5% acetic acid diluted in distilled water, dehydrated, cleared, and mounted. All sections were mounted with xylene-based mounting media (Leica Mikrosysteme Vertrieb GmbH, Germany). Cryosections of 7 µm thickness were stained with Oil Red O (ORO) (Sigma-Aldrich, Germany) following manufacturer's instructions and mounted with aqueous mounting media. Quantification of

percentage of positive area for SR and ORO was done using ImageJ 1.54b. For mCherry detection, 7µm liver sections from unfixed frozen tissue were fixed in 4% PFA for 20 minutes followed by washing in PBS before the primary and secondary antibodies. Primary antibody goat mCherry 1:500 (AB0040; OriGene Technologies GmbH, Germany) was left overnight at 4°C. Alexa 594 conjugated donkey anti-goat 1:400 (A11058; Invitrogen, Germany) was used as secondary antibody. The sections were stained with mounting medium with DAPI (Invitrogen, Germany).

RNA, cDNA synthesis and real-time qPCR

RNA isolation was carried out using kits from QIAGEN depending on the tissue and following the manufacturer's instructions. For liver, kidney, and PMH, RNA was isolated using the miRNeasy Mini kit; for BAT with the RNeasy Lipid Tissue Mini kit; muscle with RNeasy Fibrous Tissue Mini Kit; pituitary and paraventricular nucleus of the hypothalamus (PVN) with RNeasy Mini Kit (QIAGEN, Germany). A DNase step was included in all the extractions (QIAGEN, Germany). RNA concentration and purity were assessed by NanoDrop (Thermo Fisher Scientific, Germany). Next, cDNA synthesis was carried out using the Molecular Biology ReserAid cDNA Kit (Thermo Fisher Scientific, Germany) from 1µg of RNA. For real-time qPCR (qPCR) analysis, QuantStudio Applied Biosystems (Thermo Fisher Scientific, Germany) and GoTaq qPCR Master Mix (Promega, Germany) were used. Efficiency of qPCR primers (E) was determined for each plate using standard curves slope (157).

Normalization of gene expression was done with the best combination of housekeeper genes determined by NormFinder (https://moma.dk/normfindersoftware, Denmark). In that regard, gene expression was normalized with *hypoxanthine phosphoribosyltransferase (Hprt)* and *ribosomal protein lateral stalk subunit P0 (Rplp0)* for liver tissue; *Hprt* and *peptidylprolyl isomerase A (cyclophilin A) (Ppia)* for kidney; *Hprt* and *Rplp0* for BAT; *Hprt* and *peptidylprolyl isomerase D (cyclophilin D)* (*Ppid)* for muscle; *Ppid* for pituitary; *Ppia* for PVN; *Hprt* and β-*actin* (*Actb*) for PMH.

To study levels of mature microRNA (miRNA), 10 ng from total RNA of each sample was reverse transcribed into cDNA using TaqMan Advanced miRNA cDNA Synthesis Kit (Thermo Fisher Scientific, Germany). For gene expression quantification, qPCR was performed in a fast-thermal cycling protocol using TaqMan Fast Advanced Master Mix (Thermo Fisher Scientific,

Germany) with either the miR34a-5p specific primer or the endogenous control miR24-3p primer (assay ID:478048_mir; 477992_mir, respectively).

To evaluate the viral transduction efficiency, DNA was isolated from liver samples using the NucleoType™ Mouse PCR kit (Macherey-Nagel) following manufacturer's instructions. Subsequent qPCR of the Woodchuck Hepatitis Virus Posttranscriptional Regulatory Element (WPRE), present in the viral construct genome, was carried out. The calculation of viral titers was performed using the equation derived from the standard curve, described by a linear regression, which plots known viral concentrations against their corresponding Ct values. Details on the primer sequences can be found in Table 9, and the qPCR template protocol for RNA, miRNA, and DNA analysis in Table 8. qPCR data were analyzed using QuatStudio™ Design & Analysis and the $\Delta\Delta C_T$ method described by (Livak 2001) in Excel.

Table 8| Real-time qPCR protocols used in this study.

Step	***Temperature***	***Time***	***Repeats***
mRNA analysis			
Initial denaturation	95°C	10 min	1x
Denaturation	95°C	15 s	40x
Annealing and Elongation	60°C	1 min	
Melting curve program			
miRNA analysis			
Initial denaturation	95°C	20 s	1x
Denaturation	95°C	3 s	40x
Annealing and Elongation	60°C	30 s	
DNA analysis			
Initial denaturation	95°C	10 min	1x
Denaturation	95°C	10 s	45x
Annealing	60°C	20 s	
Elongation	72°C	20 s	
Melting curve program			

Table 9| Primer sequences used in this study.

Gene	***Abbreviation***	***Sequence***
Actin beta	Actb	F: GGCTGTATTCCCCTCCATCG R: CCAGTTGGTAACAATGCCATGT
B cell leukaemia/lymphoma 2	Bcl2	F: ATGCCTTTGTGGAACTATATGGC R: GGTATGCACCCAGAGTGATGC

Gene	*Abbreviation*	*Sequence*
Carnitine Palmitoyltransferase 1a	Cpt1a	F: CTCCGCCTGAGCCATGAAG R: CACCAGTGATGATGCCATTCT
CD5 antigen-like	CD5L	F: GATCGTGTTTTTCAGAGTCTCCA R: TGCAGTCAACCCCTTGAATAAG
Collagen type I, alpha 1	Col1a1	F: GCTCCTCTTAGGGGCCACT R: CCACGTCTCACCATTGGGG
CREB regulated transcription coactivator 1	Crct1	F: TGCCCAACGTGAACCAGATT R: CCCATGATGTCGTGTGGTCC
Deiodinase type I	Dio1	F: GCTGAAGCGGCTTGTGATATT R: GTTGTCAGGGGCGAATCGG
E74-like factor 3	Elf3	F: GCTGCCACCTGTGAGATCAG R: GTGCCAAAGGTAGTCGGAGG
Fatty Acid Synthase	Fasn	F: GGAGGTGGTGATAGCCGGTAT R: TGGGTAATCCATAGAGCCCAG
Fibroblast Growth Factor 21	Fgf21	F: GCTGCTGGAGGACGGTTACA R: CACAGGTCCCCAGGATGTTG
Forkhead box P1	Foxp1	F: GGTCTGAGACAAAAAGTAACGGA R: CGCACTCTAGTAAGTGGTTGC
GLIS family zinc finger 2	Glis2	F: GACGAGCCCCTCGACCTAA R: AGCTCTCGATGCAAAGCATGA
Glucose transporter 2	Glut2	F: TCAGAAGACAAGATCACCGGA R: GCTGGTGTGACTGTAAGTGGG
Hypoxanthine Phosphoribosyltransferase	Hprt	F: GCAGTACAGCCCCAAAATGG R: AACAAAGTCTGGCCTGTATCCAA
Insulin-like growth factor 1	Igf1	F: CTGGACCAGAGACCCTTTGC R: GGACGGGGACTTCTGAGTCTT
Insulin-like growth factor 1 receptor	Igf1r	F: CTTCTACAACTACGCACTGGTC R: TCGGCGTTCTTCTCAATCCTG
Interleukin 1 beta	IL1b	F: TATCACTCATTGTGGCTGTGGA R: CATCTCGGAGCCTGTAGTGC
Interleukin 10	IL10	F: ATGCAGGACTTTAAGGGTTACTTG R: TAGACACCTTGGTCTTGGAGCTTA
Interleukin 6	IL6	F: GCTACCAAACTGGATA- R: TAATCAGGA CCAGGTAGCTATGGTACTCCAGA
Krüppel-like factor 9	Klf9	F: TTATTGCACGCTGGTCACTATC R: CTCATCGGGACTCTCCAGAC
Malic enzyme 1, NADP(+)-dependent, cytosolic	Me1	F: GAAAGAGGTGTTTGCCCATGA R: AATTGCAGCAACTCCTATGAGG
Peptidylprolyl isomerase A	Ppia	F: GAGCTGTTTGCAGACAAAGTTC R: CCCTGGCACATGAATCCTGG

Gene	*Abbreviation*	*Sequence*
Peptidylprolyl isomerase D	Ppid	F: TCACAACAGTTCCGACTCCTC R: ACCTCTACATTTTCAAGCGTCC
Peroxisome proliferator activated receptor gamma	PPARγ	F: TCGCTGATGCACTGCCTATG R: GAGAGGTCCACAGAGCTGATT
Peroxisome proliferator-activated receptor alpha	PPARα	F: AGAGCCCCATCTGTCCTCTC R: ACTGGTAGTCTGCAAAACCAAA
Phosphate cytidylyltransferase 1, choline, beta isoform	Pyct1b	F: GTCACGCAAGGGCACTTATG R: GAGTAAGGTCATCACTGCAAACT
Ribosomal protein lateral stalk subunit P0	Rplp0	F: TCGGGTCCTAGACCAGTGTTC R: AGATTCGGGATATGCTGTTGGC
Sirtuin 1	Sirt1	F: GCTGACGACTTCGACGACG R: TCGGTCAACAGGAGGTTGTCT
Suppressor of cytokine signaling 3	Socs3	F: GGGTGGCAAAGAAAAGGAG R: GTTGAGCGTCAAGACCCAGT
Thyroid hormone receptor alpha 1	Thra	F: GTGACTGACCTCCGCATGAT R: ATCCTCAAAGACCTCCAGGAA
Thyroid hormone receptor beta 1	Thrb1	F: ACACCTTATCCAGGCCACTT R: GTGGTACCCTGTGGCTTTGT
Thyroid hormone responsive	Thrsp	F: CCTGCTGACAGTCATGGATCG R: TGGTCCACTTCTACACAGATGC
Transformation related protein 53	p53	F: CTCTCCCCCGCAAAAGAAAAA R: CGGAACATCTCGAAGCGTTTA
Transforming growth factor, beta 1	TGFb	F: CTCCCGTGGCTTCTAGTGC R: GCCTTAGTTTGGACAGGATCTG
Tumor necrosis factor	TNFα	F: TCTCATCAGTTCTATGGCCC R: GGGAGTAGACAAGGTACAAC
Uncoupling protein 1	Ucp1	F: ACTCAGGATTGGCCTCTACG R: CCACACCTCCAGTCATTAAGC
Woodchuck Hepatitis Virus Posttranscriptional Regulatory Element	WPRE	F: ACTGTGTTTGCTGACGCAAC R: CAACACCACGGAATTGTCAG

Serum parameters

Concentrations of serum total T3 and total T4 were quantified using enzyme-linked immunosorbent assay (ELISA) kits (for T3: DNOV053, NovaTec Immundiagnostica GmbH, Germany; for T4: EIA-1781, DRG Diagnostics, Germany). Despite these assays being validated for human samples, they have been demonstrated to yield accurate measurements for mouse samples as well (121,158). Similarly, serum C-peptide 2 levels were assessed using an ELISA kit (EZRMCP2-21K, Sigma-Aldrich, Germany). To determine the levels of hepatic damage and

triglyceride content, serum values of aspartate aminotransferase (AST) and alanine aminotransferase (ALT) and triglycerides were determined using available kits (Sigma-Aldrich, Germany). TSH levels were measured using commercially available kit (Merk Millipore, Germany). All the assays were done following the protocols provided by the manufacturers.

Intrahepatic T3/T4 and DIO1 activity

DIO1 activity assays were conducted in the Charité Universitätsmedizin Berlin by Dr. Eva Wirth following established methods as previously described (159,160). Intrahepatic TH levels were determined using liquid chromatography mass spectrometry by Prof. Dr. Anita Boelen at the Endocrine Laboratory Amsterdam UMC as described previously (161,162).

Glycogen assay

Liver and muscle glycogen content was determined according to manufacturer's instructions (Sigma Aldrich, Germany) in duplicates. To determine the sample concentration, a linear regression of the mean absorbance values of the standard curve against known concentrations provided by the manufacturer was done using GraphPad Prism 9 (GraphPad, USA) software. Then, the linear regression was used to interpolate the sample values on the standard curve, followed by normalization on tissue weight.

Statistical analysis

Data was processed either using GraphPad Prism 9 (GraphPad, USA) or Excel (Microsoft, USA) prior to statistical evaluation. The preprocessing stage involved normalization, outlier testing, and preliminary analysis of the collected data. For statistical analysis, GraphPad Prism 9 was used, and the significances of differences observed between the groups were assessed using appropriate post hoc tests, the details can be found in Supplementary Table S1. Significance levels were set as follows: *p<0.05, **p<0.01, ***p<0.001, ****p<0.0001 for diet or treatment effect; # p<0.05, ##p<0.01, ###p<0.001, ####p<0.0001 for genotype or time effect when corresponds. Data are reported as mean ± SD (standard deviation).

Given that main interest of the project was studying the diet and the genotype effects, all timepoints were analysed separately using 2-way ANOVA.

3. RESULTS

3.1. The role of TRβ on MASLD and MASH development and progression

The exact contribution of TRβ in the development and progression of liver diseases is still unknown. Given the strong association between hypothyroidism and metabolic diseases, and research in humans indicating that TRβ declines with the progression of the disease, all together it highlights the importance of local thyroid hormone regulation in liver diseases. Moreover, scientific evidence involving the recent approved drug resmetirom, a liver-specific thyromimetic with high affinity for TRβ, proved to be beneficial for the pathogenesis of MASLD and MASH. Together it supports support the idea of using TRs as potential therapeutic target for MASLD and MASH (11,15,52). However, the exact mechanism is currently unknown.

To address the role of TRβ in the development and progression of fatty liver diseases, a loss and a gain of function approach were performed.

Loss of TRβ function in mice models of MASLD and MASH

WT and TRβ knockout (TRβ -/-) mice were studied using a novel fast paradigm for MASLD and MASH at thermoneutrality for 4, 8 or 16 weeks. Thermoneutrality housing (30 ± 2°C) during the whole experiment was employed to reduce the heightened metabolism observed by the ongoing cold stress at room temperature (163–165). This approach allows to resemble better the human autonomic innervation (164,166) and it revokes the usual hyperthyroidism observed in TRβ-/- mice (131) while allowing a faster progression of the disease (167,168). Moreover, the mice were subjected to either a control diet (Control) or a choline-deficient high-fat diet (CD-HFD) to develop MASLD or MASH respectively (Figure 4A). Altogether, this animal model approach allows to study MASLD and MASH without cofounding effects in other organs and ultimately mimicking better the human condition in a fast and practical manner.

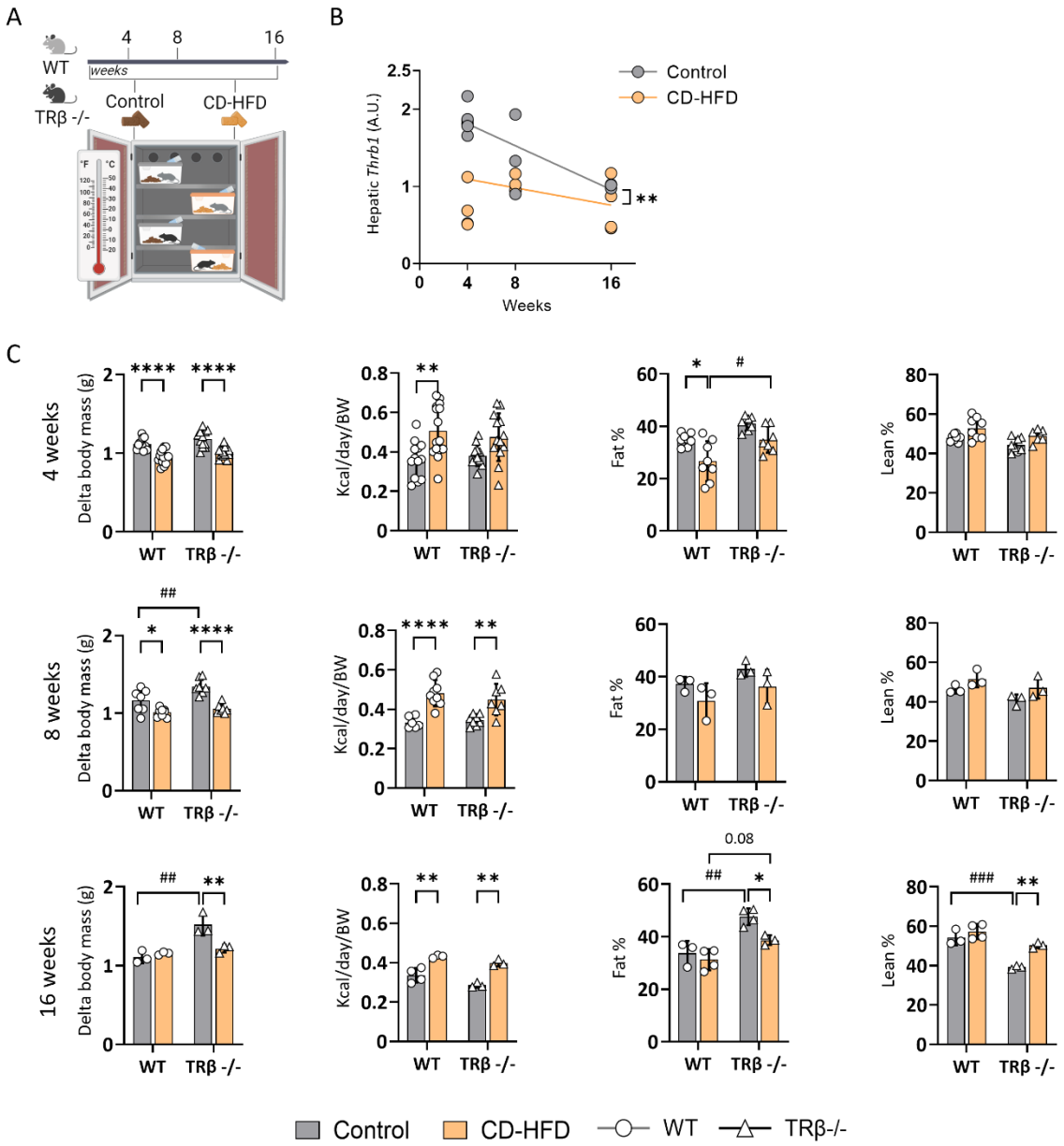

Figure 4 – Impact of MASH diet on TRβ knockout mice. A) Overview experimental design. B) Influence of CD-HFD on hepatic *Thrb1* expression in WT mice. C) Body parameters measured: body weight, food intake and body composition at 4, 8, and 16 weeks of diet. Values are mean ± SD, *: p<0.05; **: p<0.01; ***: p<0.001 for Control vs CD-HFD; #: p<0.05; ##: p<0.01; ###: p<0.001 for WT vs TRβ knockout (2-way ANOVA with Tukey's or Šídák's multiple comparison test, see Table S1).

Diet and genotype influence on body parameters and liver damage

The mice were analysed at 4, 8 and 16 weeks. Concomitant with observations in humans, WT mice showed initially an elevated *Thrb1* gene expression in early MASLD with a peak at 4 weeks which declined over time. A similar trend was observed in mice subjected to a CD-HFD although with a basal lower level of *Thrb1* expression, replicating the observations in the human MASH cohort (11) (Figure 4B).

Across all the groups, CD-HFD feeding resulted in slower body weight gain despite increased daily food intake, and reduced fat mass percentage compared to the controls (Figure 4C). This observation aligns with the existing literature on the use of this diet in other mouse studies (169). Notably, despite having similar starting body weight values across the groups (data not shown), WT mice displayed an average lower baseline fat mass at 4 weeks compared to TRβ-/- in the MASH cohort. Interestingly, at 16 weeks these differences became apparent also in the MASLD cohort, probably due to cumulative metabolic alterations that surpass the liver's compensatory capacity. Importantly, in both dietary groups the fat mass was higher than the 17-19% usually observed in wild type male mice on chow diet at room temperature (170).

Liver damage assessment was conducted through histological examination of H&E staining and biochemical measurement of serum transaminases ALT and AST (Figure 5).

Histological analysis revealed common indicators of liver injury in all the groups which became more pronounced with the increase disease severity. However, no clear differences between the genotypes were observed. Control-fed mice were presented with microsteatosis at 4 weeks, evolving into macrosteatosis along with hepatocyte-nuclear displacement to the periphery of the cell due to the enlargement of the lipid droplets by 8 weeks, which became more apparent at 16 weeks along with occasional immune cell infiltration. These observations are characteristic of MASLD pathology. On the other hand, CD-HFD fed animals exhibited a greater degree of lipid accumulation at 4 weeks characterized by both macro and microsteatosis, along with first signs of hepatocellular ballooning and nuclear displacement which were more pronounced across the weeks. Signs of immune cell infiltration were noticeable at 8 weeks and became marked by 16 weeks. These observations are characteristic of MASH.

Notably, TRβ -/- mice displayed a distinctive zonation pattern with reduced lipid deposition around the central vein (CV) in early MASLD contrary to the usual hepatic lipid accumulation pattern (Figure 21).

Observations for ALT and AST were consistent with the histology data. A marked elevation in serum transaminases was noted in the CD-HFD group, indicating a more pronounced severity of the phenotype. Importantly, no genotype differences were detected for ALT,

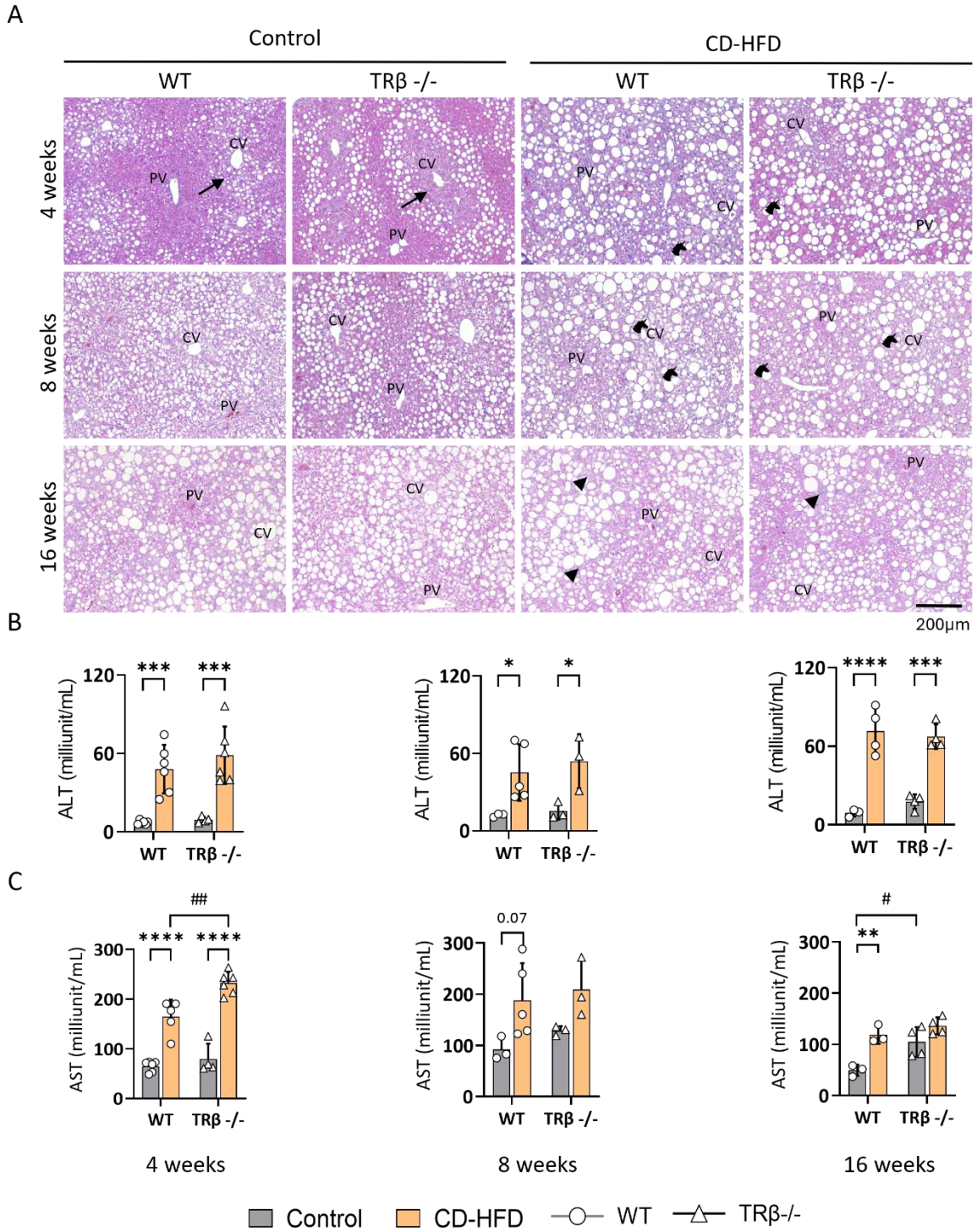

Figure 5 – Liver damage of MASH diet on TRβ knockout mice. A) Haematoxylin and eosin (H&E) staining of WT and TRβ knockout mice fed with Control or CD-HFD for 4, 8, and 16 weeks. Central vein (CV); Portal vein (PV). Arrows point to lipid deposition zonation between genotypes. Unicorn heads indicate ballooning. Arrowheads point to immune cell infiltration. Scale bar reflects 200µm. B-C) Serum levels of (B) alanine transaminase (ALT) and (C) aspartate transaminase (AST) in these mice. Values are mean ± SD, *: p<0.05; ***: p<0.001; ****: p<0.0001 for control vs CD-HFD. #: p<0.05; ##: p<0.01 for WT vs TRβ knockout (2-way ANOVA with Tukey's or Šídák's multiple comparison test, see Table S1).

considered a more reliable liver-specific biomarker, whereas AST was noted to be elevated in early MASH and late MASLD in mice lacking TRβ. These differences could be partially explained by the degree of liver damage which coincides with the first signs of inflammation and fibrotic gene expression markers (Figure 5B). Additionally, AST is known for its broader tissue distribution, as is present in all the tissues except bone.

Hepatic lipid response to dietary interventions in WT and TRß-/- mice

To investigate the combined effects of diet and genotype on disease progression, analysis of lipid accumulation and TGA content were carried out in the mice livers (Figure 6A-C).

Lipid accumulation was assessed in histology using ORO staining (Figure 6A-B). This staining target neutral lipids and lipoproteins allowing the visualization of the fat droplets in red within the cells. Analysis of the pictures showed that all the groups displayed more than the 5% of lipid accumulation, threshold for the diagnosis of steatosis in MASLD (171).

In line with previous results and with the nature of the model, the percentage of ORO positive area was higher in mice fed with CD-HFD but surprisingly it was comparable for both genotypes across the experiment. Likewise, no differences were observed in the MASLD cohort mice.

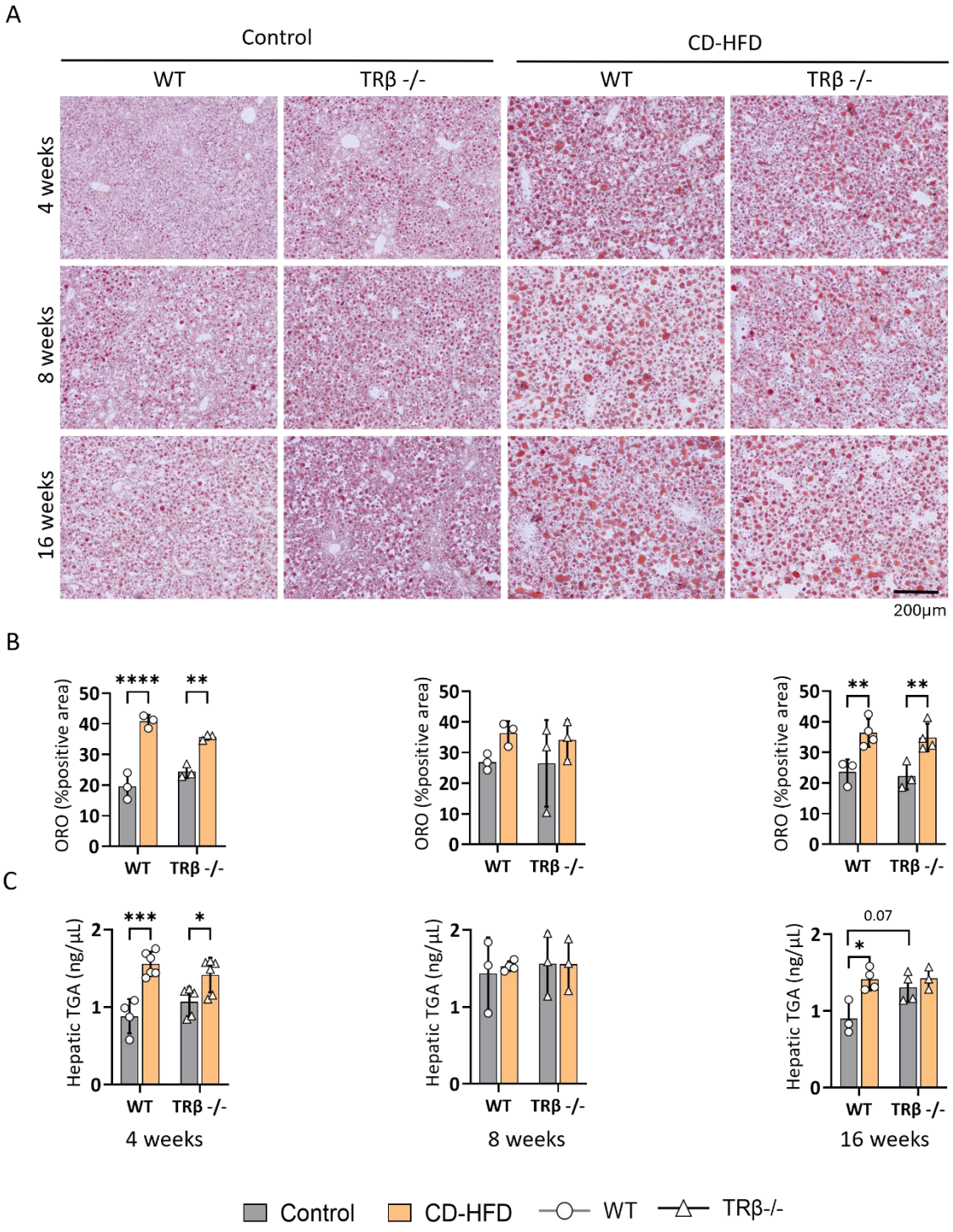

Figure 6 – Hepatic lipid response to MASH diet on TRβ knockout mice. A) Oil Red O (ORO) staining of WT and TRβ knockout mice at 4, 8, and 16 weeks of Control or CD-HFD diet. Fat droplets in red. Scale bar equals to 200µm. B) Quantification of ORO positive area. C) Hepatic triglyceride (TGA) content in these mice. Values are mean ± SD, *: p<0.05; ***: p<0.001; ****: p<0.0001 for control vs CD-HFD. (2-way ANOVA with Tukey's or Šídák's multiple comparison test, see Table S1).

Fibrosis and inflammation markers in MASH

Fibrosis assessed using SR staining showed that control diet fed mice did not develop fibrosis despite the aggravating steatosis (Figure 7A-B). This observation along with the mild liver damage observed in the biochemical and histological assessment, are typical features of MASLD. Likewise, the study of hepatic gene expression and MASH score assessment showed normal values on fibrotic genes throughout the experiment, and normal inflammatory markers in early MASLD that progressively rose by 16 weeks, consistent with the increased liver damage (Figure 8).

Surprisingly, despite no clear genotype-driven differences in lipid accumulation were seen, fibrosis staining highlighted a genotype effect, where TRβ -/- mice fed with CD-HFD exhibited less fibrosis nearly reaching statistical significance at week 16 (P=0.06) (Figure 7A-B). Gene expression analyses confirmed reduced levels of *Col1α1* and *Elf3*, genes directly involved in fibrosis. COL1A1 is the main component of fibrotic fibres and *Elf3* is involved in hepatocyte reprogramming and intra-hepatic communication during liver fibrosis. Also, reduced levels of *TNFα* and *IL6* were found in TRβ -/- MASH mice, two important gene markers for inflammation (Figure 8).

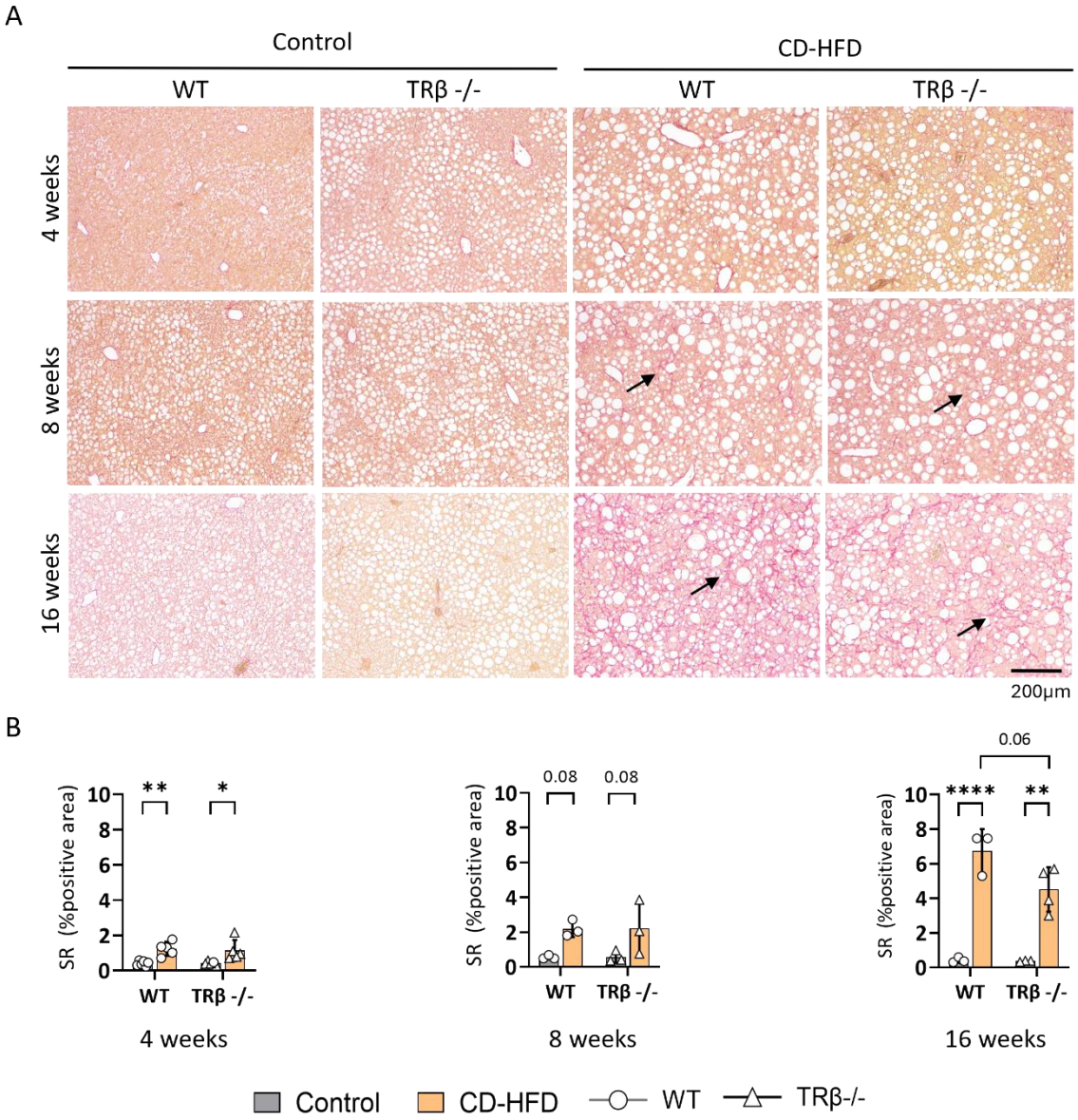

Figure 7 – Hepatic fibrosis in MASH TRβ knockout mice. A) Sirius Red (SR) staining in WT or TRβ knockout mice fed with either Control or CD-HFD at 4, 8 or 16 weeks. Collagen fibres in magenta B) SR staining quantification as percentage of positive area. Values are mean ± SD, *: p<0.05; ***: p<0.001; ****: p<0.0001 for control vs CD-HFD, #: p<0.05; ##: p<0.01 for WT vs TRβ knock-out (2-way ANOVA with Tukey's or Šídák's multiple comparison test, see Table S1).

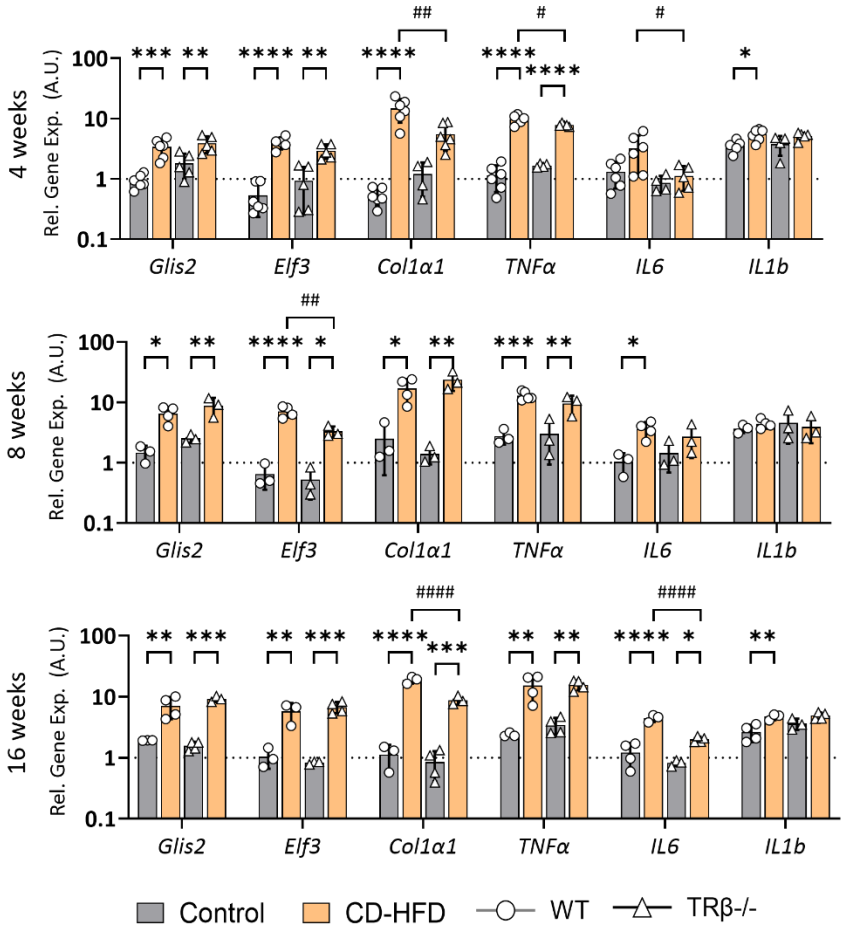

Figure 8 – Inflammation markers in MASH liver of TRβ knockout mice. Hepatic relative gene expression of fibrosis and inflammatory markers in these mice. Y axis scale as log 10. Values are mean ± SD, *: p<0.05; ***: p<0.001; ****: p<0.0001 for control vs CD-HFD, #: p<0.05; ##: p<0.01 for WT vs TRβ knockout (2-way ANOVA with Tukey's or Šídák's multiple comparison test, see Table S1).

Thyroid hormone levels and response in MASLD and MASH mice at thermoneutrality

Within the thermoneutral environment, the usual hyperthyroidism observed in the TRβ-/- mice at room temperature was partially rescued (Figure 9A). Moreover, serum levels of total T3 (tT3) and total T4 (tT4) in the MASLD and MASH cohorts at 30°C were comparable, with variations on genotype raising after 8 and 16 weeks (Figure 9A). Nonetheless, the observed differences did not exceed the 75% difference noted between WT and TRβ-/- at room temperature (131), together with the absence of genotype-driven differences in any TH- responsive genes across the cohorts studied (Figure 11). To decipher the effect of thermoneutrality on TH

levels in these mice, a comparison between WT and TRβ-/- mice housed at 22°C versus 30°C for at least 4 weeks was carried out. The results reveal that, despite the persistent high levels of TSH in the serum of TRβ-/- mice regardless of the temperature, expression levels of *TSHb* and *Trhr1* in the pituitary were reduced at 30°C (Figure 10A-C). These findings indicate that the overactive HPT axis in the TRβ-/- mice is diminished at thermoneutrality (131).

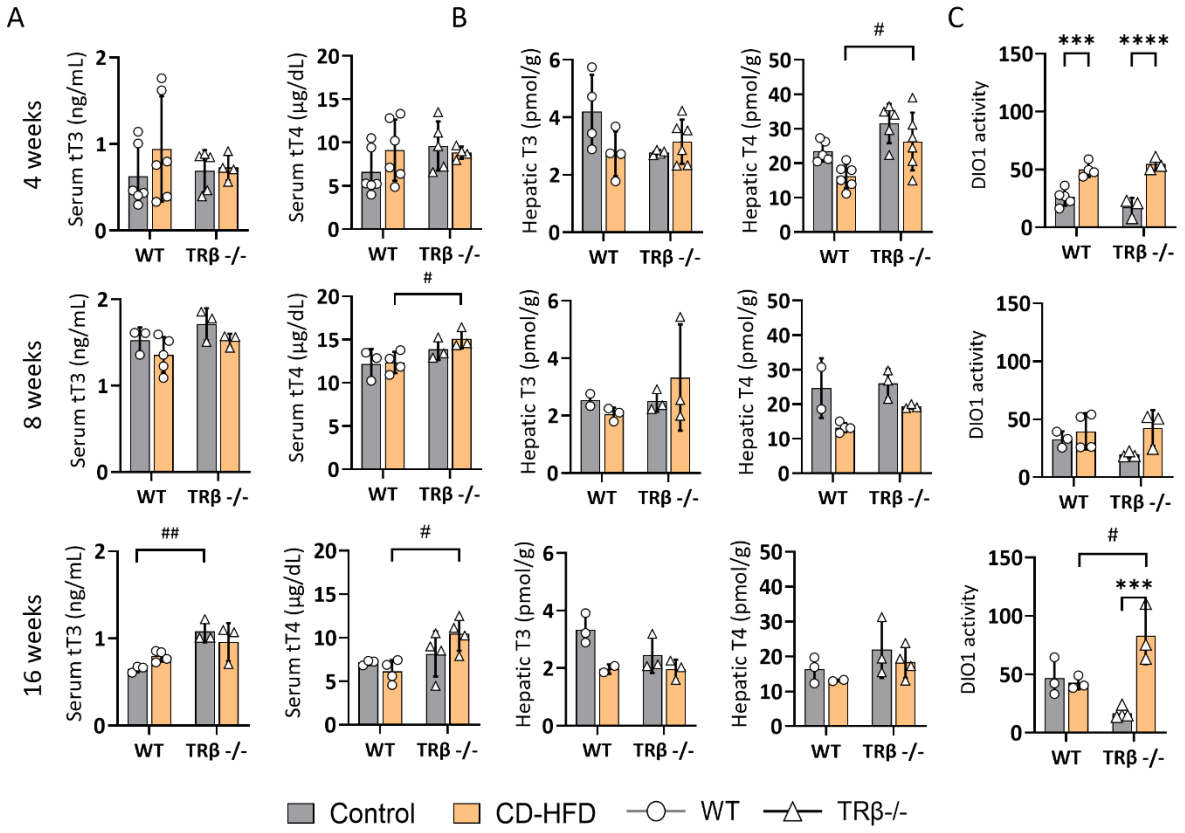

Figure 9 – Thyroid hormone status in TRβ knockout mice at thermoneutrality. A) Serum levels of total T3 and T4. B) Intrahepatic levels of T3 and T4 measured by mass spectrometry. C) DIO1 enzymatic activity. Values are mean ± SD, *: p<0.05; ***: p<0.001; ****: p<0.0001 for control vs CD-HFD, #: p<0.05; ##: p<0.01 for WT vs TRβ knockout (2-way ANOVA with Tukey's or Šídák's multiple comparison test, see Table S1).

Hepatic TH levels pattern differed from those of serum levels, underscoring the differences between tissue-specific and systemic regulation of TH (Figure 9B). Interestingly, albeit not significant, serum tT4 concentrations were when not comparable, slightly elevated, in mice fed with CD-HFD versus a control diet (Figure 9A). However, hepatic T4 levels were consistently lower in mice subjected to CD-HFD (Figure 9B). Additionally, hepatic DIO1 activity was elevated in these mice (Figure 9C).

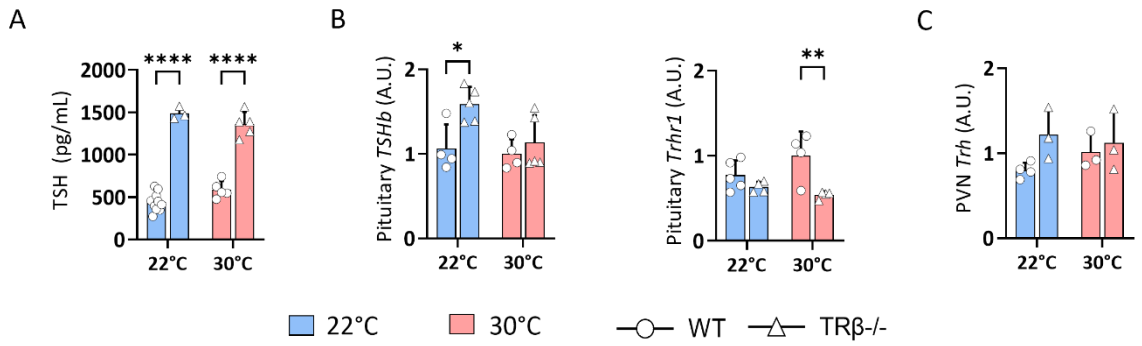

Figure 10 – Thyroid hormone status in TRβ knockout mice at RT and thermoneutrality. A) Serum values of WT mice thyroid-stimulating hormone (TSH) at 22°C and 30°C. B) Pituitary relative gene expression of these mice. C) Paraventricular nucleus of hypothalamus (PVN) relative gene expression of these mice. Values are mean ± SD, *: p<0.05; ***: p<0.001; ****: p<0.0001 for WT vs TRβ knockout (2-way ANOVA with Tukey's or Šídák's multiple comparison test, see Table S1).

Further analysis into thyroid hormone response genes (Figure 11) revealed a significant increase in the expression of *Thrsp,* particularly in MASLD in contrast to MASH mice on a CD-HFD. The reduced hepatic *Thrsp* is expected in high-fat diets, where lipid intake is the main source of energy, and partially due to lower levels of intrahepatic TH or lack of TRβ. Additionally, downregulation of the Krüppel-like factor 9 (*Klf9*) was observed in the MASH cohort which became significant in both genotypes at 16 weeks.

Surprisingly, *Dio1,* the gene encoding the DIO1 enzyme, a key regulator of local thyroid hormone control, was found to be elevated in all dietary and genotypic conditions, except in Control-fed TRβ-/-, where it remained stable yet reduced (Figure 11). The expression of *Dio1* varied significantly, displaying a strong diet-dependent response, and to a lesser extent by genotype. Nevertheless, although *Dio1* showed to be diet-dependent, and to a lesser extent genotype responsive, the gene expression was not concomitant with the enzymatic activity or intrahepatic levels of THs. These observations possibly point out to posttranscriptional mechanisms influenced by dietary changes.

In conclusion, the experimental outcomes demonstrate that TRβ exerts a variable influence on MASLD and MASH. TRβ slightly enhances lipid metabolism in the liver, while it has a

negative impact in fibrosis and inflammation. Together it suggests that TRβ's role is beneficial at early and mild MASLD, concomitant with the literature. However, it might contribute negatively at more severe disease stages by promoting inflammation and fibrosis.

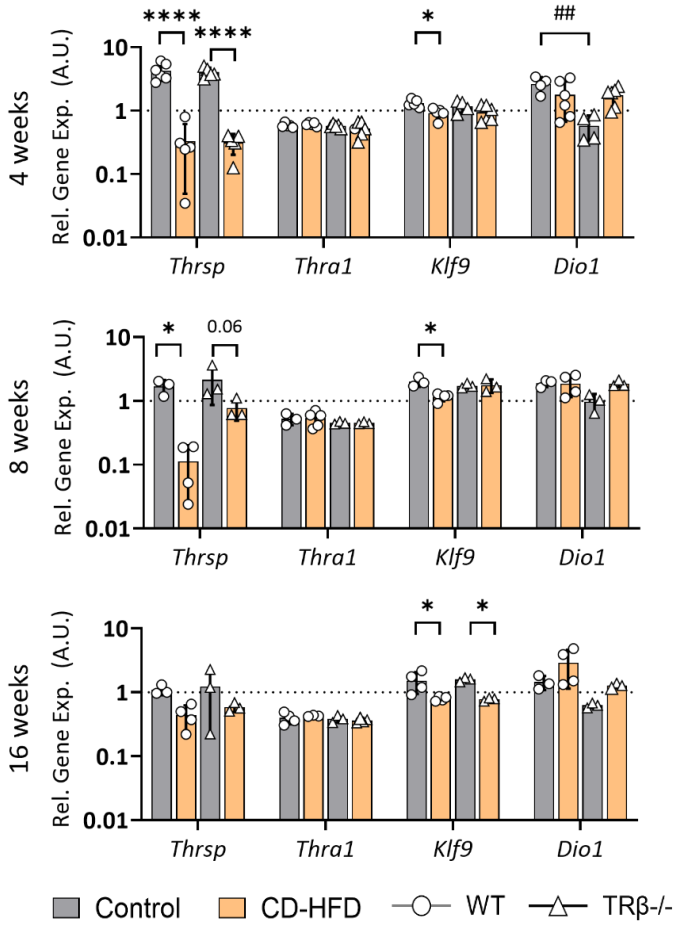

Figure 11 – Hepatic TH responsive genes in TRβ knockout mice. Relative gene expression at 4, 8, and 16 weeks. Y axis as log10. Values are mean ± SD, *: p<0.05; ***: p<0.001; ****: p<0.0001 for control vs CD-HFD, #: p<0.05; ##: p<0.01 for WT vs TRβ knockout (2-way ANOVA with Tukey's or Šídák's multiple comparison test, see Table S1).

Gain of TRβ function in mice models of MASLD and MASH

To investigate whether preventing the decline of *Thrb1* during MASH progression in hepatocytes would exert beneficial effects, an overexpression strategy using AAV was employed. WT mice on CD-HFD at thermoneutrality for 2 weeks were administered with AAV containing *Thrb1* (AAV-Thrb) or *mCherry* (Control), while maintaining housing and dietary conditions. Hepatocyte-specific expression was ensured using AAV serotype 8 (AAV8), which has high

hepatocytes affinity (172), under the hepatocyte specific human promoter TBG (153,154)(Figure 12A).

Thrb1 expression analysis indicated a successful 2-fold increase in the liver of AAV-Thrb mice relative to controls, while no upregulation was found in other organs (Figure 12B). The efficacy of viral transduction was verified by qPCR of the WPRE element, present in the viral construct genome, and mCherry staining (Figure 12C-D), showing high viral DNA copy numbers in the liver.

Measurements of body parameters including body weight gain, food intake, body composition (Figure 12E), liver weight/body weight ratio (LW/BW) (Figure 12F) or energy expenditure (Figure 12H-I) revealed no significant differences between AAV-Thrb and controls. Furthermore, glucose and insulin tolerance tests (GTT, ITT) showed no disparities in glucose metabolism between the groups. Histological analysis revealed micro-, macro- steatosis with signs of hepatocellular ballooning and nuclear displacement in both groups (Figure 8J). However, no notable differences in fibrosis or inflammation in histology were observed, which might be attributed to the early disease stage at six weeks post-diet start. No significant change in gene expression of MASH score marker genes were observed (Figure 12N), but a tendency to increased fibrosis and inflammation markers was observed in AAV-Thrb mice.

Lastly, no variations in the ratio T3/T4 or individual values of T3 and T4 values (data not shown) were detected between the groups.

Overall, these findings demonstrate the complex role of TRβ in liver diseases, showing both protective and detrimental effects depending on the stage of disease progression and the metabolic context.

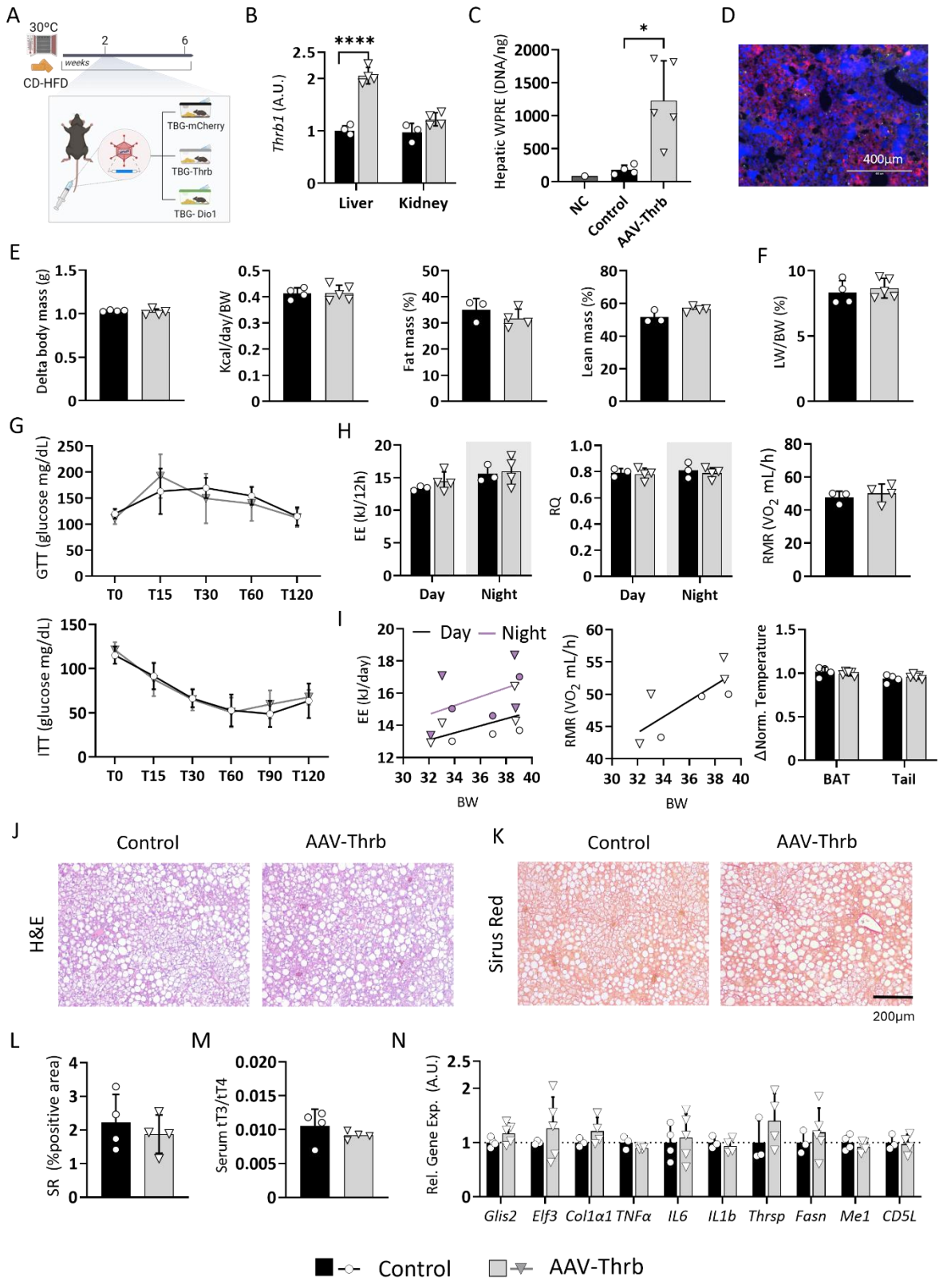
A
30°C
2
6
weeks
CD-HFD
TBG-mCherry
TBG-Thrb
TBG- Dio1
B
Thrb1 (A.U.)
****
Liver
Kidney
C
Hepatic WPRE (DNA/ng)
*
NC
Control
AAV-Thrb
D
400µm
E
Delta body mass (g)
Kcal/day/BW
Fat mass (%)
Lean mass (%)
F
LW/BW (%)
G
GTT (glucose mg/dL)
T0
T15
T30
T60
T120
ITT (glucose mg/dL)
T90
H
EE (kJ/12h)
Day
Night
RQ
RMR (VO2 mL/h)
I
EE (kJ/day)
BW
RMR (VO2 mL/h)
ΔNorm. Temperature
BAT
Tail
J
Control
AAV-Thrb
H&E
K
Sirus Red
200µm
L
SR (%positive area)
M
Serum tT3/tT4
N
Rel. Gene Exp. (A.U.)
Glis2
Elf3
Col1α1
TNFα
IL6
IL1b
Thrsp
Fasn
Me1
CD5L
Control
AAV-Thrb

Figure 12 – Effect of MASH in TRβ overexpressing mice. A) Experimental design overview. B) Relative gene expression of *Thrb1* in liver and kidney of WT and AAV-Thrb mice fed with CD-HFD. C) Hepatic transgenic copies measured by WPRE. D) *mCherry* staining of WT control mice. Scale bar reflects 400µm. E) Body parameters including body weight gain, food intake, and body composition. F) Liver/Body weight ratio. G) Glucose (top) and insulin (bottom) tolerance test. H) Calorimetry measurements as energy expenditure (EE); respiratory quotient (RQ), resting metabolic rate (RMR). I) EE and RMR versus BW; Body temperature measured by IR pictures. BAT and Tail temperature normalized to inner ear. J) Haematoxylin and eosin (H&E) staining. K-L) Sirius Red (SR) (K) staining (L) quantification as percentage of positive area. Scale bar at 200µm. M) Serum levels of THs. N) Hepatic relative expression of MASH score genes. Values are mean ± SD, *: $p<0.05$; ***: $p<0.001$; ****: $p<0.0001$ for Control vs AAV-Thrb (Un-paired Student's test or 2-way ANOVA with Šídák's post hoc test, see Table S1).

3.2. *In vitro* pharmacological modulation of *Thrb1* and *Dio1*

Given the complex pathophysiological changes occurring in MASLD and MASH, *in vitro* studies on possible single factors affecting *Thrb1* or *Dio1* expression were carried out in PMH. The selection of drugs or reagents was based on their association with MASLD, MASH, risk factors or comorbidities of these liver diseases and their relevant use in the clinic (Table 10).

PMH were isolated from WT mice as outlined in the Methods section. The hepatocytes were then exposed to different pharmacological compounds and the expression of *Thrb1* and *Dio1* levels were determined using qPCR.

The results indicated that *Thrb1* expression levels were significantly increased following a 48-hour stimulation with fatty acids, whereas it was reduced upon simvastatin (10µM) treatment for 24h (Figure 13A). While T3 stimulation did not alter *Thrb1*, *Dio1* was elevated after 48-hours of stimulation with 1nM, a concentration within the range of physiological conditions (Figure 13B). No significant changes in gene expression were noted besides those previously described.

Table 10| Overview of *in vitro* pharmacological treatments used on PMH.

Drug/Component	***Use-case***	***Impact on MASLD/MASH***	***Ref***
T3 (3,5,3'-triiodo-L-thyronine)	Thyroid hormone replacement.	Enhances metabolic rate, increases β-oxidation, may reduce lipid accumulation in hepatocytes.	(60,173)
GC-1 (Sobetirome)	Selective thyroid hormone receptor modulator.	Improves lipid metabolism, reduces cholesterol levels, promotes liver regeneration.	(60)
Fatty acids	Study of lipid metabolism and obesity in cell culture.	Promotes lipid accumulation and steatosis, used to model fatty liver disease.	(174)
Corticosterone	Anti-inflammatory, immunosuppressive drug, model of stress and metabolic syndrome.	Induces insulin resistance, may exacerbate MASLD/MASH pathogenesis.	(175)
Insulin	Diabetes treatment, model of hyperinsulinemia.	Lowers blood glucose, inhibits gluconeogenesis and glycogenolysis.	(176)
High glucose	Model for hyperglycemia and diabetes.	Increases hepatic lipid accumulation.	(177)
Metformin	Type 2 diabetes treatment.	Regulates gluconeogenesis and hepatocyte redox stage, improving insulin sensitivity.	(176)
Simvastatin	Cholesterol-lowering statin. Most common treatment to reduce risk of cardiovascular diseases.	Can induce hepatocellular and cholestatic damage.	(178)

These results underscore the effect of pharmacological interventions, commonly used for the treatment of comorbidities associated with MASLD and MASH, in selectively modulating the gene expression of *Thrb1* and *Dio1*. This modulation offers insights into how these interventions or co-treatments, might influence TH metabolism in the liver, potentially impacting the disease progression.

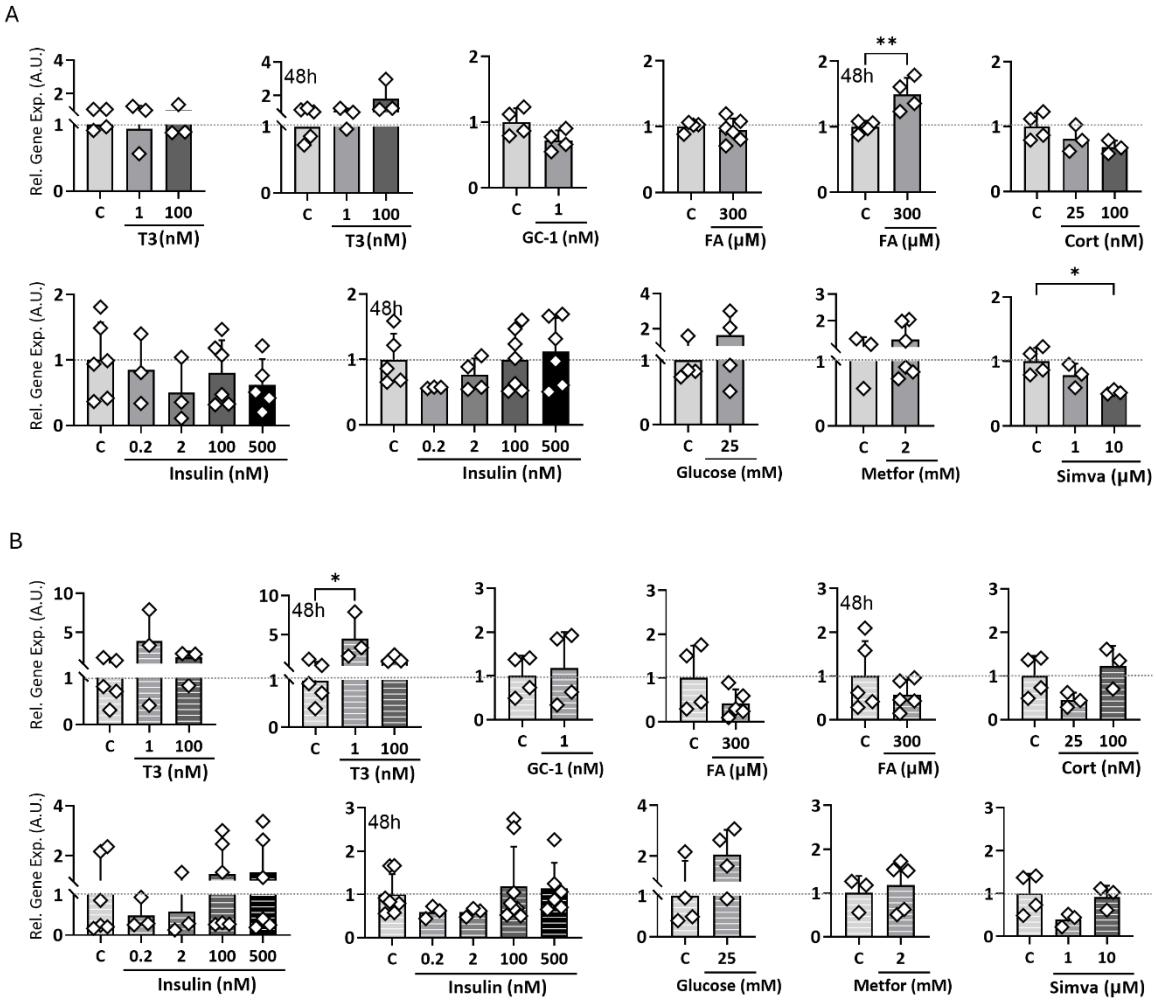

Figure 13 – Effect of pharmacological stimulation of *Thrb1* and *Dio1* in PMH. PMH isolated from WT mice A) *Thrb1* relative gene expression. B) *Dio1* relative gene expression. Values are mean ± SD, *: p<0.05; ***: p<0.001; for treatment effect (Unpaired Student's test or One-Way ANOVA, see Table S1).

3.3. The role of DIO1 on MASLD and MASH development and progression

DIO1 is another master regulator in the control of TH in the liver by converting T4 into T3. Dysfunction of DIO1 could result in local hypothyroidism which is associated to increased risk of MASLD and MASH development. However, the exact alterations and contributions of DIO1 in disease development and progression remain unclear.

To characterize the response of *Dio1* mRNA expression to changing metabolic conditions, liver samples from the study of Geißler et al., carried out in a MASLD mice model housed at room temperature were analyzed (152). In this experiment, WT mice were fed with either chow diet or HFD for up to 18 weeks. Additionally, at 14 and 18 weeks, an extra group receiving HFD was treated with metformin in the drinking water (Figure 14A). The analysis of hepatic gene expression revealed a rapid increase of *Dio1* within the first week of HFD feeding (Figure 14B). Despite the progressive declining expression of *Dio1* by age in all mice (11,179), this decline was more pronounced in the MASLD cohort, which is primarily attributable to the initial upregulation. Remarkedly, throughout the duration of the study, *Dio1* levels in the MASLD mice persisted elevated to those of the control group (Figure 14C). Interestingly, histology analysis revealed no visible features of fatty liver in mice fed with HFD before 4 weeks of diet. Even then, only minor microsteatosis was observed (Figure 14G). This finding indicates that *Dio1* induction precedes pathological changes within the tissue and further supports the observations of a diet-response effect.

For comparison with previous research conducted at room temperature compared to thermoneutrality, data from WT mice of both MASLD and MASH studies were plotted in graphs. As observed before, in all dietary intervention groups (Control or CD-HFD), there was an increase *Dio1* expression versus chow-fed mice. Notably, while statistical significance was only achieved at 4-weeks in the early MASLD group, a consistent trend toward elevated *Dio1* expression was evident across all the groups, potentially obscured by the limited sample size (Figure 9D). In alignment with prior results, hepatic DIO1 enzymatic activity did not correlate with gene expression levels in the MASLD or MASH groups (Figure 9E-F) at room or at thermoneutrality; yet, a notable correlation was observed within chow-fed mice, indicating that this discrepancy is a result of dietary changes, or the dysregulation induced by the liver disease

(Figure 9F). Together it suggests that the control of DIO1, and therefore TH, might be affected by posttranscriptional mechanisms, underscoring the complexity of the system during liver

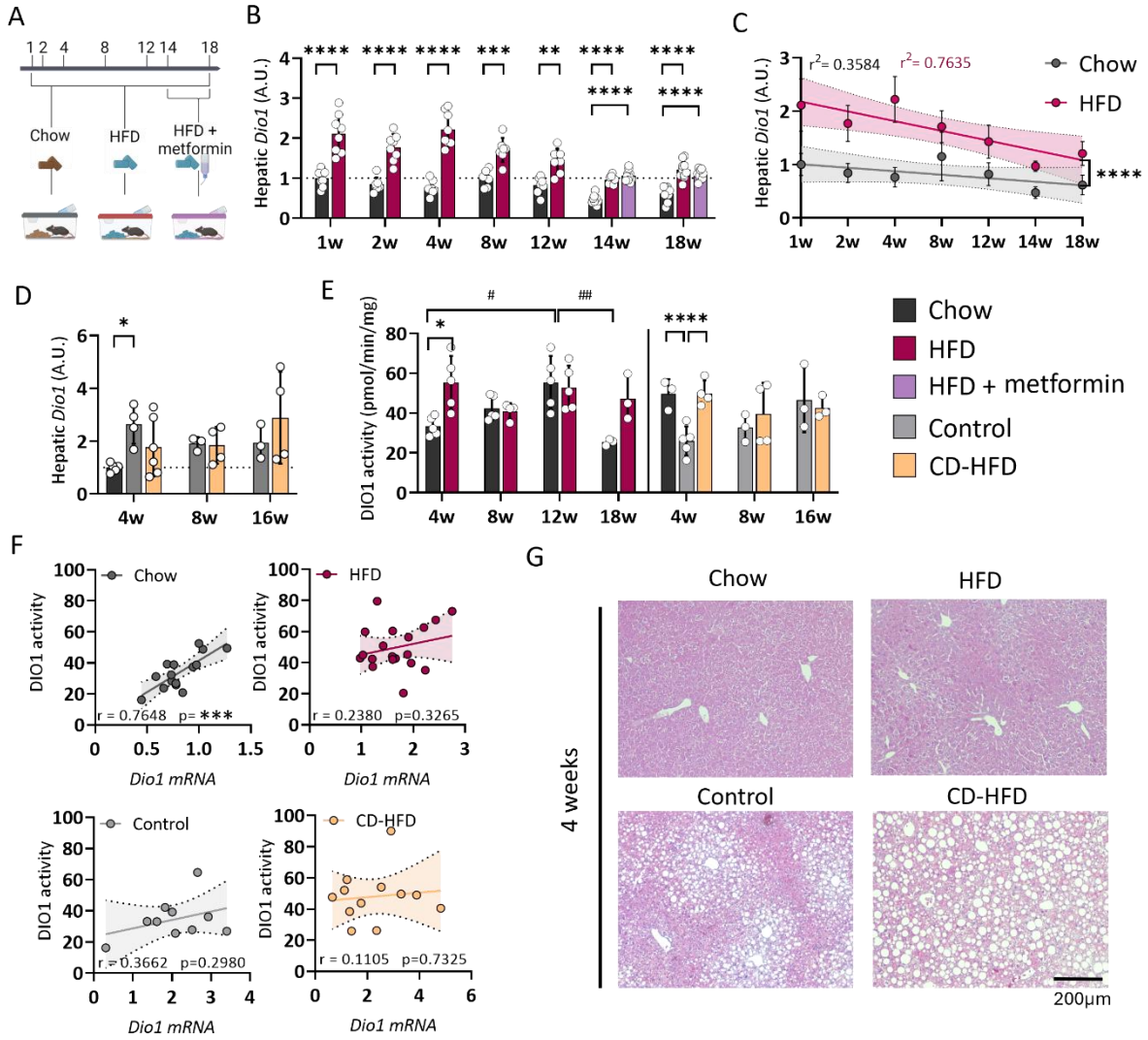

Figure 14 – DIO1 status in MASLD and MASH mice at different housing conditions. A) Animal model design. B) Hepatic *Dio1* relative gene expression in WT mice fed with chow or HFD for 1 to 18 weeks at room temperature. C) Hepatic *Dio1* expression across time. D) Liver *Dio1* expression in WT mice fed with Control or CD-HFD at thermoneutrality for 4, 8 and 16 weeks. E) DIO1 enzymatic activity in these animals. F) DIO1 activity correlation with *Dio1* mRNA expression. G) Haematoxylin and eosin staining of each of the models. Scale bar represents 200µm. Values are mean ± SD, *: p<0.05; ***: p<0.001; ****: p<0.0001 for diet effect; #: p<0.05 for time effect (Unpaired Student's test, One-way ANOVA or 2-way ANOVA with Tukey's post hoc test, see Table S1)

diseases.

Effect of Dio1 upregulation in MASH

To investigate the potential benefits of *Dio1* overexpression in early MASH, mice were treated with AAV8 with *Dio1* (AAV-Dio1) or *mCherry* (Control), driven by the TBG promoter as detailed in the methods section while maintained at thermoneutrality (Figure 12A). To confirm successful transfection, qPCR of the viral WPRE element was carried out revealing high viral DNA copies in the AAV-Dio1 mice (Figure 15B). Despite the lack of an increased hepatic *Dio1* mRNA expression, mice receiving AAV-Dio1 displayed elevated DIO1 enzymatic activity in the liver (Figure 15A,C). This discrepancy between gene expression and enzymatic activity was unexpected and suggest that post-transcriptional mechanisms might play a role.

Contrary to expectations, the increased DIO1 activity did not translate into elevated hepatic T3 (Figure 15N) in MASH mice. Despite comparable values of hepatic T3 and T4 between groups, the slightly decrease in T3 and an increase in T4 observed in the AAV-Dio1 group resulted in statistically significant lower T3/T4 ratio. These subtle differences did not significantly impact the expression of TH-responsive genes (Figure 15L).

Comprehensive analysis of body parameters including body weight gain, food intake, fat mass, lean mass, and the ratio LW/BW revealed no differences between control and AAV-Dio1 mice (Figure 15D-E). Similarly, assessment of glucose metabolism and energy expenditure at thermoneutrality was comparable in both groups (Figure 15F-H). Histological analysis of the liver confirmed similar degree of lipid accumulation (Figure 15I), with only a marginal reduction in fibrosis in the AAV-Dio1 mice that was not significant for the timeframe of the experiment (Figure 15J-K). Notably, no genetic markers commonly associated with fibrosis or MASH score differ between the groups, except for TNFα levels which were reduced after *Dio1* gene therapy (Figure 15L). Together these results suggest a potential anti-inflammatory effect of *Dio1* overexpression that did not translate into broad metabolic improvements.

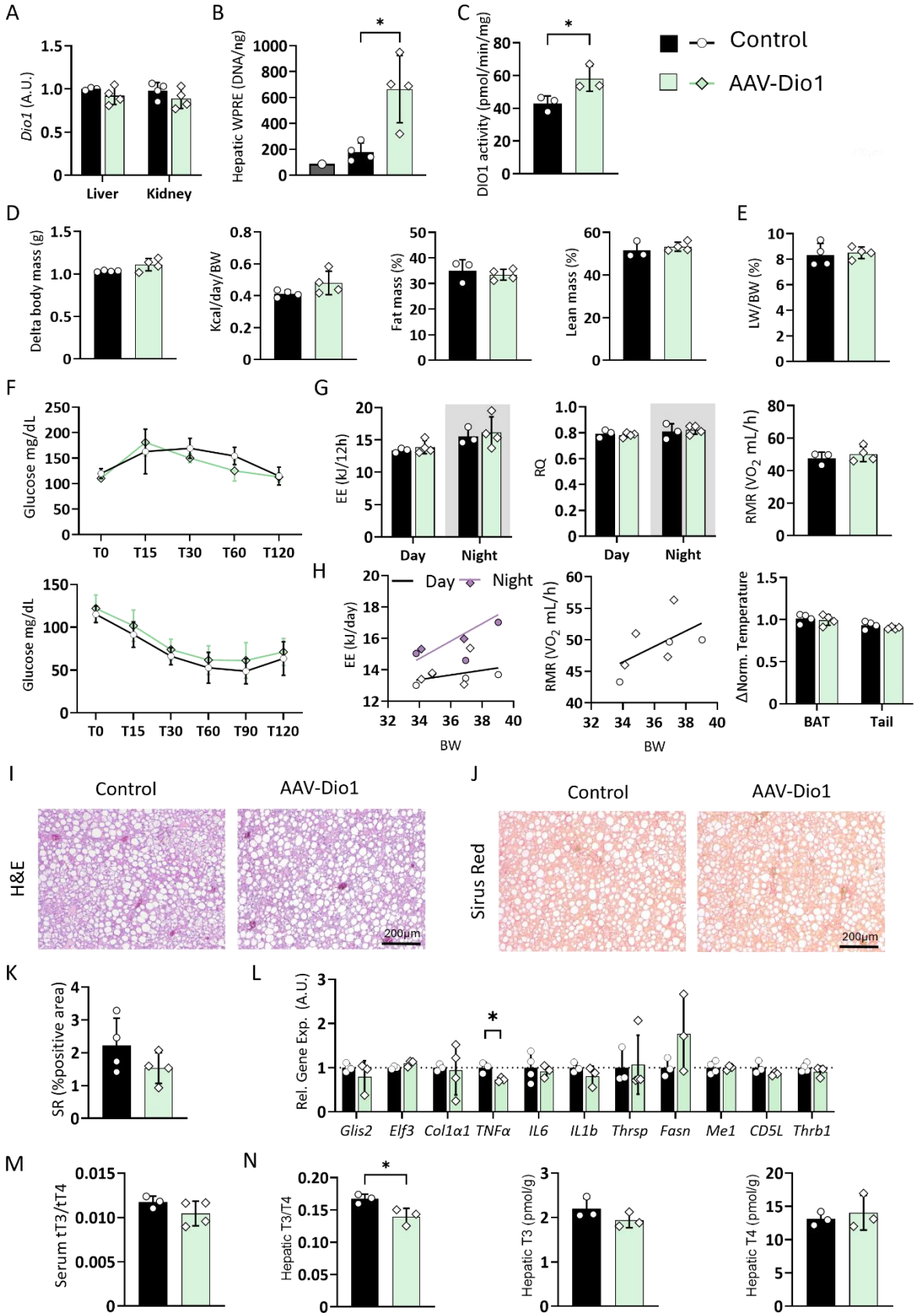
A
Dio1 (A.U.)
Liver
Kidney
B
Hepatic WPRE (DNA/ng)
C
DIO1 activity (pmol/min/mg)
Control
AAV-Dio1
D
Delta body mass (g)
Kcal/day/BW
Fat mass (%)
Lean mass (%)
E
LW/BW (%)
F
Glucose mg/dL
T0
T15
T30
T60
T90
T120
G
EE (kJ/12h)
Day
Night
RQ
RMR (VO2 mL/h)
H
EE (kJ/day)
BW
RMR (VO2 mL/h)
ΔNorm. Temperature
BAT
Tail
I
Control
AAV-Dio1
H&E
200µm
J
Sirus Red
K
SR (%positive area)
L
Rel. Gene Exp. (A.U.)
Glis2
Elf3
Col1α1
TNFα
IL6
IL1b
Thrsp
Fasn
Me1
CD5L
Thrb1
M
Serum tT3/tT4
N
Hepatic T3/T4
Hepatic T3 (pmol/g)
Hepatic T4 (pmol/g)

Figure 15 – Role of Dio1 in MASH. Results from Control or AAV-Dio1 mice fed with CD-HFD. A) Hepatic and renal *Dio1* relative gene expression. B) Transgene efficiency measured by WPRE qPCR. C) DIO1 activity. D) Body parameters as body weight gain, food intake, and body composition. E) Liver/Body weight. F) Glucose (top), insulin (bottom) tolerance test. G) Energy expenditure (EE); respiratory quotient (RQ) and resting metabolic rate (RMR). H) EE and RMR versus BW; BAT and Tail temperature normalized to inner ear. I)Haematoxylin and eosin (H&E) staining. J-K) Sirius Red (SR) (J) staining (K) quantification as percentage of positive area. Scale bar at 200µm. L) Hepatic relative expression of MASH score genes. M) Serum levels of the ratio total THs. N) Intrahepatic levels of THs. Values are mean ± SD, *: $p<0.05$; ***: $p<0.001$; ****: $p<0.0001$ for Control vs AAV-Dio1 (Unpaired Student's test or 2-way ANOVA with Šídák's post hoc test, see Table S1).

The metabolic phenotype of these mice was evaluated at room temperature (22°C ± 0.5) using indirect calorimetry for a 24-hours period before returning them to thermoneutrality conditions (30°C ± 0.5) until sacrifice. Notably, while there were no clear differences at thermoneutrality, AAV-Dio1 mice exhibited increased RMR at room temperature (Figure 16A) indicating enhanced energy expenditure. Subsequent analysis after sacrifice revealed elevated hepatic glycogen levels in AAV-Dio1 mice and *Igf1* (Figure 16C-D), suggesting a compensatory metabolic response potentially mediated by T3, a known enhancer of glycogen storage and *Igf1*. Despite these findings, no increase in intrahepatic TH levels (Figure 16N) or TH-responsive gene expression were observed (Figure 16L), indicating that this compensatory response might be T3-independent in this set up. Moreover IGF-1 has been linked to M2 macrophages and anti-inflammatory effects and treatment with IGF-1 has been shown to improve fibrosis in MASLD mice models (180–182). Its elevation is in alignment with the observed reductions in TNFα in AAV-Dio1 mice and the tendency in lower fibrosis.

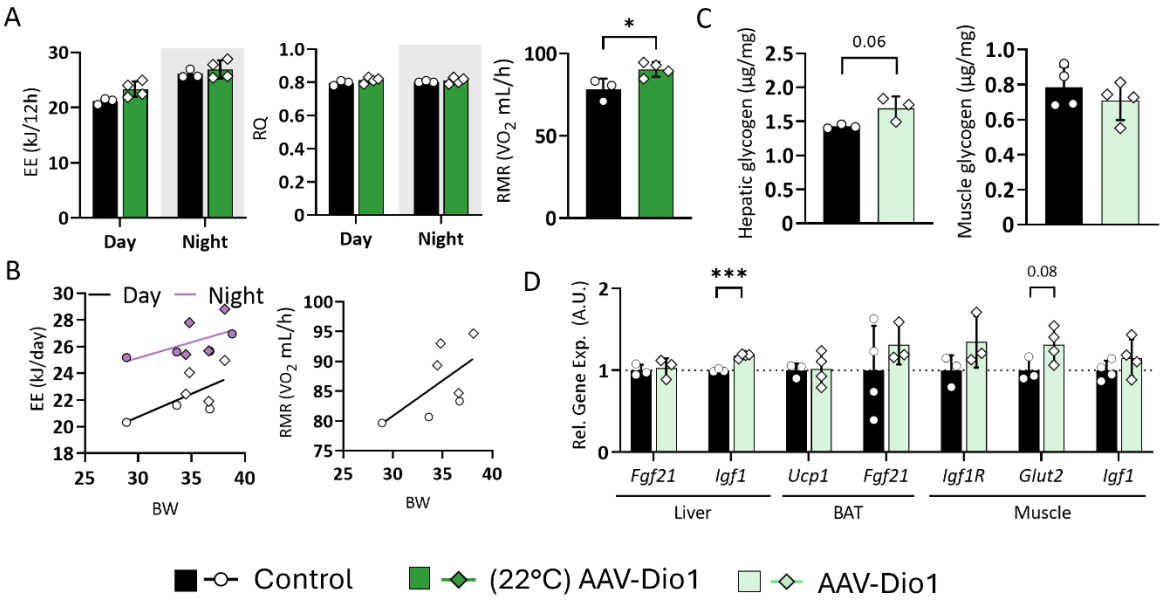

Figure 16 – DIO1 impact on metabolism in mice housed at 22°C. Control or AAV-Dio1 mice fed with CD-HFD. A) Calorimetry study including energy expenditure (EE); Respiratory quotient (RQ); Resting metabolic rate (RMR). B) EE and RMR on BW. C) Glycogen content in liver and muscle after sacrifice. D) Relative gene expression of metabolic markers in liver, brown adipose tissue (BAT) and muscle after sacrifice. Values are mean ± SD, *: p<0.05; ***: p<0.001; ****: p<0.0001 for Control vs AAV-Dio1 (Unpaired Student's test or 2-way ANOVA with Šídák's post hoc test, see Table S1).

3.4. *Dio1* posttranscriptional modifications: modulation by miRNA and inflammation during MASLD and MASH

Due to the lack of significant elevation in *Dio1* mRNA levels with the direct AAV approach, two indirect strategies were subsequently employed.

A recent investigation identified the miR34a-5p as a possible regulator of hepatic TH action in developing human MASH, including modulation of *Dio1* mRNA translation (Naujack et al., *in Revision*). These findings were corroborated at transcript level in MASLD mice housed at room temperature, where miR34a-5p levels progressively increased with the disease severity (Figure 17). A similar trend was observed under thermoneutrality conditions in both MASLD and MASH, with the MASH group displaying higher miR34a-5p levels, concomitant with more severe liver damage (Figure 17). Consequently, it was hypothesized that reducing the expression levels of miR34a-5p in a hepatocyte-specific manner could restore DIO1

enzymatic activity, thereby potentially slowing down or halting the progression of the disease. To achieve it, a targeted approach was employed using AAV8 engineered to express a miRNA sponge for miR34a-5p under the TBG promoter (AAV-miR34a-5p-S) as detailed in the method section (Figure 18A) . The sponge strategy consists of consecutive sequences that are complementary to the one of miR34a-5p, allowing it to bind the miR34a-5p with high affinity. The binding subsequently sequesters miR34a-5p, significantly reducing its availability in the cytoplasm and therefore its interaction with DIO1.

Inflammation is another critical factor known to influence gene expression, protein translation and enzymatic activity. The pro-inflammatory cytokine IL-6 has shown to impact the biosynthesis of hepatic selenoproteins, leading to reduced DIO1 expression and activity through the STAT3 pathway *in vitro* (183). To explore the effects of IL-6 inhibition on DIO1 expression and activity within hepatocytes in MASH, a genetic approach was used aiming to inhibit the STAT3 pathway in these cells. The strategy used the suppressor of cytokine signaling 3 (SOCS3), known to inhibit the STAT3 pathway (184,185). Hence, overexpressing *Socs3* specifically in hepatocytes was hypothesized as potential mitigator of the IL-6 mediated suppression of DIO1. The experimental design, included the AAV8 with *Socs3*, was designed as described in the methods section (Figure 18A).

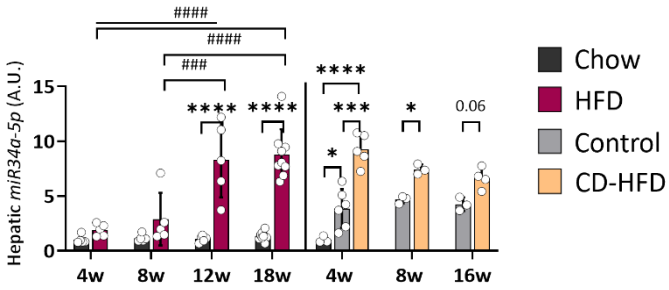

Figure 17 – Hepatic miR34a-5p in MASLD and MASH. Analysis of WT mice at room temperature (left) and thermoneutrality (right). Values are mean ± SD, *: p<0.05; ***: p<0.001; ****: p<0.0001 for diet effect; #: p<0.05 for time effect (Unpaired Student's test, One-way ANOVA or 2-way ANOVA with Tukey's post hoc test, see Table S1)

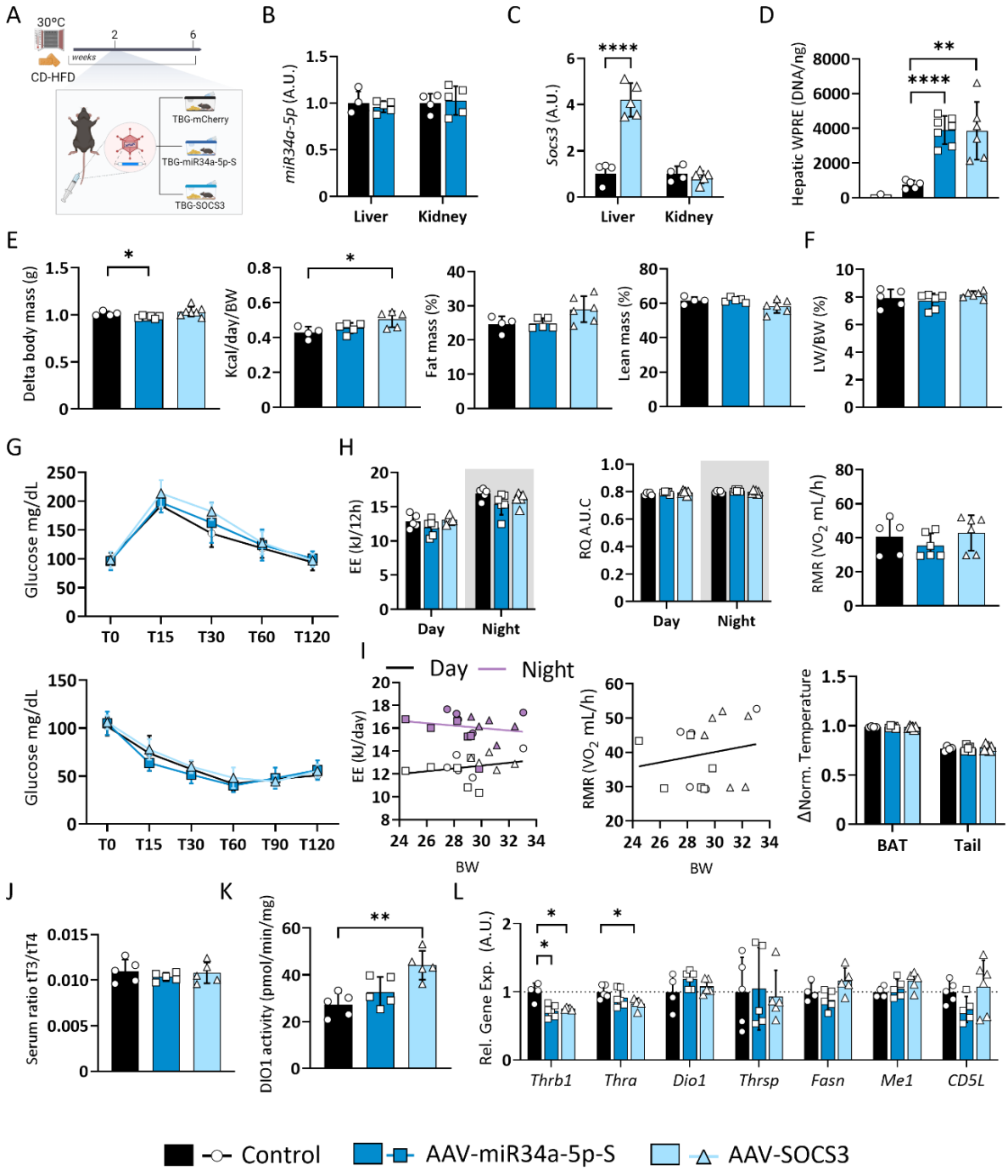
A
30°C
2
6
weeks
CD-HFD
TBG-mCherry
TBG-miR34a-5p-S
TBG-SOCS3
B
miR34a-5p (A.U.)
Liver
Kidney
C
Socs3 (A.U.)
****
Liver
Kidney
D
Hepatic WPRE (DNA/ng)
**
****
E
Delta body mass (g)
*
Kcal/day/BW
*
Fat mass (%)
Lean mass (%)
F
LW/BW (%)
G
Glucose mg/dL
T0
T15
T30
T60
T120
H
EE (kJ/12h)
Day
Night
RQ.A.U.C
Day
Night
RMR (VO2 mL/h)
Glucose mg/dL
T0
T15
T30
T60
T90
T120
I
Day
Night
EE (kJ/day)
BW
RMR (VO2 mL/h)
BW
ΔNorm. Temperature
BAT
Tail
J
Serum ratio tT3/tT4
K
DIO1 activity (pmol/min/mg)
**
L
Rel. Gene Exp. (A.U.)
*
*
*
Thrb1
Thra
Dio1
Thrsp
Fasn
Me1
CD5L
Control
AAV-miR34a-5p-S
AAV-SOCS3

Figure 18 – Effect of miR34a-5p and STAT3 pathway on DIO1 and its impact on MASH. A) Overview of experimental design. B-C) Liver and kidney relative gene expression of (B) miR34a-5p and (C) *Socs3*. D) Transgene levels measured via WPRE qPCR. E) Study of body parameters including body weight, food intake, and body composition. F) Liver/Body weight. G) Glucose (top), insulin (bottom) tolerance test H) Energy expenditure (EE); respiratory quotient (RQ) and resting metabolic rate (RMR). I) EE and RMR versus BW; BAT and Tail temperature normalized to inner ear. J) Serum levels of the ratio total THs. K) DIO1 enzymatic activity. L) Liver relative gene expression of TH-responsive genes. Values are mean ± SD, *: $p<0.05$; ***: $p<0.001$; ****: $p<0.0001$ for AAV-miR34a-5p-S or AAV-SOCS3 comparisons to the control group (Unpaired Student's test or 2-way ANOVA with Šídák's post hoc test, see Table S1).

Analysis of the liver of these mice revealed high number of viral DNA particles in both AAV-miR34a-5p-S and AAV-SOCS3 (Figure 18D) indicative of a successful viral transduction. Noticeably, while gene expression of *Socs3* was elevated in livers of AAV8-SOCS3 (Figure 18C), analysis of *miR34a-5p* did not reveal differences between control and treated mice (Figure 18B). However, as this strategy was based on a sponge construct where the miR34a-5p is sequestered within the sponge sequence rather than absence, during the RNA isolation process it can be released from its binding and therefore not accurately reflect the functional availability of miR34a-5p. Despite some target genes of miR34a-5p followed the expected trend of a model with decreased miR34a-5p expression (Bcl2, p53), none of the differences were significant (186–188) Moreover, *Sirt1,* a well stablished marker of this miRNA did not increase (189,190)(Figure 20).

The study of body parameters across the two mice models indicated no differences compared to controls, except for reduced body weight gain in the AAV-miR34a-5p-S model despite similar caloric intake. In contrast, the AAV-SOCS3 model exhibited increased food intake and slightly higher percentage of body fat, although this last was not statistically significance (Figure 18E). Glucose metabolism, as measured by GTT and ITT, along with energy expenditure, showed no differences between the groups at thermoneutrality (Figure 18G-I).

Importantly, DIO1 enzymatic activity was significantly elevated in AAV-SOCS3 mice but not in AAV-miR34a-S mice (Figure 18K). These results could be related to heightened hepatic T3 content, however, no significant upregulation in TH-responsive gene expression (*Fasn,*

Me1, CD5L) was observed, only minor elevation which could be explained by the experiment's duration. Interestingly, in both mice models there was a downregulation of *Thrb1* and *Thra,* (Figure 18L). Furthermore, markers of fibrosis and inflammation, such as *Glis2, Elf3, Col1a1, TNFα* and *IL10,* showed to be improved in the AAV-miR34a-5p (Figure 19B). A similar pattern was noted in AAV-SOCS3 mice, with reductions in *Glis2* and *TNFα*, indicating decreased fibrosis and inflammation (Figure 19B). However, both models preformed worse in lipid accumulation assessed by ORO staining (Figure 19A). In that regard, both models displayed reduced expression of *Cpt1a*, the gene encoding for the rate-limiting enzyme CPT1A, involved in mitochondrial fatty acid oxidation. Knockout mice for *Cpt1a* display more severe hepatosteatosis (191). Similarly, reduced *Crtc1* has been attributed with increased hepatic steatosis. Notably, Kim et al. demonstrated that *Crtc1* is negatively regulated by miR34a-5p, therefore its significant reduction in AAV-miR34a-5p-S was an unexpected finding (192) (Figure 19B).

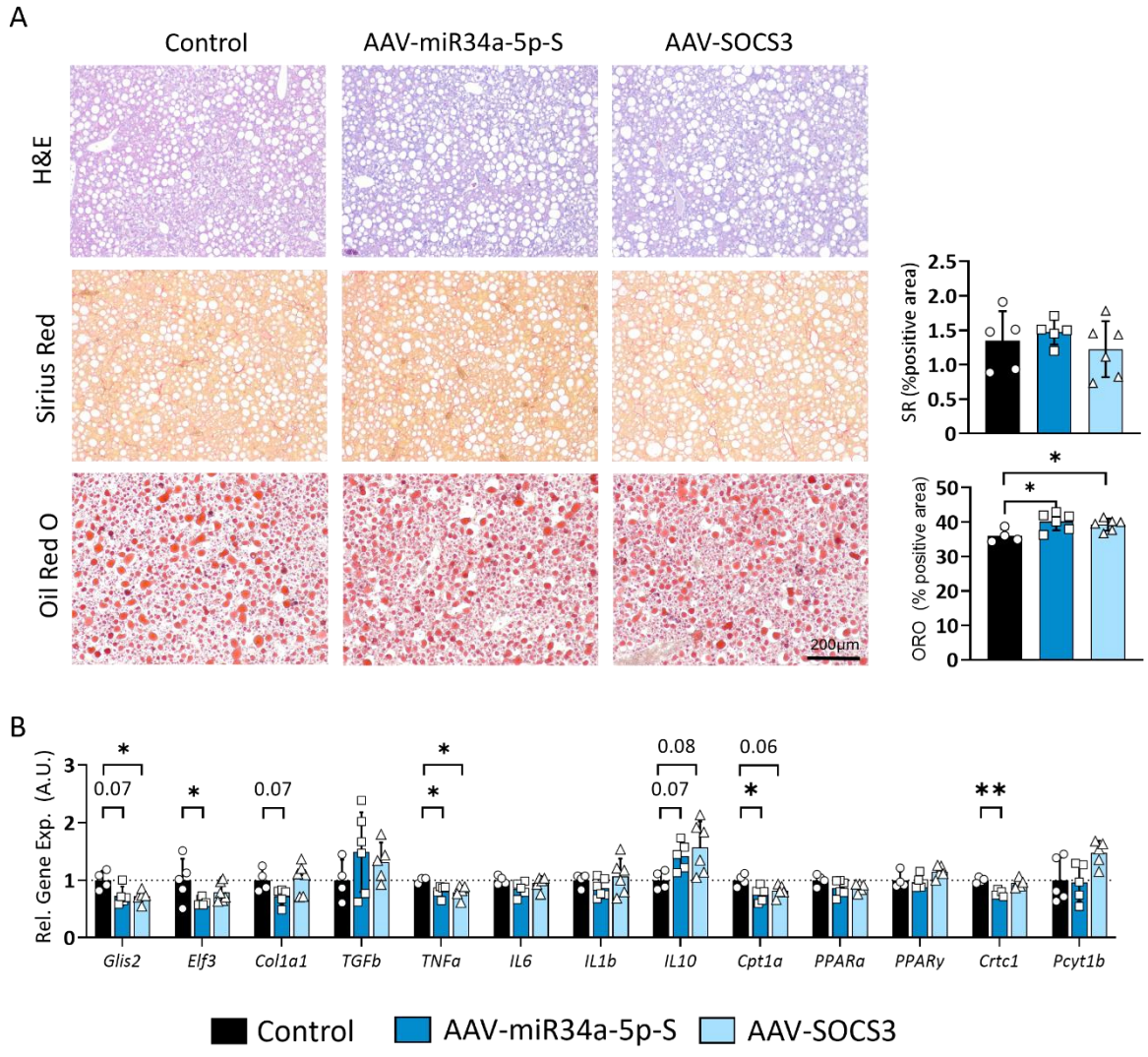

Figure 19 – Liver damage, fibrosis, and steatosis levels in MASH mice treated with associated adenovirus. Mice fed with CD-HFD received AAV-miR34a-5p-S or AAV-SOCS3 mice at thermoneutrality. A) Haematoxylin and eosin (H&E) staining; Sirius Red (SR) staining and quantification; Oil Red O (ORO) staining and quantification. B) Hepatic relative mRNA levels of MASH score and fatty acid oxidation markers. Values are mean ± SD, *: p<0.05; ***: p<0.001; ****: p<0.0001 for AAV-miR34a-5p-S or AAV-SOCS3 comparisons to the control group (Unpaired Student's test, see Table S1).

In summary, modulating miR34a-5p using a sponge AAV approach and the STAT3 pathway via upregulating *Socs3* resulted in minor ameliorated disease progression via diminishing inflammation and fibrosis genetic markers. Additionally, although the findings provide information on the role of posttranscriptional modifications affecting DIO1 activity, no enhanced hepatic T3 content was observed. Noteworthy were unexpected findings that highlighted the complexity of the disease and the involvement of these pathways, suggesting the possibility of off-targets and compensatory mechanisms triggered by the gene therapy. Furthermore, the obtained results in fibrosis markers align with previous results conducted in this work in TRβ knockout models.

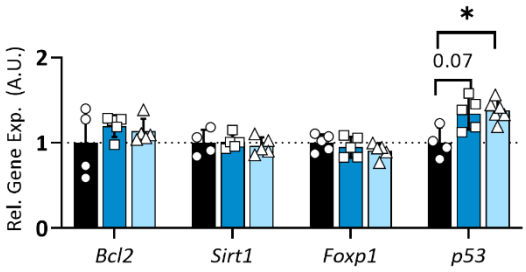

Figure 20 – Hepatic miR34a-5p target genes in MASH. Mice fed with CD-HFD received AAV-miR34a-5p-S or AAV-SOCS3 mice at thermoneutrality. Values are mean ± SD, *: p<0.05; ***: p<0.001; ****: p<0.0001 for AAV-miR34a-5p-S or AAV-SOCS3 comparisons to the control group (Unpaired Student's test, see Table S1).

4. DISCUSSION

The relationship between TH and metabolic diseases has been widely studied, yet the numerous molecular pathways remain poorly understood. In particular, the role of TRβ, the predominant TR isoform in the liver and its contribution to the progression of MASLD and MASH is not fully elucidated. Patients with these conditions present with reduced levels of TRβ mRNA, which declines further as the diseases progresses, correlating with the MASH score severity (11). Moreover, thyroid hormone resistant β(RTHβ) patients with mutations on TRβ ligand domain, also display elevated hepatic steatosis (193). Notably, TH replacement therapy reduces MASLD and MASH severity, similarly to observations in hyperthyroidism (12,52,53). Furthermore, resmetirom, a TRβ agonist, was recently approved by the FDA for its benefits improving MASH, underscoring the significance of local TH action in the liver for MASH progression (15). However, the exact mechanism of action remains unclear.

Together, these observations suggest that TH action in the liver is altered during disease progression, partially by a reduced T3 responsiveness due to declining TRβ expression, which could dampen the liver response to thyromimetics. The local TH availability is largely regulated by hepatic DIOs, specially Dio1. This dissertation aims to investigate TH metabolism during the progression of MASH, focusing on TRβ and other regulators of local hepatic TH action.

4.1. Impact of pharmacological modulation on *Thrb* in primary mouse hepatocytes

Pharmacological stimulation of primary mouse hepatocytes showed that *Thrb1* expression is significantly influenced by both FA stimulation and simvastatin treatment. Specifically, *Thrb1* is upregulated after 48 hours of fatty acid stimulation, while simvastatin treatment results in a decrease in Thrb expression.

The upregulation of *Thrb1* in response to FA stimulation aligns with a compensatory mechanism where TRβ enhances lipid metabolism to manage the increased lipid load. Conversely, the decrease in *Thrb1* expression following simvastatin treatment in a dose-dependent manner indicates that statins may negatively impact TRβ. Simvastatin is a drug primarily indicated for the treatment of CVDs targeting HMG-CoA reductase, an enzyme involved in

cholesterol synthesis, which is also affected by T3. While simvastatin effectively lowers cholesterol levels and reduces cardiovascular risk, its effects on liver metabolism, particularly *Thrb1* expression are unclear.

Some studies have reported beneficial effects of statins on liver diseases, while others have shown no significant improvement or even potential adverse effects (178,194). This inconsistency suggests that the hepatic effects of simvastatin on TRβ are not fully understood. The data from this thesis indicate that there is an urgent need for further research into potential TH resistance induced by statins. Nonetheless, statin treatment is recommended for patients with MASH when CVD is suspected, or the risk is high (194). However, the observed reduction in *Thrb1* by simvastatin raises important questions regarding the combined use of simvastatin with TRβ agonists.

4.2. Development and characterization of MASLD and MASH mouse models

In this thesis, a mouse model of MASLD and MASH replicating the reduction of TRβ observed in humans along with disease severity was developed. To this end, mice were housed at thermoneutrality together with CD-HFD. In the study of metabolic diseases, the housing temperature proved to be an important factor and a limitation. Most existing research in mouse models has been conducted at room temperature (22±2°C), introducing another variable in the study of complex systemic diseases. Room temperature is associated with chronic cold stress in mice, impacting their physiology, immune responses, and elevated sympathetic activation (131,163,165,195). Examples include elevated heart rate, higher arterial blood pressure, increased energy expenditure, altered immune response and cytokine production, etc (164,196–198). These altered responses are resolved at thermoneutrality housing conditions, which for mice is considered 30±2°C (199). In the context of MASLD and MASH, thermoneutrality exacerbates steatosis and hepatocyte ballooning together with increased inflammatory and fibrogenic responses and results in increased hepatocellular damage (167,168). Additionally, it removes the sex-based differences typically observed between female and male mice (167).

The CD-HFD model, employed in this research, offers several advantages in studying the pathological features of MASH without the drawbacks observed in other dietary intervention models. Commonly used diets like MCDD often result in significant weight loss, failing to

mimic the gradual progression of MASLD to MASH. Meanwhile HFD or WD alone, while mimicking the metabolic features of MASLD, typically do not result in advance stages of the disease as they fail to induce fibrosis without additional pharmacological interventions such as CCl_4.

Despite the use of CD-HFD has faced criticism in the past, as this diet alone showed to improve glucose metabolism and insulin sensitivity in mouse models, potentially representing a problem when studying MASH pathogenesis. This limitation was addressed by combining CD-HFD with an optimized methionine content of 0.4%, which not only prevents the weight loss but also induces obesity and insulin resistance in mice (151). Together with thermoneutral housing conditions, this model enables the study of the full spectrum of MASH while capturing the TRβ reduction observed in humans without cofounding effects as this model closely resembles the human condition. A comparison of the models of MASLD and MASH can be found in Table 11.

Table 11| Comparison of mice models for MASLD and MASH housed at room temperature.

	Human	HFD/HCD	WD	MCD	CD	CD-HFD	CD-HFD + 0.4% met	WD + CCl_4	Ob/Ob	Db/Db
Genetic knockout	-	-	-	-	-	-	-	-	+	+
Weight gain	+	+	+	-	-	+	+	+	+	+
Obesity	+/-	+	+	-	-	-	+	-	+	+
Liver steatosis	+	+	+	+	+	+	+	+	+	+
Hypercholesterolemia (serum)	+	+	+	-	-	-	+	+	+	+
Hypertriglyceridemia (serum)	+	-	-	-	-	-	-	-	-	-
Hypercholesterolemia (hepatic)	+	-	+	-	+	+	+	+	+	-
Hypertriglyceridemia (hepatic)	+	+	+	+	+	+	+	+	+	+
Transaminases	+	+/-	+	+	+/-	+	+	+	+	+
Insulin resistance	+	+	+	+*	+/-	-	+	+	+	+
Diabetes	+/-	+	+	-	-	-	-	-	+	+
Ballooning	+	-	+	+	+	+	+	+	-	-

Inflammation	+	-	+	+	+	+	+	+	-	-
Advance fibrosis	+	-	-	+	+	+	+	+	-	-
MASH	+	-	+	+	+	+	+	+	-	-
HCC	+	-	-	-	+	+	+	+	-	-
References	(25,47,200)	(147,148,150,201)	(145,147,201)	(150,202)	(150,203,204)	(150,151,205)	(151)	(145)	(206)	(207,208)

(+) Presence, (-) Absence; *only hepatic

To investigate the role of TRβ during disease progression, a loss and a gain of function approaches were carried out using this novel mouse MASH model. For the loss of function, using TRβ knockout mice instead of mutated TRβ was preferred as it allows to study the role of TRβ without the pronounced phenotype derived by the state of unliganded apo-receptor observed in mutant TRβ mice. This constant state of actively suppression on gene expression often results in a more pronounced phenotype than the absence of the receptor (126–128). Moreover, a mutated TRβ might interfere with the normal functioning of TRα1, potentially through mechanisms like dimerization, leading to cofounding effects which could complicate the interpretation of the results.

4.3. The role of TRβ in MASLD and MASH disease progression

The thermoneutrality housing conditions resulted in a notable restoration of the usual hyperthyroid observed in mice lacking TRβ as compared to room temperature. This observation can primarily be attributed to a reduced hyperactive HPT axis at thermoneutral conditions (131,168). Moreover, this approach allows to reduce cofounding effects derived from a hyperthyroid state in other organs while developing the liver disease faster (167,168).

Body parameters including body weight gain, food intake or body composition were minimally affected by the absence or overexpression of TRβ at thermoneutrality. However, mice lacking TRβ displayed a consistently higher average fat mass percentage throughout the experiment. Similar results were observed in studies conducted at room temperature, where body weight was comparable between TRβs and controls (107,209). Additionally, Oelkrug et al. reported that TRβ knockout male offsprings had a slightly elevated fat mass percentage

compared to their littermates. Notably, the differences in body composition between genotypes were significant during early MASH at thermoneutrality, suggesting a critical role of TRβ during MASLD progression which eventually, the cumulative effects of the diet diminish this difference. Additionally, the absence of TRβ did not result in clear differences in hepatic steatosis levels or other histopathological features associated with MASH.

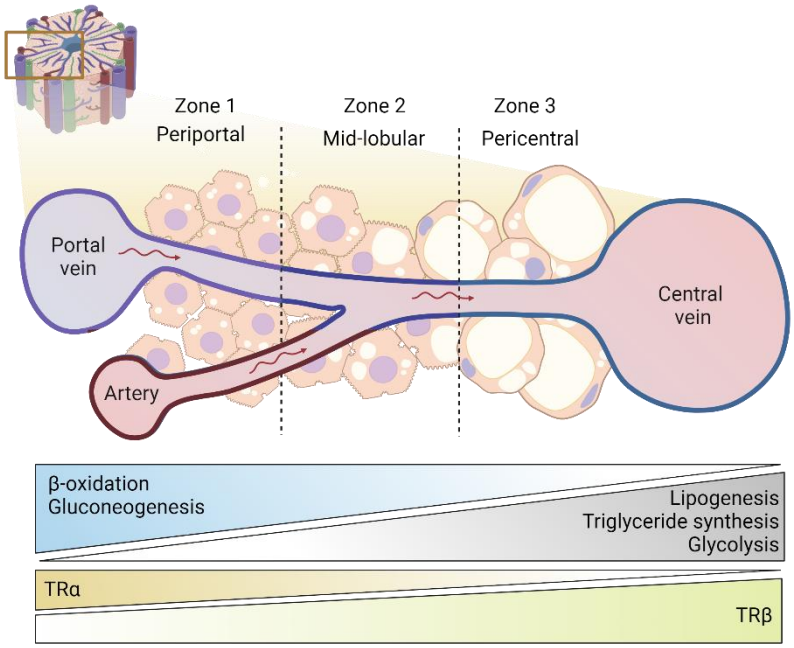

Figure 21 – Liver parenchyma architecture, functions, and TRβ expression. Blood from the hepatic artery, rich in oxygen, mixes with nutrient-rich blood from the portal vein (PV) as it flows towards the central vein (CV). Hepatic lobes are structure into periportal (zone 1), mid-lobular (zone 2), and pericentral (zone 3) areas, which function as distinct metabolic zones. Near the PV, β-oxidation and gluconeogenesis are increased, whereas closer to CV, lipogenesis, TGAs synthesis, and glycolysis are elevated. Thyroid hormone receptors (TRs) show different spatial gene expression with TRβ, the predominant isoform, highest levels close to CV and TRα levels higher near PV. Figure adapted from 210-211, created with Biorender.

Interestingly, TRβ knockout mice exhibited a distinctive lipid deposition pattern around the CV in early MASLD, where most of the lipids were deposited in the intermediate zone, contrary to the usual hepatic lipid accumulation pattern (Figure 21). Typically, steatosis begins near the CV and progresses towards the PV in a gradient-manner, opposite to the

direction of the blood flow (210). This observation agrees with thyroid hormone crucial spatial and temporal importance within organs, regulated by differential expression of transporters, deiodinases, and receptors, which is altered in TRβ knockout mice. Public hepatocyte transcriptome data analysis indicates that the highest TRβ expression is found close to CV and decreases towards the PV (211). However, as metabolic challenges accumulate in the liver thorough the weeks, the lipid deposition occurs without regard to localization. A possible explanation for the marked steatosis in zone 2 in TRβ knockout mice could be due to the liver architecture and the physiological roles of each of the zones which are not exclusively regulated by TH action (Figure 21) (211–215). In zone 3, marked by increased lipogenesis and TGA synthesis, the lack of TRβ might result in increased lipogenesis and TGAs together with reduced beta-oxidation. However, zone 3 is adapted to handle high levels of lipids, possibly being able to trigger compensatory mechanisms in the absence of TRβ delaying lipid accumulation but is not sufficient as disease severity increases (214,215). On the other hand, zone 1 relies on beta-oxidation and gluconeogenesis, suggesting the lack of TRβ might result in reduction of these processes. However, as zone 1 displays less TRβ, could indicate that this zone relies less on TRβ for metabolic regulation. In zone 2, the loss of TRβ results in a significant metabolic imbalance, possibly because is a less specialized area and may rely more on TRβ. Consequently, lipid accumulation starts in zone 2 in TRβ knockout as it fails to compensate for TRβ loss. Together it suggests that TRβ's might be more relevant in the context of lipid deposition during early stages of the disease, whereas in severe stages its role is overshadowed by cumulative effects of the diet and disease progression.

This observation is supported by results of liver transaminases in these mice, which indicated a similar degree of liver damage across all mice belonging to the same dietary group, implying a minor role for TRβ in hepatic damage. Although AST was elevated in early MASH in TRβ knockout mice, the ALT, a considered more reliable transaminase for detecting liver damage, showed no differences compared to WT mice. Given AST's broader distribution in the body, this elevation might indicate that other organs are contributing to AST levels. However, whether this is due to greater liver disease progression in the absence of TRβ, or the direct impact of the absence of TRβ in those tissues, was not further explored.

Despite the minimal impact of TRβ on average fat percentage, the lack of TRβ resulted in elevated hepatic TGA content in early MASH. TH action in the liver is associated with

regulation of lipid metabolism by influencing pathways related to fatty acid oxidation and lipogenesis (60,61). In TRβ knockout mice, similar to observed in hypothyroidism, reduced or absent TRβ leads to an imbalance in lipid homeostasis, resulting in increased hepatic TGA content (62,139,140). These findings suggest that TRβ helps maintaining hepatic TGA levels during disease progression.

Although steatosis was not affected by TRβ, fibrosis assessment revealed that the absence of TRβ resulted in improved fibrosis during MASH progression by reducing the expression of pro-fibrotic genes, such as *Col1α1*, *Elf3,* and inflammatory cytokines *TNFα* and *IL6*. These observations are in alignment with a recent study using TRβ knockout mice, where that lack of TRβ prevented the upregulation of *Col1α1* in the heart after T3 administration (131). Moreover, mice studies using thyromimetics including resmetirom or GC-1 to activate TRβ in the liver, resulted in reduced steatosis in metabolic and histological parameters and a modest down-regulation of genes involved in fibrogenesis, but this last was not reflected in histological improvements (216). In humans, resmetirom double-blind, placebo-controlled trail set up gathered 966 participants where 95% were presented with fibrosis in stage 2 to 3, and the mean BMI was 36 kg/m^2. The drug tested dosage was 80 mg and 100mg. Results on steatosis indicated a reduction on 42.5% and 51% from baseline for the 80mg and 100mg groups respectively. Despite these promising results, only 26% and 39% of the double-blind individuals subjected to 80mg and 100 mg groups, had improved fibrosis. Notably, 21% of the placebo group participants had also improved fibrosis (14,15). Together these findings suggest a role of TRβ in fibrosis development, which are concomitant with TRβ role in inhibiting the TGFβ/SMAD pathway (133). However, a role of TRα cannot be discarded.

Fibrosis is predominantly regulated by hepatic stellate cells (HSCs), where TRα is the dominant isoform while TRβ is mainly found in hepatocytes (122). Studies with TRα knockdown mice indicate that reduced TRα levels results in high basal levels of fibrogenic markers in the liver. When TRα knockdown are subjected to pro-fibrogenic intervention (e.g. MCDD, CCl_4), there is an increased activation of HSCs and exacerbation of fibrosis. Conversely, administration of T3 or GC-1 inhibits TGFβ/SMAD signaling in HSCs *in vitro* and *in vivo* dependent of TRα (122,215). These findings suggest that TRβ might be more relevant for maintaining the overall liver metabolic health and its activation in MASH results in indirect fibrosis improvement via improved steatosis (15,52,134). On the other hand, TRα appears to play a more direct

role in regulating fibrosis. Therefore, it might explain the modest fibrosis improvement in clinical trials of thyromimetics, which although can bind to TRα, they have high affinity for TRβ.

In this dissertation, thermoneutral housing condition revokes the usual hyperthyroidism in TRβ knockouts, therefore allowing to observe the individual roles of the TRs without cofounding effects. In that regard, TRα might partially compensate for the lack of TRβ in MASH, however its low expression in the liver, restricted to HSCs and immune cells, is not sufficient to restore the disease without TRβ activation. More studies focusing on the individual roles of TRβ and TRα in the liver metabolism and on the different cell types is needed.

Regarding TH status in these mice, measurements in serum and liver underscored the distinction between tissue-specific and systemic TH status. In TRβ knockout mice fed with CD-HFD, serum T4 levels were elevated along with increased DIO1 activity compared to control-fed mice. DIO1 preferentially metabolizes rT3>T4>T3. This suggests that T4 is transported into the liver where undergoes conversion by DIO1 to other metabolites, resulting in a reduced T4 intrahepatic concentration. However, the increased enzymatic activity did not result in increased hepatic or serum T3 levels, nor a clear induction of TH-responsive genes in the liver. Collectively, it indicates that the liver's capacity for intrahepatic TH regulation may be compromised during disease progression. Importantly, intrahepatic results should be carefully interpreted as local TH concentrations might differ between various areas of the liver (Figure 21). A potential solution could be the use of hepatocyte-specific luciferase mice to better understand and visualize the differences in TH activity in the liver.

Dio1 expression levels is a sensitive marker of T3 action in the liver (99,106). *Dio1* was increased in all CD-HFD fed mice and in WTs on control diet except in TRβ knockout mice on a control diet when compared to healthy mice. In contrast the TH-responsive genes *Klf9* and *Thsrp,* were downregulated in CD-HFD fed mice. *Thrsp* is typically reduced in high-fat diets, where lipid intake is the main source of energy. *Thrsp* contains carbohydrate response elements (ChoRE) besides TREs upstream the promoter region, which may explain its upregulation under a carbohydrate-rich diet like the control diet compared to CD-HFD in the same genotype (217). Sustained upregulation of *Thrsp in vitro* is linked to enhanced in DNL (218) and impaired mitochondrial fatty acid oxidation, potentially worsening MASLD condition at early stages. These findings suggest that alterations on *Dio1* and *Thrsp* mRNA expression are

initially diet-dependent rather than driven by TH action, as no differences between the genotypes in gene expression or intrahepatic TH levels were found.

Overall, these findings demonstrate the complex role of TRβ in liver diseases, showing both protective and detrimental effects depending on the stage of disease progression and the metabolic context. The loss of function model underscores TRβ's potential to exacerbate liver damage in advanced stages of disease, particularly through fibrosis and inflammation. The gain of function, however, suggests a nuanced role where TRβ expression does not necessarily translate to better outcome. These experiments outcomes, and the vast results using TRβ selective ligands with proven benefits, further supports the important role of TH in liver metabolism. However, our findings suggest that the precise levels of *Thrb* are of minor importance, and it might be more relevant to focus on liver specific ligands or in deiodinases. Additionally, TRα action might compensate for TRβ, thus activating both receptors while maintaining liver specificity could be beneficial for MASH.

4.4. The role of Dio1 in MASLD and MASH disease progression

DIO1 is the main deiodinase in the liver of human and mice and plays a crucial role in managing local TH metabolism (103). Dysfunction on DIO1 can result in local hypothyroidism, potentially heightening the risk of MASLD and MASH.

Prior studies using animal models reported that DIO1 expression and activity increases in early MASLD and goes back to baseline after 24 weeks of WD. In the same study, DIO1 enzymatic activity was also increased and further associated with elevated T3/T4 ratio, which resulted from unchanged T3 levels and reduced T4 intrahepatic levels (84). In this dissertation, the characterization of a MASLD mouse cohort housed at room temperature, showed a rapid increase of hepatic *Dio1* within the first week of HFD feeding, which remained elevated throughout the study despite the general decline in *Dio1* expression with age (220). Histological assessment of the liver revealed that *Dio1* induction preceded visible pathological changes, which become apparent after 4 weeks of HFD feeding. These findings suggest that *Dio1* induction might be an initial response to diet. This is not surprising as multiple studies have found DIO1 to be affected by overnutrition (84), fasting (161), food restriction (221), or insulin (222). Moreover, preventing the increase of *Dio1* mRNA using shRNA, led to increased hepatic TGAs and cholesterol in the liver of WD-fed mice (84). Together these findings indicate

that early induction of *Dio1*, might represent a protective mechanism for the progression of MASLD and MASH by increasing the T3 content in the liver. However, these experiments were conducted at room temperature, overlooking the critical influence of temperature on TH dynamics and against a background of elevated energy turnover.

To investigate the possible benefit of *Dio1* overexpression in early MASH at thermoneutrality, a hepatocyte-specific *Dio1* overexpressing mouse model approach was used (AAV-Dio1). DIO1 enzymatic activity was increased in these mice but it failed to correlate with elevated hepatic TH levels at thermoneutrality. Intrahepatic T3 and T4 level, although individually were not different from those of the control group, combined resulted in a lower ratio T3/T4. Nonetheless, no differences in TH-responsive genes were observed in AAV-Dio1 compared to control mice. With this approach, the endogenous *Dio1* and the AAV triggered *Dio1* are indistinguishable, hence the discrepancies between *Dio1* mRNA and enzymatic activity can only be speculated. On one hand, the transgene-encoded product might lead to an increased degradation of the endogenous counterpart by triggering compensatory mechanisms (e.g. miRNA), or it exhibits greater enzymatic activity than its endogenous counterpart. The presence of WPRE element in the construct may partly account for these observations, as WPRE is known to enhance mRNA stability and nuclear export, facilitating more efficient translation of the transgene (223,224). Given that qPCR analysis typically focuses on exon regions, this method may overlook variation between pre-mRNA and mature mRNA. Maturation of mRNA is a spatial-dependent process, therefore the enhanced export of transgenic *Dio1* mRNA into the cytoplasm likely accelerates the translation process, maintaining the total mRNA levels. These findings align with earlier observations in this work where an increased *Dio1* expression did not necessarily correlate to enhanced DIO1 activity during disease progression. This lack of correlation suggests that posttranscriptional modifications affecting mRNA maturation play an important role, illustrating a complex interplay of TH regulation within MASLD and MASH progression.

Further analysis showed that *Dio1* mRNA and DIO1 activity correlate in healthy mice whereas the rest of the dietary interventions did not, indicating possible posttranscriptional mechanisms affecting *Dio1* mRNA. Thus, the protective effect of *Dio1* upregulation might be overshadowed by the impact of posttranscriptional mechanism in the liver of MASH mice.

Inflammation is a common feature of liver diseases and its impact on DIO1 has been observed in multiple models of inflammation. *In vitro,* HepG2 cells treated with the proinflammatory interleukin 1β (IL-1β) display reduced mRNA and activity of DIO1 (225,226). Similar results were obtained in HepG2 treated with interleukin 6 (IL-6) (183) and in primary rat hepatocytes exposed to IL-1 and IL-6 (227).

To investigate the impact of inflammation on liver DIO1, an alternative gene therapy approach to reduce liver inflammation was performed. Hepatocyte-specific overexpression of *Socs3*, a well-known inhibitor of the STAT3 pathway (184,185), resulted in significant increase of DIO1 enzymatic activity at thermoneutrality. However, no changes in serum TH levels or liver TH-responsive genes were observed. Mice overexpressing *Socs3* showed increased food intake together with elevated fat mass percentage which could explain the increased lipid accumulation in the liver assessed in histology. Moreover, although some inflammation and fibrogenic markers were decreased, these changes were minor and did not translate into improvements in histology.

In addition to inflammation, miR34a-5p was recently proposed as candidate regulator of local TH action in human MASH livers (Naujack et al *in Revision*). MicroRNAs are highly conserved small non-coding RNAs that regulate gene expression at posttranscriptional level. By binding to *Dio1* mRNA, miR34a-5p may exert a negative regulatory action, promoting the degradation of its target. Upregulation of miR34a-5p was confirmed in livers of MASLD and MASH mice at room temperature as well as thermoneutrality. This increase, parallel to disease progression, reached the peak at late-MASLD and early-MASH. Reducing levels of miR34a-5p was hypothesized to be beneficial for MASH progression by affecting DIO1 activity. For that, the use of a microRNA sponge strategy was chosen. The microRNA sponge was designed to directly target the miR34a-5p in a hepatocyte-specific manner, hence sequestering miR34a-5p in these cells and preventing them from binding to *Dio1* mRNA. Although there was no significant increase in DIO1 enzymatic activity after the viral administration, a regulation of miR34a-5p on *Dio1* cannot be discarded. The results of this mouse model were inconclusive as miR34a-5p levels were not reduced and target genes of miR34a-5p were not altered. Similar approach was done by Bianca et al., using miR34 in the heart without noticeable effect (228). The miRNA sponge is a difficult approach due to reduce stability of the construct that results in the inability to sequester enough of the miRNA target to produce a noticeable effect. Therefore, it is

possible that the observed outcomes in the phenotype of these mice are a result of off-target effects or compensatory mechanisms triggered by the gene therapy approach.

Collectively, although these strategies provide insights into the posttranscriptional modifications influencing DIO1 during liver diseases, they did not translate into increased TH action in the liver neither into histological changes during MASH progression. On the other hand, it has been suggested that DIO3 might play an important role during liver diseases. DIO3 is the main inactivating deiodinase catalysing the conversion of T4 and T3 to rT3 or T2 respectively, thus an increase of DIO3 may enhance TH clearance independently of DIO1 action during disease progression. However, although several studies reported elevated DIO3 expression in HCC or partial hepatectomy (229), there is no solid evidence that it also happens in MASLD. Bruinstroop et at., showed that elevation of *Dio3* during early MASLD, did not resulted in increased DIO3 activity in the liver (84). Similar evidence was found for MASLD patients (11,230). Together it suggests that DIO3 has negligible biological relevance during MASLD development and progression. Instead, its increase during HCC and partial hepatectomy may be likely linked primarily to the activation of various fetal genes usually induced under these conditions (231).

5. CONCLUSION AND OUTLOOK

Local control of TH regulation in MASH progression is a complex process involving lipid metabolism, inflammation, and fibrosis processes. The experimental outcomes of this study demonstrated that TRβ exerts a variable influence on MASLD and MASH. Specifically, lack of TRβ slightly worsened lipid metabolism in the liver, suggesting a potential therapeutic role in modulating hepatic lipid homeostasis. However, it was also observed that the lack of TRβ had a positive impact on fibrosis and inflammation.

In early and mild MASLD stages, TRβ's activation appears beneficial. Enhanced lipid metabolism could reduce hepatic steatosis, thereby mitigating the disease progression. This aligns with existing literature on the beneficial effects of TRβ activation in improving lipid profiles and reducing liver fat accumulation. Conversely, in more severe stages of MASLD, TRβ presence without a ligand might be detrimental. Additionally, the role of TRα cannot be overlooked, particularly in the context of liver fibrosis. While TRβ activation has a broader effect on improving overall liver function, TRα activation might be crucial for improving fibrosis.

To better understand the individual roles of TRs in liver, future research should include single-cell analysis of the liver cell types in health and disease conditions. Developing a mouse model that use hepatic-specific antagonists for TRβ in late MASH could also provide valuable insights into TH action in the liver. Additionally, studying fibrosis development in resmetirom studies would yield important data from patients.

Dio1 was found to be upregulated in MASH progression, likely as a compensatory response initially triggered by the diet to regulate TH in the mice liver. Although gene therapy aimed at increasing DIO1 did not result in improvements during MASH progression, the observed discrepancies between gene expression, enzymatic activity, and T3 content suggest that posttranscriptional mechanisms may play a role overshading this protective action of *Dio1*. A potential solution to enhance our understanding of TH activity in the liver could be the use of hepatocyte-specific luciferase mice, which would enable better understanding of TH and DIO1 activity across various stages of disease progression.

Importantly, the role of temperature over TH regulation may explain the discrepancies between our study and previous studies conducted at room temperature. Thermoneutrality closely resembles the human condition and allows to study the role of TRβ without cofounding effects, as it restores the usual hyperthyroidism observed in TRβ knockout mice. Future preclinical studies should include thermoneutrality experiments as it not only improves the comparability of animal models and translation to humans but also represents a practical solution as it enables fast development of MASH.

References

1. the EMIL-Study, Ludwig U, Holzner D, Denzer C, Greinert A, Haenle MM, et al. Subclinical and clinical hypothyroidism and non-alcoholic fatty liver disease: a cross-sectional study of a random population sample aged 18 to 65 years. BMC Endocr Disord. 2015 Dec;15(1):41.

2. Chung GE, Kim D, Kim W, Yim JY, Park MJ, Kim YJ, et al. Non-alcoholic fatty liver disease across the spectrum of hypothyroidism. J Hepatol. 2012 Jul;57(1):150–6.

3. Kim D, Kim W, Joo SK, Bae JM, Kim JH, Ahmed A. Subclinical Hypothyroidism and Low-Normal Thyroid Function Are Associated With Nonalcoholic Steatohepatitis and Fibrosis. Clin Gastroenterol Hepatol. 2018 Jan;16(1):123-131.e1.

4. Duntas LH. Thyroid Disease and Lipids. Thyroid. 2002 Apr;12(4):287–93.

5. Roti E, Minelli R, Salvi M. Thyroid hormone metabolism in obesity. Int J Obes. 2000 Jun;24(S2):S113–5.

6. Dimitriadis G, Parry-Billings M, Bevan S, Leighton B, Krause U, Piva T, et al. The effects of insulin on transport and metabolism of glucose in skeletal muscle from hyperthyroid and hypothyroid rats. Eur J Clin Invest. 1997 Jun;27(6):475–83.

7. Beer SF, Parr JH, Temple RC, Hales CN. THE EFFECT OF THYROID DISEASE ON PROINSULIN AND C-PEPTIDE LEVELS. Clin Endocrinol (Oxf). 1989 Apr;30(4):379–83.

8. Sinha RA, You SH, Zhou J, Siddique MM, Bay BH, Zhu X, et al. Thyroid hormone stimulates hepatic lipid catabolism via activation of autophagy. J Clin Invest. 2012 Jul 2;122(7):2428–38.

9. Sinha RA, Singh BK, Zhou J, Wu Y, Farah BL, Ohba K, et al. Thyroid hormone induction of mitochondrial activity is coupled to mitophagy via ROS-AMPK-ULK1 signaling. Autophagy. 2015 Aug 3;11(8):1341–57.

10. Bohinc BN, Michelotti G, Xie G, Pang H, Suzuki A, Guy CD, et al. Repair-Related Activation of Hedgehog Signaling in Stromal Cells Promotes Intrahepatic Hypothyroidism. Endocrinology. 2014 Nov 1;155(11):4591–601.

11. Krause C, Grohs M, El Gammal AT, Wolter S, Lehnert H, Mann O, et al. Reduced expression of thyroid hormone receptor β in human nonalcoholic steatohepatitis. Endocr Connect. 2018 Dec;7(12):1448–56.

12. Liu L, Yu Y, Zhao M, Zheng D, Zhang X, Guan Q, et al. Benefits of Levothyroxine Replacement Therapy on Nonalcoholic Fatty Liver Disease in Subclinical Hypothyroidism Patients. Int J Endocrinol. 2017;2017:1–10.

13. Baxter JD, Webb P. Thyroid hormone mimetics: potential applications in atherosclerosis, obesity and type 2 diabetes. Nat Rev Drug Discov. 2009 Apr;8(4):308–20.

14. Harrison SA, Bashir MR, Guy CD, Zhou R, Moylan CA, Frias JP, et al. Resmetirom (MGL-3196) for the treatment of non-alcoholic steatohepatitis: a multicentre, randomised, double-blind, placebo-controlled, phase 2 trial. The Lancet. 2019 Nov;394(10213):2012–24.

15. Harrison SA, Taub R, Neff GW, Lucas KJ, Labriola D, Moussa SE, et al. Resmetirom for nonalcoholic fatty liver disease: a randomized, double-blind, placebo-controlled phase 3 trial. Nat Med. 2023 Nov;29(11):2919–28.

16. Rinella ME, Lazarus JV, Ratziu V, Francque SM, Sanyal AJ, Kanwal F, et al. A multisociety Delphi consensus statement on new fatty liver disease nomenclature. J Hepatol. 2023 Dec;79(6):1542–56.

17. Hagström H, Vessby J, Ekstedt M, Shang Y. 99% of patients with NAFLD meet MASLD criteria and natural history is therefore identical. J Hepatol. 2023 Sep;S0168827823050808.

18. Yang A, Zhu X, Zhang L, Ding Y. Transitioning from NAFLD to MAFLD and MASLD: Consistent prevalence and risk factors in a Chinese cohort. J Hepatol. 2023 Oct;S0168827823051619.

19. Song SJ, Lai JCT, Wong GLH, Wong VWS, Yip TCF. Can we use old NAFLD data under the new MASLD definition? J Hepatol. 2023 Aug;S0168827823050006.

20. Younossi ZM, Golabi P, Paik JM, Henry A, Van Dongen C, Henry L. The global epidemiology of nonalcoholic fatty liver disease (NAFLD) and nonalcoholic steatohepatitis (NASH): a systematic review. Hepatology. 2023 Apr;77(4):1335–47.

21. Golabi P, Paik JM, AlQahtani S, Younossi Y, Tuncer G, Younossi ZM. Burden of non-alcoholic fatty liver disease in Asia, the Middle East and North Africa: Data from Global Burden of Disease 2009-2019. J Hepatol. 2021 Oct;75(4):795–809.

22. Younossi ZM, Koenig AB, Abdelatif D, Fazel Y, Henry L, Wymer M. Global epidemiology of nonalcoholic fatty liver disease—Meta-analytic assessment of prevalence, incidence, and outcomes. Hepatology. 2016 Jul;64(1):73–84.

23. Paik JM, Golabi P, Younossi Y, Srishord M, Mishra A, Younossi ZM. The Growing Burden of Disability Related to Nonalcoholic Fatty Liver Disease: Data From the Global Burden of Disease 2007-2017. Hepatol Commun. 2020 Dec;4(12):1769–80.

24. Younossi ZM, Stepanova M, Ong J, Trimble G, AlQahtani S, Younossi I, et al. Nonalcoholic Steatohepatitis Is the Most Rapidly Increasing Indication for Liver Transplantation in the United States. Clin Gastroenterol Hepatol. 2021 Mar;19(3):580-589.e5.

25. Ye Q, Zou B, Yeo YH, Li J, Huang DQ, Wu Y, et al. Global prevalence, incidence, and outcomes of non-obese or lean non-alcoholic fatty liver disease: a systematic review and meta-analysis. Lancet Gastroenterol Hepatol. 2020 Aug;5(8):739–52.

26. Quek J, Chan KE, Wong ZY, Tan C, Tan B, Lim WH, et al. Global prevalence of non-alcoholic fatty liver disease and non-alcoholic steatohepatitis in the overweight and obese population: a systematic review and meta-analysis. Lancet Gastroenterol Hepatol. 2023 Jan;8(1):20–30.

27. Gastaldelli A, Cusi K. From NASH to diabetes and from diabetes to NASH: Mechanisms and treatment options. JHEP Rep. 2019 Oct;1(4):312–28.

28. Cao L, An Y, Liu H, Jiang J, Liu W, Zhou Y, et al. Global epidemiology of type 2 diabetes in patients with NAFLD or MAFLD: a systematic review and meta-analysis. BMC Med. 2024 Mar 6;22(1):101.

29. Makki K, Froguel P, Wolowczuk I. Adipose Tissue in Obesity-Related Inflammation and Insulin Resistance: Cells, Cytokines, and Chemokines. ISRN Inflamm. 2013 Dec 22;2013:1–12.

30. Seki E, De Minicis S, Österreicher CH, Kluwe J, Osawa Y, Brenner DA, et al. TLR4 enhances TGF-β signaling and hepatic fibrosis. Nat Med. 2007 Nov;13(11):1324–32.

31. Kim D, Adejumo AC, Yoo ER, Iqbal U, Li AA, Pham EA, et al. Trends in Mortality From Extrahepatic Complications in Patients With Chronic Liver Disease, From 2007 Through 2017. Gastroenterology. 2019 Oct;157(4):1055-1066.e11.

32. Roca-Fernandez A, Banerjee R, Thomaides-Brears H, Telford A, Sanyal A, Neubauer S, et al. Liver disease is a significant risk factor for cardiovascular outcomes – A UK Biobank study. J Hepatol. 2023 Nov;79(5):1085–95.

33. Baratta F, Pastori D, Angelico F, Balla A, Paganini AM, Cocomello N, et al. Nonalcoholic Fatty Liver Disease and Fibrosis Associated With Increased Risk of Cardiovascular Events in a Prospective Study. Clin Gastroenterol Hepatol. 2020 Sep;18(10):2324-2331.e4.

34. Chen S, Xue H, Huang R, Chen K, Zhang H, Chen X. Associations of MAFLD and MAFLD subtypes with the risk of the incident myocardial infarction and stroke. Diabetes Metab. 2023 Sep;49(5):101468.

35. Li G, Peng Y, Chen Z, Li H, Liu D, Ye X. Bidirectional Association between Hypertension and NAFLD: A Systematic Review and Meta-Analysis of Observational Studies. Galani A, editor. Int J Endocrinol. 2022 Mar 24;2022:1–10.

36. Sartori C, Scherrer U. Insulin, nitric oxide and the sympathetic nervous system: at the crossroads of metabolic and cardiovascular regulation. J Hypertens. 1999 Nov;17(11):1517–25.

37. Harith HH, Di Bartolo BA, Cartland SP, Genner S, Kavurma MM. Insulin promotes vascular smooth muscle cell proliferation and apoptosis via differential regulation of tumor necrosis factor-related apoptosis-inducing ligand: **胰**岛素通过肿瘤坏死因子相关凋亡诱导配体的差异调节来促进血管平滑肌细胞的增殖与凋亡. J Diabetes. 2016 Jul;8(4):568–78.

38. Golubeva JA, Sheptulina AF, Elkina AYu, Liusina EO, Kiselev AR, Drapkina OM. Which Comes First, Nonalcoholic Fatty Liver Disease or Arterial Hypertension? Biomedicines. 2023 Sep 5;11(9):2465.

39. Mantovani A, Zaza G, Byrne CD, Lonardo A, Zoppini G, Bonora E, et al. Nonalcoholic fatty liver disease increases risk of incident chronic kidney disease: A systematic review and meta-analysis. Metabolism. 2018 Feb;79:64–76.

40. Liu HW, Liu JS, Kuo KL. Association of nonalcoholic fatty liver and chronic kidney disease: An analysis of 37,825 cases from health checkup center in Taiwan. Tzu Chi Med J. 2020;32(1):65.

41. Cao Y, Deng Y, Wang J, Zhao H, Zhang J, Xie W. The association between NAFLD and risk of chronic kidney disease: a cross-sectional study. Ther Adv Chronic Dis. 2021 Jan;12:204062232110486.

42. Sung H, Ferlay J, Siegel RL, Laversanne M, Soerjomataram I, Jemal A, et al. Global Cancer Statistics 2020: GLOBOCAN Estimates of Incidence and Mortality Worldwide for 36 Cancers in 185 Countries. CA Cancer J Clin. 2021 May;71(3):209–49.

43. Siegel RL, Giaquinto AN, Jemal A. Cancer statistics, 2024. CA Cancer J Clin. 2024 Jan;74(1):12–49.

44. Villanueva A. Hepatocellular Carcinoma. Longo DL, editor. N Engl J Med. 2019 Apr 11;380(15):1450–62.

45. Powell EE, Cooksley WGE, Hanson R, Searle J, Halliday JW, Powell W. The natural history of nonalcoholic steatohepatitis: A follow-up study of forty-two patients for up to 21 years. Hepatology. 1990 Jan;11(1):74–80.

46. Younossi Z, Stepanova M, Ong JP, Jacobson IM, Bugianesi E, Duseja A, et al. Nonalcoholic Steatohepatitis Is the Fastest Growing Cause of Hepatocellular Carcinoma in Liver Transplant Candidates. Clin Gastroenterol Hepatol. 2019 Mar;17(4):748-755.e3.

47. Zhang QQ, Lu LG. Nonalcoholic Fatty Liver Disease: Dyslipidemia, Risk for Cardiovascular Complications, and Treatment Strategy. J Clin Transl Hepatol. 2015 Mar;3(1):78–84.

48. Mullur R, Liu YY, Brent GA. Thyroid Hormone Regulation of Metabolism. Physiol Rev. 2014 Apr;94(2):355–82.

49. Bano A, Chaker L, Plompen EPC, Hofman A, Dehghan A, Franco OH, et al. Thyroid Function and the Risk of Nonalcoholic Fatty Liver Disease: The Rotterdam Study. J Clin Endocrinol Metab. 2016 Aug;101(8):3204–11.

50. Pagadala MR, Zein CO, Dasarathy S, Yerian LM, Lopez R, McCullough AJ. Prevalence of Hypothyroidism in Nonalcoholic Fatty Liver Disease. Dig Dis Sci. 2012 Feb;57(2):528–34.

51. Manka P, Bechmann L, Best J, Sydor S, Claridge LC, Coombes JD, et al. Low Free Triiodothyronine Is Associated with Advanced Fibrosis in Patients at High Risk for Nonalcoholic Steatohepatitis. Dig Dis Sci. 2019 Aug;64(8):2351–8.

52. Miyake T, Matsuura B, Furukawa S, Todo Y, Yamamoto S, Yoshida O, et al. Hyperthyroidism Improves the Pathological Condition of Nonalcoholic Steatohepatitis: A Case of Nonalcoholic Steatohepatitis with Graves' Disease. Intern Med. 2016;55(15):2019–23.

53. Bruinstroop E, Dalan R, Cao Y, Bee YM, Chandran K, Cho LW, et al. Low-Dose Levothyroxine Reduces Intrahepatic Lipid Content in Patients With Type 2 Diabetes Mellitus and NAFLD. J Clin Endocrinol Metab. 2018 Jul 1;103(7):2698–706.

54. Shin DJ, Osborne TF. Thyroid Hormone Regulation and Cholesterol Metabolism Are Connected through Sterol Regulatory Element-binding Protein-2 (SREBP-2). J Biol Chem. 2003 Sep;278(36):34114–8.

55. Madison BB. Srebp2: A master regulator of sterol and fatty acid synthesis. J Lipid Res. 2016 Mar;57(3):333–5.

56. Lammel Lindemann JA, Angajala A, Engler DA, Webb P, Ayers SD. Thyroid hormone induction of human cholesterol 7 alpha-hydroxylase (Cyp7a1) in vitro. Mol Cell Endocrinol. 2014 May;388(1–2):32–40.

57. Lin JZ, Martagón AJ, Hsueh WA, Baxter JD, Gustafsson JÅ, Webb P, et al. Thyroid Hormone Receptor Agonists Reduce Serum Cholesterol Independent of the LDL Receptor. Endocrinology. 2012 Dec 1;153(12):6136–44.

58. Bonde Y, Plösch T, Kuipers F, Angelin B, Rudling M. Stimulation of murine biliary cholesterol secretion by thyroid hormone is dependent on a functional ABCG5/G8 complex. Hepatology. 2012 Nov;56(5):1828–37.

59. Willard DL, Leung AM, Pearce EN. Thyroid Function Testing in Patients With Newly Diagnosed Hyperlipidemia. JAMA Intern Med. 2014 Feb 1;174(2):287.

60. Perra A, Simbula G, Simbula M, Pibiri M, Kowalik MA, Sulas P, et al. Thyroid hormone (T3) and TRβ agonist GC-1 inhibit/reverse nonalcoholic fatty liver in rats. FASEB J. 2008 Aug;22(8):2981–9.

61. Valdemarsson S, Hansson P, Hedner P, Nilsson-Ehle P. Relations between thyroid function, hepatic and lipoprotein lipase activities, and plasma lipoprotein concentrations. Acta Endocrinol (Copenh). 1983 Sep;104(1):50–6.

62. Brenta G, Berg G, Miksztowicz V, Lopez G, Lucero D, Faingold C, et al. Atherogenic Lipoproteins in Subclinical Hypothyroidism and Their Relationship with Hepatic Lipase Activity: Response to Replacement Treatment with Levothyroxine. Thyroid. 2016 Mar;26(3):365–72.

63. Saggerson ED, Carpenter CA. Carnitine palmitoyltransferase in liver and five extrahepatic tissues in the rat. Inhibition by DL -2-bromopalmitoyl-CoA and effect of hypothyroidism. Biochem J. 1986 May 15;236(1):137–41.

64. Jackson-Hayes L, Song S, Lavrentyev EN, Jansen MS, Hillgartner FB, Tian L, et al. A Thyroid Hormone Response Unit Formed between the Promoter and First Intron of the Carnitine Palmitoyltransferase-Iα Gene Mediates the Liver-specific Induction by Thyroid Hormone. J Biol Chem. 2003 Mar;278(10):7964–72.

65. Mynatt RL, Park EA, Thorngate FE, Das HK, Cook GA. Changes in Carnitine Palmitoyltransferase-I mRNA Abundance Produced by Hyperthyroidism and Hypothyroidism Parallel Changes in Activity. Biochem Biophys Res Commun. 1994 Jun;201(2):932–7.

66. Batchuluun B, Pinkosky SL, Steinberg GR. Lipogenesis inhibitors: therapeutic opportunities and challenges. Nat Rev Drug Discov. 2022 Apr;21(4):283–305.

67. Zhang Y, Yin L, Hillgartner FB. Thyroid Hormone Stimulates Acetyl-CoA Carboxylase-α Transcription in Hepatocytes by Modulating the Composition of Nuclear Receptor Complexes Bound to a Thyroid Hormone Response Element. J Biol Chem. 2001 Jan;276(2):974–83.

68. Hodnett DW, Fantozzi DA, Thurmond DC, Klautky SA, MacPhee KG, Estrem ST, et al. The Chicken Malic Enzyme Gene: Structural Organization and Identification of Triiodothyronine Response Elements in the 5'-Flanking DNA. Arch Biochem Biophys. 1996 Oct;334(2):309–24.

69. Wang Y, Urs S, Kim S, Soltani-Bejnood M, Quigley N, Heo YR, et al. The Human Fatty Acid Synthase Gene and De Novo Lipogenesis Are Coordinately Regulated in Human Adipose Tissue. J Nutr. 2004 May;134(5):1032–8.

70. Petty KJ, Desvergne B, Mitsuhashi T, Nikodem VM. Identification of a thyroid hormone response element in the malic enzyme gene. J Biol Chem. 1990 May;265(13):7395–400.

71. Campbell MC, Anderson GW, Mariash CN. Human Spot 14 Glucose and Thyroid Hormone Response: Characterization and Thyroid Hormone Response Element Identification. Endocrinology. 2003 Dec;144(12):5242–8.

72. Kingwell K. NASH field celebrates 'hurrah moment' with a first FDA drug approval for the liver disease. Nat Rev Drug Discov. 2024 Apr;23(4):235–7.

73. Kádár A, Sánchez E, Wittmann G, Singru PS, Füzesi T, Marsili A, et al. Distribution of hypophysiotropic thyrotropin-releasing hormone (TRH)-synthesizing neurons in the hypothalamic paraventricular nucleus of the mouse. J Comp Neurol. 2010 Oct;518(19):3948–61.

74. Soundarrajan M, Kopp PA. Thyroid Hormone Biosynthesis and Physiology. In: Eaton JL, editor. Thyroid Disease and Reproduction [Internet]. Cham: Springer International Publishing; 2019 [cited 2024 Jan 13]. p. 1–17. Available from: http://link.springer.com/10.1007/978-3-319-99079-8_1

75. Bartalena L, Robbins J. Thyroid Hormone Transport Proteins. Clin Lab Med. 1993 Sep;13(3):583–98.

76. Dyess EM, Segerson TP, Liposits Z, Paull WK, Kaplan MM, Wu P, et al. Triiodothyronine Exerts Direct Cell-Specific Regulation of Thyrotropin-Releasing Hormone Gene Expression in the Hypothalamic Paraventricular Nucleus*. Endocrinology. 1988 Nov;123(5):2291–7.

77. Groeneweg S, Van Geest FS, Peeters RP, Heuer H, Visser WE. Thyroid Hormone Transporters. Endocr Rev. 2020 Apr 1;41(2):146–201.

78. Fagerberg L, Hallström BM, Oksvold P, Kampf C, Djureinovic D, Odeberg J, et al. Analysis of the Human Tissue-specific Expression by Genome-wide Integration of Transcriptomics and Antibody-based Proteomics. Mol Cell Proteomics. 2014 Feb;13(2):397–406.

79. Yue F, Cheng Y, Breschi A, Vierstra J, Wu W, Ryba T, et al. A comparative encyclopedia of DNA elements in the mouse genome. Nature. 2014 Nov 20;515(7527):355–64.

80. Dumitrescu AM, Liao XH, Best TB, Brockmann K, Refetoff S. A Novel Syndrome Combining Thyroid and Neurological Abnormalities Is Associated with Mutations in a Monocarboxylate Transporter Gene. Am J Hum Genet. 2004 Jan;74(1):168–75.

81. Friesema EC, Jansen J, Heuer H, Trajkovic M, Bauer K, Visser TJ. Mechanisms of Disease: psychomotor retardation and high T3 levels caused by mutations in monocarboxylate transporter 8. Nat Clin Pract Endocrinol Metab. 2006 Sep;2(9):512–23.

82. Dumitrescu AM, Liao XH, Weiss RE, Millen K, Refetoff S. Tissue-Specific Thyroid Hormone Deprivation and Excess in Monocarboxylate Transporter (Mct) 8-Deficient Mice. Endocrinology. 2006 Sep 1;147(9):4036–43.

83. Mebis L, Paletta D, Debaveye Y, Ellger B, Langouche L, D'Hoore A, et al. Expression of thyroid hormone transporters during critical illness. Eur J Endocrinol. 2009 Aug;161(2):243–50.

84. Bruinstroop E, Zhou J, Tripathi M, Yau WW, Boelen A, Singh BK, et al. Early induction of hepatic deiodinase type 1 inhibits hepatosteatosis during NAFLD progression. Mol Metab. 2021 Nov;53:101266.

85. Campbell SD, De Morais SM, Xu JJ. Inhibition of human organic anion transporting polypeptide OATP 1B1 as a mechanism of drug-induced hyperbilirubinemia. Chem Biol Interact. 2004 Nov;150(2):179–87.

86. Zhang B, Lauschke VM. Genetic variability and population diversity of the human SLCO (OATP) transporter family. Pharmacol Res. 2019 Jan;139:550–9.

87. Niemi M, Pasanen MK, Neuvonen PJ. Organic Anion Transporting Polypeptide 1B1: a Genetically Polymorphic Transporter of Major Importance for Hepatic Drug Uptake. Koulu M, editor. Pharmacol Rev. 2011 Mar;63(1):157–81.

88. Abe T, Kakyo M, Tokui T, Nakagomi R, Nishio T, Nakai D, et al. Identification of a Novel Gene Family Encoding Human Liver-specific Organic Anion Transporter LST-1. J Biol Chem. 1999 Jun;274(24):17159–63.

89. Hönes GS, Sivakumar RG, Hoppe C, König J, Führer D, Moeller LC. Cell-Specific Transport and Thyroid Hormone Receptor Isoform Selectivity Account for Hepatocyte-Targeted Thyromimetic Action of MGL-3196. Int J Mol Sci. 2022 Nov 8;23(22):13714.

90. Teumer A, Chaker L, Groeneweg S, Li Y, Di Munno C, Barbieri C, et al. Genome-wide analyses identify a role for SLC17A4 and AADAT in thyroid hormone regulation. Nat Commun. 2018 Oct 26;9(1):4455.

91. Stieger B, Hagenbuch B, Landmann L, Höchli M, Schroeder A, Meier PJ. In situ localization of the hepatocytic na+/taurocholate cotransporting polypeptide in rat liver. Gastroenterology. 1994 Dec;107(6):1781–7.

92. Visser WE, Wong WS, Van Mullem AAA, Friesema ECH, Geyer J, Visser TJ. Study of the transport of thyroid hormone by transporters of the SLC10 family. Mol Cell Endocrinol. 2010 Feb;315(1–2):138–45.

93. Friesema ECH, Docter R, Moerings EPCM, Stieger B, Hagenbuch B, Meier PJ, et al. Identification of Thyroid Hormone Transporters. Biochem Biophys Res Commun. 1999 Jan;254(2):497–501.

94. Donkers JM, Roscam Abbing RLP, Van Weeghel M, Levels JHM, Boelen A, Schinkel AH, et al. Inhibition of Hepatic Bile Acid Uptake by Myrcludex B Promotes Glucagon-Like Peptide-1 Release and Reduces Obesity. Cell Mol Gastroenterol Hepatol. 2020;10(3):451–66.

95. Idowu JY, Hagenbuch B. Free Cholesterol Affects the Function and Localization of Human Na+/Taurocholate Cotransporting Polypeptide (NTCP) and Organic Cation Transporter 1 (OCT1). Int J Mol Sci. 2022 Jul 30;23(15):8457.

96. Sinha RA, Bruinstroop E, Singh BK, Yen PM. Nonalcoholic Fatty Liver Disease and Hypercholesterolemia: Roles of Thyroid Hormones, Metabolites, and Agonists. Thyroid. 2019 Sep 1;29(9):1173–91.

97. Berry MJ, Banu L, Larsen PR. Type I iodothyronine deiodinase is a selenocysteine-containing enzyme. Nature. 1991 Jan;349(6308):438–40.

98. Curcio-Morelli C, Gereben B, Zavacki AM, Kim BW, Huang S, Harney JW, et al. In Vivo Dimerization of Types 1, 2, and 3 Iodothyronine Selenodeiodinases. Endocrinology. 2003 Mar 1;144(3):937–46.

99. Bianco AC, Salvatore D, Gereben B, Berry MJ, Larsen PR. Biochemistry, Cellular and Molecular Biology, and Physiological Roles of the Iodothyronine Selenodeiodinases. Endocr Rev. 2002 Feb 1;23(1):38–89.

100. Hernandez A, Martinez ME, Ng L, Forrest D. Thyroid Hormone Deiodinases: Dynamic Switches in Developmental Transitions. Endocrinology. 2021 Aug 1;162(8):bqab091.

101. Baqui MMA, Gereben B, Harney JW, Larsen PR, Bianco AC. Distinct Subcellular Localization of Transiently Expressed Types 1 and 2 Iodothyronine Deiodinases as Determined by Immunofluorescence Confocal Microscopy. Endocrinology. 2000 Nov 1;141(11):4309–12.

102. Baqui M, Botero D, Gereben B, Curcio C, Harney JW, Salvatore D, et al. Human Type 3 Iodothyronine Selenodeiodinase Is Located in the Plasma Membrane and Undergoes Rapid Internalization to Endosomes. J Biol Chem. 2003 Jan;278(2):1206–11.

103. Köhrle J, Frädrich C. Deiodinases control local cellular and systemic thyroid hormone availability. Free Radic Biol Med. 2022 Nov;193:59–79.

104. Theo J Visser. Metabolism of thyroid hormone. In: Cooke, B. A., Van Der Molen, H. J., King, R. J. B., editor. Hormones and Their Actions, Part 1. Elsevier; 1988. p. 81–100.

105. Toyoda N, Zavacki AM, Maia AL, Harney JW, Larsen PR. A Novel Retinoid X Receptor-Independent Thyroid Hormone Response Element Is Present in the Human Type 1 Deiodinase Gene. Mol Cell Biol. 1995 Sep 1;15(9):5100–12.

106. Maia AL, Kieffer JD, Harney JW, Larsen PR. Effect of 3,5,3'-Triiodothyronine (T3) administration on dio1 gene expression and T3 metabolism in normal and type 1 deiodinase-deficient mice. Endocrinology. 1995 Nov;136(11):4842–9.

107. Hönes GS, Rakov H, Logan J, Liao XH, Werbenko E, Pollard AS, et al. Noncanonical thyroid hormone signaling mediates cardiometabolic effects in vivo. Proc Natl Acad Sci [Internet]. 2017 Dec 26 [cited 2024 Feb 7];114(52). Available from: https://pnas.org/doi/full/10.1073/pnas.1706801115

108. Amma LL, Campos-Barros A, Wang Z, Vennström B, Forrest D. Distinct Tissue-Specific Roles for Thyroid Hormone Receptors β and α1 in Regulation of Type 1 Deiodinase Expression. Mol Endocrinol. 2001 Mar 1;15(3):467–75.

109. Panicker V, Cluett C, Shields B, Murray A, Parnell KS, Perry JRB, et al. A Common Variation in Deiodinase 1 Gene DIO1 Is Associated with the Relative Levels of Free Thyroxine and Triiodothyronine. J Clin Endocrinol Metab. 2008 Aug 1;93(8):3075–81.

110. De Jong FJ, Peeters RP, Den Heijer T, Van Der Deure WM, Hofman A, Uitterlinden AG, et al. The Association of Polymorphisms in the Type 1 and 2 Deiodinase Genes with Circulating Thyroid Hormone Parameters and Atrophy of the Medial Temporal Lobe. J Clin Endocrinol Metab. 2007 Feb 1;92(2):636–40.

111. Yamauchi I, Sakane Y, Yamashita T, Hakata T, Sugawa T, Fujita H, et al. Thyroid hormone economy in mice overexpressing iodothyronine deiodinases. FASEB J [Internet]. 2022 Feb [cited 2023 Sep 7];36(2). Available from: https://onlinelibrary.wiley.com/doi/10.1096/fj.202101288RR

112. Chanoine JP, Braverman LE, Farwell AP, Safran M, Alex S, Dubord S, et al. The thyroid gland is a major source of circulating T3 in the rat. J Clin Invest. 1993 Jun 1;91(6):2709–13.

113. França MM, German A, Fernandes GW, Liao XH, Bianco AC, Refetoff S, et al. Human Type 1 Iodothyronine Deiodinase (*DIO1*) Mutations Cause Abnormal Thyroid Hormone Metabolism. Thyroid. 2021 Feb 1;31(2):202–7.

114. Schoenmakers CH, Pigmans IG, Poland A, Visser TJ. Impairment of the selenoenzyme type I iodothyronine deiodinase in C3H/He mice. Endocrinology. 1993 Jan;132(1):357–61.

115. Fonseca TL, Fernandes GW, McAninch EA, Bocco BMLC, Abdalla SM, Ribeiro MO, et al. Perinatal deiodinase 2 expression in hepatocytes defines epigenetic susceptibility to liver steatosis and obesity. Proc Natl Acad Sci. 2015 Nov 10;112(45):14018–23.

116. Bates JM, St. Germain DL, Galton VA. Expression Profiles of the Three Iodothyronine Deiodinases, D1, D2, and D3, in the Developing Rat [1]. Endocrinology. 1999 Feb;140(2):844–51.

117. Hernandez A. Type 3 deiodinase is critical for the maturation and function of the thyroid axis. J Clin Invest. 2006 Jan 19;116(2):476–84.

118. Lazar MA. Thyroid Hormone Receptors: Multiple Forms, Multiple Possibilities*. Endocr Rev. 1993 Apr;14(2):184–93.

119. Zhang X kun, Hoffmann B, Tran PBV, Graupner G, Pfahl M. Retinoid X receptor is an auxiliary protein for thyroid hormone and retinoic acid receptors. Nature. 1992 Jan;355(6359):441–6.

120. Koenig RJ. Thyroid Hormone Receptor Coactivators and Corepressors. Thyroid. 1998 Aug;8(8):703–13.

121. Dore R, Watson L, Hollidge S, Krause C, Sentis SC, Oelkrug R, et al. Resistance to thyroid hormone induced tachycardia in RTHα syndrome. Nat Commun. 2023 Jun 7;14(1):3312.

122. Manka P, Coombes JD, Sydor S, Swiderska-Syn MK, Best J, Gauthier K, et al. Thyroid hormone receptor alpha modulates fibrogenesis in hepatic stellate cells. Liver Int. 2024 Jan;44(1):125–38.

123. Yen PM, Sunday ME, Darling DS, Chin WW. Isoform-specific thyroid hormone receptor antibodies detect multiple thyroid hormone receptors in rat and human pituitaries. Endocrinology. 1992 Mar;130(3):1539–46.

124. Sjöberg M, Vennström B, Forrest D. Thyroid hormone receptors in chick retinal development: differential expression of mRNAs for *α* and N-terminal variant *β* receptors. Development. 1992 Jan 1;114(1):39–47.

125. Bradley DJ, Towle HC, Young WS. Alpha and beta thyroid hormone receptor (TR) gene expression during auditory neurogenesis: evidence for TR isoform-specific transcriptional regulation in vivo. Proc Natl Acad Sci. 1994 Jan 18;91(2):439–43.

126. Forrest D, Hanebuth E, Smeyne RJ, Everds N, Stewart CL, Wehner JM, et al. Recessive resistance to thyroid hormone in mice lacking thyroid hormone receptor beta: evidence for tissue-specific modulation of receptor function. EMBO J. 1996 Jun 17;15(12):3006–15.

127. Ferrara AM, Onigata K, Ercan O, Woodhead H, Weiss RE, Refetoff S. Homozygous Thyroid Hormone Receptor β-Gene Mutations in Resistance to Thyroid Hormone: Three New Cases and Review of the Literature. J Clin Endocrinol Metab. 2012 Apr;97(4):1328–36.

128. Takeda K, Sakurai A, DeGroot LJ, Refetoff S. Recessive inheritance of thyroid hormone resistance caused by complete deletion of the protein-coding region of the thyroid hormone receptor-beta gene. J Clin Endocrinol Metab. 1992 Jan;74(1):49–55.

129. Flores-Morales A, Gullberg H, Fernandez L, Ståhlberg N, Lee NH, Vennström B, et al. Patterns of Liver Gene Expression Governed by TRβ. Mol Endocrinol. 2002 Jun;16(6):1257–68.

130. Yen PM, Feng X, Flamant F, Chen Y, Walker RL, Weiss RE, et al. Effects of ligand and thyroid hormone receptor isoforms on hepatic gene expression profiles of thyroid hormone receptor knockout mice. EMBO Rep. 2003 Jun;4(6):581–7.

131. Dore R, Sentis SC, Johann K, Lopez-Alcantara N, Resch J, Chandrasekar A, et al. Partial resistance to thyroid hormone-induced tachycardia and cardiac hypertrophy in mice lacking thyroid hormone receptor β. Thyroid®. 2024 Mar 25;thy.2023.0638.

132. Gauthier K. Different functions for the thyroid hormone receptors TRalpha and TRbeta in the control of thyroid hormone production and post-natal development. EMBO J. 1999 Feb 1;18(3):623–31.

133. Alonso-Merino E, Martín Orozco R, Ruíz-Llorente L, Martínez-Iglesias OA, Velasco-Martín JP, Montero-Pedrazuela A, et al. Thyroid hormones inhibit TGF-β signaling and attenuate fibrotic responses. Proc Natl Acad Sci [Internet]. 2016 Jun 14 [cited 2024 May 5];113(24). Available from: https://pnas.org/doi/full/10.1073/pnas.1506113113

134. Vatner DF, Weismann D, Beddow SA, Kumashiro N, Erion DM, Liao XH, et al. Thyroid hormone receptor-β agonists prevent hepatic steatosis in fat-fed rats but impair insulin sensitivity via discrete pathways. Am J Physiol-Endocrinol Metab. 2013 Jul 1;305(1):E89–100.

135. Berkenstam A, Kristensen J, Mellström K, Carlsson B, Malm J, Rehnmark S, et al. The thyroid hormone mimetic compound KB2115 lowers plasma LDL cholesterol and stimulates bile acid synthesis without cardiac effects in humans. Proc Natl Acad Sci. 2008 Jan 15;105(2):663–7.

136. Ladenson PW, Kristensen JD, Ridgway EC, Olsson AG, Carlsson B, Klein I, et al. Use of the Thyroid Hormone Analogue Eprotirome in Statin-Treated Dyslipidemia. N Engl J Med. 2010 Mar 11;362(10):906–16.

137. Angelin B, Kristensen JD, Eriksson M, Carlsson B, Klein I, Olsson AG, et al. Reductions in serum levels of LDL cholesterol, apolipoprotein B, triglycerides and lipoprotein(a) in hypercholesterolaemic patients treated with the liver-selective thyroid hormone receptor agonist eprotirome. J Intern Med. 2015 Mar;277(3):331–42.

138. Chiellini G, Apriletti JW, Yoshihara HA, Baxter JD, Ribeiro RCJ, Scanlan TS. A high-affinity subtype-selective agonist ligand for the thyroid hormone receptor. Chem Biol. 1998 Jun;5(6):299–306.

139. Trost SU, Swanson E, Gloss B, Wang-Iverson DB, Zhang H, Volodarsky T, et al. The Thyroid Hormone Receptor-β-Selective Agonist GC-1 Differentially Affects Plasma Lipids and Cardiac Activity [1]. Endocrinology. 2000 Sep;141(9):3057–64.

140. Grover GJ, Egan DM, Sleph PG, Beehler BC, Chiellini G, Nguyen NH, et al. Effects of the Thyroid Hormone Receptor Agonist GC-1 on Metabolic Rate and Cholesterol in Rats and Primates: Selective Actions Relative to 3,5,3'-Triiodo- L -Thyronine. Endocrinology. 2004 Apr;145(4):1656–61.

141. Columbano A, Pibiri M, Deidda M, Cossu C, Scanlan TS, Chiellini G, et al. The Thyroid Hormone Receptor-β Agonist GC-1 Induces Cell Proliferation in Rat Liver and Pancreas. Endocrinology. 2006 Jul;147(7):3211–8.

142. Puliga E, Min Q, Tao J, Zhang R, Pradhan-Sundd T, Poddar M, et al. Thyroid Hormone Receptor-β Agonist GC-1 Inhibits Met-β-Catenin–Driven Hepatocellular Cancer. Am J Pathol. 2017 Nov;187(11):2473–85.

143. Amorim BS, Ueta CB, Freitas BCG, Nassif RJ, Gouveia CHDA, Christoffolete MA, et al. A TRβ-selective agonist confers resistance to diet-induced obesity. J Endocrinol. 2009 Nov;203(2):291–9.

144. Teufel A, Itzel T, Erhart W, Brosch M, Wang XY, Kim YO, et al. Comparison of Gene Expression Patterns Between Mouse Models of Nonalcoholic Fatty Liver Disease and Liver Tissues From Patients. Gastroenterology. 2016 Sep;151(3):513-525.e0.

145. Tsuchida T, Lee YA, Fujiwara N, Ybanez M, Allen B, Martins S, et al. A simple diet- and chemical-induced murine NASH model with rapid progression of steatohepatitis, fibrosis and liver cancer. J Hepatol. 2018 Aug;69(2):385–95.

146. Yang P, Wang Y, Tang W, Sun W, Ma Y, Lin S, et al. Western diet induces severe nonalcoholic steatohepatitis, ductular reaction, and hepatic fibrosis in liver CGI-58 knockout mice. Sci Rep. 2020 Mar 13;10(1):4701.

147. Kohli R, Kirby M, Xanthakos SA, Softic S, Feldstein AE, Saxena V, et al. High-fructose, medium chain trans fat diet induces liver fibrosis and elevates plasma coenzyme Q9 in a novel murine model of obesity and nonalcoholic steatohepatitis. Hepatology. 2010 Sep;52(3):934–44.

148. Charlton M, Krishnan A, Viker K, Sanderson S, Cazanave S, McConico A, et al. Fast food diet mouse: novel small animal model of NASH with ballooning, progressive fibrosis, and high physiological fidelity to the human condition. Am J Physiol-Gastrointest Liver Physiol. 2011 Nov;301(5):G825–34.

149. Ikawa-Yoshida A, Matsuo S, Kato A, Ohmori Y, Higashida A, Kaneko E, et al. Hepatocellular carcinoma in a mouse model fed a choline-deficient, L-amino acid-defined, high-fat diet. Int J Exp Pathol. 2017 Aug;98(4):221–33.

150. Matsumoto M, Hada N, Sakamaki Y, Uno A, Shiga T, Tanaka C, et al. An improved mouse model that rapidly develops fibrosis in non-alcoholic steatohepatitis. Int J Exp Pathol. 2013 Apr;94(2):93–103.

151. Suzuki-Kemuriyama N, Abe A, Nakane S, Uno K, Ogawa S, Watanabe A, et al. Nonobese mice with nonalcoholic steatohepatitis fed on a choline-deficient, L-amino acid-defined, high-fat diet exhibit alterations in signaling pathways. FEBS Open Bio. 2021 Nov;11(11):2950–65.

152. Geißler C, Krause C, Neumann AM, Britsemmer JH, Taege N, Grohs M, et al. Dietary induction of obesity and insulin resistance is associated with changes in Fgf21 DNA methylation in liver of mice. J Nutr Biochem. 2022 Feb;100:108907.

153. Hayashi Y, Mori Y, Janssen OE, Sunthornthepvarakul T, Weiss RE, Takeda K, et al. Human thyroxine-binding globulin gene: complete sequence and transcriptional regulation. Mol Endocrinol. 1993 Aug;7(8):1049–60.

154. Yan Z, Yan H, Ou H. Human thyroxine binding globulin (TBG) promoter directs efficient and sustaining transgene expression in liver-specific pattern. Gene. 2012 Sep;506(2):289–94.

155. Heldmaier G. The influence of the social thermoregulation on the cold-adaptive growth of BAT in hairless and furred mice. Pfl□gers Arch Eur J Physiol. 1975;355(3):261–6.

156. Oelkrug R, Mittag J. An improved method for the precise unravelment of non-shivering brown fat thermokinetics. Sci Rep. 2021 Feb 26;11(1):4799.

157. Pfaffl MW, Tichopad A, Prgomet C, Neuvians TP. Determination of stable housekeeping genes, differentially regulated target genes and sample integrity: BestKeeper – Excel-based tool using pair-wise correlations. Biotechnol Lett. 2004 Mar;26(6):509–15.

158. Nicolaisen TS, Klein AB, Dmytriyeva O, Lund J, Ingerslev LR, Fritzen AM, et al. Thyroid hormone receptor α in skeletal muscle is essential for T3-mediated increase in energy expenditure. FASEB J. 2020 Nov;34(11):15480–91.

159. Wirth EK, Rijntjes E, Meyer F, Köhrle J, Schweizer U. High T3, Low T4 Serum Levels in Mct8 Deficiency Are Not Caused by Increased Hepatic Conversion through Type I Deiodinase. Eur Thyroid J. 2015;4(Suppl. 1):87–91.

160. Renko K, Kerp H, Pape J, Rijntjes E, Burgdorf T, Führer D, et al. Tentative Application of a Streamlined Protocol to Determine Organ-Specific Regulations of Deiodinase 1 and Dehalogenase Activities as Readouts of the Hypothalamus-Pituitary-Thyroid-Periphery-Axis. Front Toxicol. 2022 Mar 21;4:822993.

161. De Vries EM, Eggels L, Van Beeren HC, Ackermans MT, Kalsbeek A, Fliers E, et al. Fasting-Induced Changes in Hepatic Thyroid Hormone Metabolism in Male Rats Are Independent of Autonomic Nervous Input to the Liver. Endocrinology. 2014 Dec 1;155(12):5033–41.

162. Boelen A, Van Der Spek AH, Bloise F, De Vries EM, Surovtseva OV, Van Beeren M, et al. Tissue thyroid hormone metabolism is differentially regulated during illness in mice. J Endocrinol. 2017 Apr;233(1):25–36.

163. Sentis SC, Dore R, Oelkrug R, Kolms B, Iwen KA, Mittag J. Hypothalamic Thyroid Hormone Receptor α1 Signaling Controls Body Temperature. Thyroid®. 2024 Feb 1;34(2):243–51.

164. Swoap SJ, Li C, Wess J, Parsons AD, Williams TD, Overton JM. Vagal tone dominates autonomic control of mouse heart rate at thermoneutrality. Am J Physiol-Heart Circ Physiol. 2008 Apr;294(4):H1581–8.

165. Fischer AW, Cannon B, Nedergaard J. The answer to the question “What is the best housing temperature to translate mouse experiments to humans?” is: thermoneutrality. Mol Metab. 2019 Aug;26:1–3.

166. Ganeshan K, Chawla A. Warming the mouse to model human diseases. Nat Rev Endocrinol. 2017 Aug;13(8):458–65.

167. Giles DA, Moreno-Fernandez ME, Stankiewicz TE, Graspeuntner S, Cappelletti M, Wu D, et al. Thermoneutral housing exacerbates nonalcoholic fatty liver disease in mice and allows for sex-independent disease modeling. Nat Med. 2017 Jul 1;23(7):829–38.

168. Püschel GP. Control of hepatocyte metabolism by sympathetic and parasympathetic hepatic nerves. Anat Rec A Discov Mol Cell Evol Biol. 2004 Sep;280A(1):854–67.

169. Raubenheimer PJ, Nyirenda MJ, Walker BR. A Choline-Deficient Diet Exacerbates Fatty Liver but Attenuates Insulin Resistance and Glucose Intolerance in Mice Fed a High-Fat Diet. Diabetes. 2006 Jul 1;55(7):2015–20.

170. Oelkrug R, Krause C, Herrmann B, Resch J, Gachkar S, El Gammal AT, et al. Maternal Brown Fat Thermogenesis Programs Glucose Tolerance in the Male Offspring. Cell Rep. 2020 Nov;33(5):108351.

171. Liang W, Menke AL, Driessen A, Koek GH, Lindeman JH, Stoop R, et al. Establishment of a General NAFLD Scoring System for Rodent Models and Comparison to Human Liver Pathology. Sookoian SC, editor. PLoS ONE. 2014 Dec 23;9(12):e115922.

172. Sands MS. AAV-Mediated Liver-Directed Gene Therapy. In: Snyder RO, Moullier P, editors. Adeno-Associated Virus [Internet]. Totowa, NJ: Humana Press; 2012 [cited 2023 Sep 7]. p. 141–57. (Methods in Molecular Biology; vol. 807). Available from: https://link.springer.com/10.1007/978-1-61779-370-7_6

173. Warner A, Mittag J. Thyroid hormone and the central control of homeostasis. J Mol Endocrinol. 2012 Aug;49(1):R29–35.

174. Moravcová A, Červinková Z, Kučera O, Mezera V, Rychtrmoc D, Lotková H. The Effect of Oleic and Palmitic Acid on Induction of Steatosis and Cytotoxicity on Rat Hepatocytes in Primary Culture. Physiol Res. 2015 Dec 30;S627–36.

175. Woods CP, Hazlehurst JM, Tomlinson JW. Glucocorticoids and non-alcoholic fatty liver disease. J Steroid Biochem Mol Biol. 2015 Nov;154:94–103.

176. Utzschneider KM, Kahn SE. The Role of Insulin Resistance in Nonalcoholic Fatty Liver Disease. J Clin Endocrinol Metab. 2006 Dec 1;91(12):4753–61.

177. Davidson MD, Ballinger KR, Khetani SR. Long-term exposure to abnormal glucose levels alters drug metabolism pathways and insulin sensitivity in primary human hepatocytes. Sci Rep. 2016 Jun 17;6(1):28178.

178. Casula M, Mozzanica F, Scotti L, Tragni E, Pirillo A, Corrao G, et al. Statin use and risk of new-onset diabetes: A meta-analysis of observational studies. Nutr Metab Cardiovasc Dis. 2017 May;27(5):396–406.

179. Silvestri E, Lombardi A, De Lange P, Schiavo L, Lanni A, Goglia F, et al. Age-related changes in renal and hepatic cellular mechanisms associated with variations in rat serum thyroid hormone levels. Am J Physiol-Endocrinol Metab. 2008 Jun;294(6):E1160–8.

180. Muhič M, Vardjan N, Chowdhury HH, Zorec R, Kreft M. Insulin and Insulin-like Growth Factor 1 (IGF-1) Modulate Cytoplasmic Glucose and Glycogen Levels but Not Glucose Transport across the Membrane in Astrocytes. J Biol Chem. 2015 Apr;290(17):11167–76.

181. Spadaro O, Camell CD, Bosurgi L, Nguyen KY, Youm YH, Rothlin CV, et al. IGF1 Shapes Macrophage Activation in Response to Immunometabolic Challenge. Cell Rep. 2017 Apr;19(2):225–34.

182. Takahashi Y. The Role of Growth Hormone and Insulin-Like Growth Factor-I in the Liver. Int J Mol Sci. 2017 Jul 5;18(7):1447.

183. Martitz J, Becker NP, Renko K, Stoedter M, Hybsier S, Schomburg L. Gene-specific regulation of hepatic selenoprotein expression by interleukin-6. Metallomics. 2015;7(11):1515–21.

184. Carow B, Rottenberg ME. SOCS3, a Major Regulator of Infection and Inflammation. Front Immunol [Internet]. 2014 [cited 2024 Apr 21];5. Available from: http://journal.frontiersin.org/article/10.3389/fimmu.2014.00058/abstract

185. Zhang L, Badgwell DB, Bevers JJ, Schlessinger K, Murray PJ, Levy DE, et al. IL-6 signaling via the STAT3/SOCS3 pathway: Functional Analysis of the Conserved STAT3 N-domain. Mol Cell Biochem. 2006 Aug;288(1–2):179–89.

186. Yao S, Gao M, Wang Z, Wang W, Zhan L, Wei B. Upregulation of MicroRNA-34a Sensitizes Ovarian Cancer Cells to Resveratrol by Targeting Bcl-2. Yonsei Med J. 2021;62(8):691.

187. Zhao Y, Wang X. miR-34a targets BCL-2 to suppress the migration and invasion of sinonasal squamous cell carcinoma. Oncol Lett [Internet]. 2018 Sep 11 [cited 2024 Jun 13]; Available from: http://www.spandidos-publications.com/10.3892/ol.2018.9427

188. Zhao M, Qi Q, Liu S, Huang R, Shen J, Zhu Y, et al. MicroRNA-34a: A Novel Therapeutic Target in Fibrosis. Front Physiol. 2022 Jun 20;13:895242.

189. Zhou M, Liu B, Ye HM, Hou JN, Huang YC, Zhang P, et al. ROS-induced imbalance of the miR-34a-5p/SIRT1/p53 axis triggers chronic chondrocyte injury and inflammation. Heliyon. 2024 Jun;10(11):e31654.

190. Deng XJ, Zheng HL, Ke XQ, Deng M, Ma ZZ, Zhu Y, et al. Hsa-miR-34a-5p reverses multidrug resistance in gastric cancer cells by targeting the 3′-UTR of SIRT1 and inhibiting its expression. Cell Signal. 2021 Aug;84:110016.

191. Sun W, Nie T, Li K, Wu W, Long Q, Feng T, et al. Hepatic CPT1A Facilitates Liver–Adipose Cross Talk via Induction of FGF21 in Mice. Diabetes. 2022 Jan 1;71(1):31–42.

192. Kim H. The transcription cofactor CRTC1 protects from aberrant hepatic lipid accumulation. Sci Rep. 2016 Nov 21;6(1):37280.

193. Chaves C, Bruinstroop E, Refetoff S, Yen PM, Anselmo J. Increased Hepatic Fat Content in Patients with Resistance to Thyroid Hormone Beta. Thyroid. 2021 Jul 1;31(7):1127–34.

194. Chalasani N, Younossi Z, Lavine JE, Charlton M, Cusi K, Rinella M, et al. The diagnosis and management of nonalcoholic fatty liver disease: Practice guidance from the American Association for the Study of Liver Diseases. Hepatology. 2018 Jan;67(1):328–57.

195. Škop V, Guo J, Liu N, Xiao C, Hall KD, Gavrilova O, et al. Mouse Thermoregulation: Introducing the Concept of the Thermoneutral Point. Cell Rep. 2020 Apr;31(2):107501.

196. Maloney SK, Fuller A, Mitchell D, Gordon C, Overton JM. Translating Animal Model Research: Does It Matter That Our Rodents Are Cold? Physiology. 2014 Nov;29(6):413–20.

197. Stemmer K, Kotzbeck P, Zani F, Bauer M, Neff C, Müller TD, et al. Thermoneutral housing is a critical factor for immune function and diet-induced obesity in C57BL/6 nude mice. Int J Obes. 2015 May;39(5):791–7.

198. Giles DA, Ramkhelawon B, Donelan EM, Stankiewicz TE, Hutchison SB, Mukherjee R, et al. Modulation of ambient temperature promotes inflammation and initiates atherosclerosis in wild type C57BL/6 mice. Mol Metab. 2016 Nov;5(11):1121–30.

199. Gordon CJ. Thermal physiology of laboratory mice: Defining thermoneutrality. J Therm Biol. 2012 Dec;37(8):654–85.

200. Kartsoli S, Kostara CE, Tsimihodimos V, Bairaktari ET, Christodoulou DK. Lipidomics in non-alcoholic fatty liver disease. World J Hepatol. 2020 Aug 27;12(8):436–50.

201. Heinonen I, Rinne P, Ruohonen ST, Ruohonen S, Ahotupa M, Savontaus E. The effects of equal caloric high fat and western diet on metabolic syndrome, oxidative stress and vascular endothelial function in mice. Acta Physiol. 2014 Jul;211(3):515–27.

202. Rizki G, Arnaboldi L, Gabrielli B, Yan J, Lee GS, Ng RK, et al. Mice fed a lipogenic methionine-choline-deficient diet develop hypermetabolism coincident with hepatic suppression of SCD-1. J Lipid Res. 2006 Oct;47(10):2280–90.

203. Kucsera D, Tóth VE, Gergő D, Vörös I, Onódi Z, Görbe A, et al. Characterization of the CDAA Diet-Induced Non-alcoholic Steatohepatitis Model: Sex-Specific Differences in Inflammation, Fibrosis, and Cholesterol Metabolism in Middle-Aged Mice. Front Physiol. 2021 Feb 22;12:609465.

204. Miura K, Kodama Y, Inokuchi S, Schnabl B, Aoyama T, Ohnishi H, et al. Toll-Like Receptor 9 Promotes Steatohepatitis by Induction of Interleukin-1β in Mice. Gastroenterology. 2010 Jul;139(1):323-334.e7.

205. Yasuda D, Torii H, Shimizu R, Hiraoka Y, Kume N. Reduced Serum Cholesterol and Triglyceride Levels in a Choline-Deficient L-Amino Acid-Defined High-Fat Diet (CDAHFD)-Induced Mouse Model of Non-alcoholic Steatohepatitis (NASH). Biol Pharm Bull. 2020 Apr 1;43(4):616–8.

206. Hasty AH, Shimano H, Osuga J ichi, Namatame I, Takahashi A, Yahagi N, et al. Severe Hypercholesterolemia, Hypertriglyceridemia, and Atherosclerosis in Mice Lacking Both Leptin and the Low Density Lipoprotein Receptor. J Biol Chem. 2001 Oct;276(40):37402–8.

207. Kobayashi K, Forte TM, Taniguchi S, Ishida BY, Oka K, Chan L. The db/db mouse, a model for diabetic dyslipidemia: Molecular characterization and effects of western diet feeding. Metabolism. 2000 Jan;49(1):22–31.

208. Suriano F, Vieira-Silva S, Falony G, Roumain M, Paquot A, Pelicaen R, et al. Novel insights into the genetically obese (ob/ob) and diabetic (db/db) mice: two sides of the same coin. Microbiome. 2021 Dec;9(1):147.

209. Weiss RE, Forrest D, Pohlenz J, Cua K, Curran T, Refetoff S. Thyrotropin Regulation by Thyroid Hormone in Thyroid Hormone Receptor β-Deficient Mice [1]. Endocrinology. 1997 Sep;138(9):3624–9.

210. Tiniakos DG. Nonalcoholic fatty liver disease/nonalcoholic steatohepatitis: histological diagnostic criteria and scoring systems: Eur J Gastroenterol Hepatol. 2009 May;1.

211. Park SR, Cho CS, Xi J, Kang HM, Lee JH. Holistic characterization of single-hepatocyte transcriptome responses to high-fat diet. Am J Physiol-Endocrinol Metab. 2021 Feb 1;320(2):E244–58.

212. Birchmeier W. Orchestrating Wnt signalling for metabolic liver zonation. Nat Cell Biol. 2016 May;18(5):463–5.

213. Cunningham RP, Porat-Shliom N. Liver Zonation – Revisiting Old Questions With New Technologies. Front Physiol. 2021 Sep 9;12:732929.

214. Hall A, Covelli C, Manuguerra R, Luong TV, Buzzetti E, Tsochatzis E, et al. Transaminase abnormalities and adaptations of the liver lobule manifest at specific cut-offs of steatosis. Sci Rep. 2017 Jan 20;7(1):40977.

215. Santos AA, Delgado TC, Marques V, Ramirez-Moncayo C, Alonso C, Vidal-Puig A, et al. Spatial metabolomics and its application in the liver. Hepatology. 2024 May;79(5):1158–79.

216. Kannt A, Wohlfart P, Madsen AN, Veidal SS, Feigh M, Schmoll D. Activation of thyroid hormone receptor-β improved disease activity and metabolism independent of body weight in a mouse model of non-alcoholic steatohepatitis and fibrosis. Br J Pharmacol. 2021 Jun;178(12):2412–23.

217. Tsatsos NG, Augustin LB, Anderson GW, Towle HC, Mariash CN. Hepatic Expression of the SPOT 14 (S14) Paralog S14-Related (Mid1 Interacting Protein) Is Regulated by Dietary Carbohydrate. Endocrinology. 2008 Oct 1;149(10):5155–61.

218. Moreau A, Téruel C, Beylot M, Albalea V, Tamasi V, Umbdenstock T, et al. A novel pregnane X receptor and S14-mediated lipogenic pathway in human hepatocyte. Hepatology. 2009 Jun;49(6):2068–79.

219. Bruinstroop E, Van Der Spek AH, Boelen A. Role of hepatic deiodinases in thyroid hormone homeostasis and liver metabolism, inflammation, and fibrosis. Eur Thyroid J. 2023 Mar 9;12(3):e220211.

220. Barnhoorn S, Meima ME, Peeters RP, Darras VM, Leeuwenburgh S, Hoeijmakers JHJ, et al. Decreased hepatic thyroid hormone signaling in systemic and liver-specific but not brain-specific accelerated aging due to DNA repair deficiency in mice. Eur Thyroid J. 2023 Oct 25;12(6):e220231.

221. Araujo RL, De Andrade BM, De Figueiredo ÁSP, Da Silva ML, Marassi MP, Dos Santos Pereira V, et al. Low replacement doses of thyroxine during food restriction restores type 1 deiodinase activity in rats and promotes body protein loss. J Endocrinol. 2008 Jul;198(1):119–25.

222. Liu J, Hernandez-Ono A, Graham MJ, Galton VA, Ginsberg HN. Type 1 *Deiodinase* Regulates *ApoA-I* Gene Expression and ApoA-I Synthesis Independent of Thyroid Hormone Signaling. Arterioscler Thromb Vasc Biol. 2016 Jul;36(7):1356–66.

223. Zufferey R, Donello JE, Trono D, Hope TJ. Woodchuck Hepatitis Virus Posttranscriptional Regulatory Element Enhances Expression of Transgenes Delivered by Retroviral Vectors. J Virol. 1999 Apr;73(4):2886–92.

224. Mastroyiannopoulos NP, Feldman ML, Uney JB, Mahadevan MS, Phylactou LA. Woodchuck post-transcriptional element induces nuclear export of myotonic dystrophy 3' untranslated region transcripts. EMBO Rep. 2005 May;6(5):458–63.

225. Kwakkel J, Wiersinga WM, Boelen A. Differential involvement of nuclear factor-κB and activator protein-1 pathways in the interleukin-1β-mediated decrease of deiodinase type 1 and thyroid hormone receptor β1 mRNA. J Endocrinol. 2006 Apr;189(1):37–44.

226. Jakobs T, Mentrup B, Schmutzler C, Dreher I, Kohrle J. Proinflammatory cytokines inhibit the expression and function of human type I 5'-deiodinase in HepG2 hepatocarcinoma cells. Eur J Endocrinol. 2002 Apr 1;559–66.

227. Yu J, Koenig RJ. Regulation of Hepatocyte Thyroxine 5'-Deiodinase by T3 and Nuclear Receptor Coactivators as a Model of the Sick Euthyroid Syndrome. J Biol Chem. 2000 Dec;275(49):38296–301.

228. Bernardo BC, Gregorevic P, Ritchie RH, McMullen JR. Generation of MicroRNA-34 Sponges and Tough Decoys for the Heart: Developments and Challenges. Front Pharmacol. 2018 Sep 21;9:1090.

229. Kester MHA, Toussaint MJM, Punt CA, Matondo R, Aarnio AM, Darras VM, et al. Large Induction of Type III Deiodinase Expression After Partial Hepatectomy in the Regenerating Mouse and Rat Liver. Endocrinology. 2009 Jan 1;150(1):540–5.

230. Day K, Seale LA, Graham RM, Cardoso BR. Selenotranscriptome Network in Non-alcoholic Fatty Liver Disease. Front Nutr. 2021 Nov 17;8:744825.

231. Tanimizu N, Miyajima A. Molecular Mechanism of Liver Development and Regeneration. In: International Review of Cytology [Internet]. Elsevier; 2007 [cited 2024 May 7]. p. 1–48. Available from: https://linkinghub.elsevier.com/retrieve/pii/S0074769606590011

232. EASL–EASD–EASO Clinical Practice Guidelines for the management of non-alcoholic fatty liver disease. J Hepatol. 2016 Jun;64(6):1388–402.

Appendix

Table S 1| Statistical analysis details

<table>
<tr><th colspan="8">Figure 4: – Impact of MASH diet on TRβ knockout mice</th></tr>
<tr><td colspan="8">Figure 4B</td></tr>
<tr><td colspan="2" rowspan="2">Gene</td><td colspan="6">Simple linear regression</td></tr>
<tr><td>Diet</td><td colspan="2">F (DFn, DFd)</td><td>Equation</td><td>R²</td><td>P value</td></tr>
<tr><td colspan="2" rowspan="8">Thrb1</td><td>Control</td><td colspan="2">F (1, 9) = 16,09</td><td>Y = -0.07095*X + 2.095</td><td>0.6414</td><td>0.0031 (**)</td></tr>
<tr><td>CD-HFD</td><td colspan="2">F (1, 12) = 1,453</td><td>Y = -0.02805*X + 1.206</td><td>0.1080</td><td>0.2513</td></tr>
<tr><td colspan="6">Differences in the lines</td></tr>
<tr><td colspan="3">Slope</td><td colspan="3">Elevation or intercepts</td></tr>
<tr><td colspan="2">F (DFn, DFd)</td><td>P value</td><td>F (DFn, DFd)</td><td colspan="2">P value</td></tr>
<tr><td colspan="2">F (1, 21) = 0.1774</td><td>0.1774</td><td>F (1, 22) = 11.35</td><td colspan="2">0.0028 (**)</td></tr>
<tr><td colspan="6">2-way ANOVA</td></tr>
<tr><td colspan="2">Interaction</td><td colspan="2">Time</td><td colspan="2">Diet</td></tr>
<tr><td>F (2, 19) = 1.146</td><td>P=0.3391</td><td>F (2, 19) = 4.879</td><td>P=0.0195 (*)</td><td>F (1, 19) = 8.508</td><td>P=0.0088 (**)</td></tr>
<tr><td colspan="8">Figure 4C</td></tr>
<tr><td colspan="2" rowspan="2">Parameter</td><td colspan="6">2-way ANOVA, post hoc: Tukey's[1] or Šídák's[2] multiple comparisons test</td></tr>
<tr><td colspan="2">Interaction</td><td colspan="2">Genotype</td><td colspan="2">Diet</td></tr>
<tr><td rowspan="3">Delta Body mass (g)</td><td>4w[1]</td><td>F (1, 48) = 0.0055</td><td>P=0.9412</td><td>F (1, 48) = 7.935</td><td>P=0.0070 (**)</td><td>F (1, 48) = 51.50</td><td>P<0.0001 (****)</td></tr>
<tr><td>8w[1]</td><td>F (1, 25) = 3.471</td><td>P=0.0743</td><td>F (1, 25) = 10.15</td><td>P=0.0038 (**)</td><td>F (1, 25) = 36.71</td><td>P<0.0001 (****)</td></tr>
<tr><td>16w[1]</td><td>F (1, 8) = 13.33</td><td>P=0.0065 (**)</td><td>F (1, 8) = 23.94</td><td>P=0.0012 (**)</td><td>F (1, 8) = 6.908</td><td>P=0.0303 (*)</td></tr>
<tr><td>Kcal/day/BW</td><td>4w[2]</td><td>F (1, 49) = 0.7909</td><td>P=0.3782</td><td>F (1, 49) = 0.0525</td><td>P=0.8197</td><td>F (1, 49) = 16.88</td><td>P=0.0002 (***)</td></tr>
</table>

	8w[2]	F (1, 26) = 1.129	P=0.2978	F (1, 26) = 0.2575	P=0.6161	F (1, 26) = 36.45	P<0.0001 (****)
	16w[1]	F (1, 9) = 0.4136	P=0.5362	F (1, 9) = 9.741	P=0.0123 (*)	F (1, 9) = 61.97	P<0.0001 (****)
Fat %	4w[1]	F (1, 26) = 0.3303	P=0.5704	F (1, 26) = 15.64	P=0.0005 (***)	F (1, 26) = 15.44	P=0.0006 (***)
	8w[1]	F (1, 8) = 0.0016	P=0.9690	F (1, 8) = 3.626	P=0.0934	F (1, 8) = 5.041	P=0.0550
	16w[1]	F (1, 10) = 2.704	P=0.1311	F (1, 10) = 29.97	P=0.0003 (***)	F (1, 10) = 8.554	P=0.0152 (*)
Lean %	4w[1]	F (1, 26) = 0.0137	P=0.9077	F (1, 26) = 7.471	P=0.0111 (*)	F (1, 26) = 11.05	P=0.0026 (**)
	8w[1]	F (1, 8) = 0.027	P=0.8735	F (1, 8) = 4.915	P=0.0574	F (1, 8) = 6.605	P=0.0331 (*)
	16w[1]	F (1, 9) = 5.715	P=0.0405 (*)	F (1, 9) = 43.69	P<0.0001 (****)	F (1, 9) = 18.64	P=0.0019 (**)

Figure 5: – Liver damage of MASH diet on TRβ knockout mice

Figure 5B

Parameter		2-way ANOVA, post hoc: Tukey's[1] or Šídák's[2] multiple comparisons test					
		Interaction		**Genotype**		**Diet**	
ALT	4w[2]	F (1, 18) = 0.4060	P=0.5320	F (1, 18) = 0.9380	P=0.3456	F (1, 18) = 46.79	P<0.0001 (****)
	8w[2]	F (1, 10) = 0.09045	P=0.7698	F (1, 10) = 0.3961	P=0.5432	F (1, 10) = 14.91	P=0.0032 (**)
	16w[2]	F (1, 11) = 1.231	P=0.2910	F (1, 11) = 0.1433	P=0.7122	F (1, 11) = 95.77	P<0.0001 (****)

Figure 5C

Parameter		2-way ANOVA, post hoc: Tukey's[1] or Šídák's[2] multiple comparisons test					
		Interaction		**Genotype**		**Diet**	
AST	4w[1]	F (1, 17) = 5.764	P=0.0281 (*)	F (1, 17) = 13.95	P=0.0016 (**)	F (1, 17) = 131.3	P<0.0001 (****)
	8w[2]	F (1, 10) = 0.0694	P=0.7976	F (1, 10) = 0.9504	P=0.3526	F (1, 10) = 8.920	P=0.0137 (*)
	16w[1]	F (1, 10) = 2.946	P=0.1169	F (1, 10) = 10.84	P=0.0081 (**)	F (1, 10) = 20.87	P=0.0010 (**)

Figure 6 – Hepatic lipid response to MASH diet on TRβ knockout mice.

Figure 6B							
Parameter		2-way ANOVA, post hoc: Tukey's[1] or Šídák's[2] multiple comparisons test					
		Interaction		**Genotype**		**Diet**	
ORO	4w[1]	F (1, 8) = 10.33	P=0.0124 (*)	F (1, 8) = 0.0056	P=0.9424	F (1, 8) = 108.6	P<0.0001 (****)
	8w	F (1, 8) = 0.0376	P=0.8511	F (1, 8) = 0.079	P=0.7857	F (1, 8) = 3.295	P=0.1070
	16w[2]	F (1, 10) = 0.0021	P=0.9645	F (1, 10) = 0.3334	P=0.5765	F (1, 10) = 28.38	P=0.0003 (***)
Figure 6C							
Parameter		2-way ANOVA, post hoc: Tukey's[1] or Šídák's[2] multiple comparisons test					
		Interaction		**Genotype**		**Diet**	
Hepatic TGA	4w[2]	F (1, 17) = 3.624	P=0.0740	F (1, 17) = 0.0669	P=0.7990	F (1, 17) = 34.11	P<0.0001 (****)
	8w	F (1, 9) = 0.0759	P=0.7891	F (1, 9) = 0.1677	P=0.6918	F (1, 9) = 0.0554	P=0.8192
	16w[1]	F (1, 10) = 4.373	P=0.0630	F (1,10) = 4.880	P=0.0516	F (1,10) = 10.93	P=0.0079 (**)
Figure 7 - Hepatic fibrosis in MASH TRβ knockout mice.							
Figure 7B							
Parameter		2-way ANOVA, post hoc: Tukey's[1] or Šídák's[2] multiple comparisons test					
		Interaction		**Genotype**		**Diet**	
SR	4w[2]	F (1, 17) = 0.1119	P=0.7421	F (1, 17) = 0.0550	P=0.8174	F (1, 17) = 24.18	P=0.0001 (***)
	8w[2]	F (1, 8) = 0.0003	P=0.9856	F (1, 8) = 0.0033	P=0.9556	F (1, 8) = 11.67	P=0.0091 (**)
	16w[1]	F (1, 9) = 4.167	P=0.0716	F (1, 9) = 4.58	P=0.0610	F (1, 9) = 96.55	P<0.0001 (****)
Figure 8 - Inflammation markers in MASH liver of TRβ knockout mice.							
Gene		2-way ANOVA, post hoc: Tukey's[1] or Šídák's[2] multiple comparisons test					
		Interaction		**Genotype**		**Diet**	
Glis2	4w[2]	F (1, 18) = 0.2115	P=0.6511	F (1, 18) = 3.093	P=0.0956	F (1, 18) = 32.50	P<0.0001 (****)

	8w[2]	F (1, 9) = 0.3457	P=0.5710	F (1, 9) = 2.625	P=0.1396	F (1, 9) = 29.80	P=0.0004 (***)
	16w[2]	F (1, 10) = 2.118	P=0.1762	F (1, 10) = 1.085	P=0.3221	F (1, 10) = 54.96	P<0.0001 (****)
Elf3	4w[1]	F (1, 17) = 5.775	P=0.0279 (*)	F (1, 17) = 1.194	P=0.2897	F (1, 17) = 81.46	P<0.0001 (****)
	8w[1]	F (1, 9) = 12.13	P=0.0069 (**)	F (1, 9) = 13.76	P=0.0048 (**)	F (1, 9) = 76.68	P<0.0001 (****)
	16w[2]	F (1, 9) = 0.7162	P=0.4193	F (1, 9) = 0.3218	P=0.5844	F (1, 9) = 53.17	P<0.0001 (****)
Col1α	4w[1]	F (1, 18) = 10.20	P=0.0050 (**)	F (1, 18) = 7.643	P=0.0128 (*)	F (1, 18) = 35.52	P<0.0001 (****)
	8w[2]	F (1, 9) = 1.381	P=0.2701	F (1, 9) = 0.6893	P=0.4279	F (1, 9) = 32.13	P=0.0003 (***)
	16w[1]	F (1, 9) = 40.15	P=0.0001 (***)	F (1, 9) = 44.93	P<0.0001 (****)	F (1, 9) = 278.3	P<0.0001 (****)
TNFα	4w[1]	F (1, 16) = 8.464	P=0.0102 (*)	F (1, 16) = 2.849	P=0.1108	F (1, 16) = 283.1	P<0.0001 (****)
	8w[2]	F (1, 10) = 2.181	P=0.1705	F (1, 10) = 1.631	P=0.2304	F (1, 10) = 46.94	P<0.0001 (****)
	16w[2]	F (1, 11) = 0.0222	P=0.8844	F (1, 11) = 0.1359	P=0.7194	F (1, 11) = 36.76	P<0.0001 (****)
IL6	4w[2]	F (1, 17) = 2.446	P=0.1362	F (1, 17) = 5.880	P=0.0267 (*)	F (1, 17) = 4.303	P=0.0535
	8w[2]	F (1, 9) = 1.342	P=0.2765	F (1, 9) = 0.2006	P=0.6648	F (1, 9) = 11.00	P=0.0090 (**)
	16w[1]	F (1, 10) = 21.58	P=0.0009 (***)	F (1, 10) = 41.06	P<0.0001 (****)	F (1, 10) = 97.82	P<0.0001 (****)
IL1b	4w[2]	F (1, 16) = 0.3101	P=0.5854	F (1, 16) = 0.0033	P=0.9547	F (1, 16) = 11.70	P=0.0035 (**)
	8w	F (1, 9) = 0.6588	P=0.4379	F (1, 9) = 0.0392	P=0.8475	F (1, 9) = 0.0040	P=0.9510
	16w[2]	F (1, 10) = 1.047	P=0.3304	F (1, 10) = 2.459	P=0.1479	F (1, 10) = 20.13	P=0.0012 (**)
Figure 9: Thyroid hormone status in TRβ knockout mice at thermoneutrality.							
Figure 9A							

Serum hormone		2-way ANOVA, post hoc: Šídák's multiple comparisons test					
		Interaction		**Genotype**		**Diet**	
tT3	4w	F (1, 17) = 0.6124	P=0.4447	F (1, 17) = 0.1773	P=0.6790	F (1, 17) = 0.9813	P=0.3358
	8w	F (1, 10) = 0.0109	P=0.9189	F (1, 10) = 3.596	P=0.0871	F (1, 10) = 3.661	P=0.0847
	16w	F (1, 9) = 3.701	P=0.0865	F (1, 9) = 17.69	P=0.0023 (**)	F (1, 9) = 0.0314	P=0.8633
tT4	4w	F (1, 17) = 1.802	P=0.1971	F (1, 17) = 1.232	P=0.2825	F (1, 17) = 0.5079	P=0.4857
	8w	F (1, 9) = 0.5655	P=0.4713	F (1, 9) = 8.853	P=0.0156 (*)	F (1, 9) = 0.8776	P=0.3733
	16w	F (1, 11) = 3.100	P=0.1060	F (1, 11) = 7.823	P=0.0174 (*)	F (1, 11) = 0.4567	P=0.5131
Figure 9B							
Hepatic hormone		2-way ANOVA, post hoc: Tukey's multiple comparison test					
		Interaction		**Genotype**		**Diet**	
T3	4w[1]	F (1, 14) = 5.292	P=0.0373 (*)	F (1, 14) = 1.581	P=0.2292	F (1, 14) = 1.855	P=0.1948
	8w	F (1, 7) = 1.115	P=0.3261	F (1, 7) = 0.9757	P=0.3562	F (1, 7) = 0.06740	P=0.8026
	16w	F (1, 7) = 2.206	P=0.1810	F (1, 7) = 2.273	P=0.1754	F (1, 7) = 10.41	P=0.0145 (*)
T4	4w[1]	F (1, 18) = 0.1767	P=0.6792	F (1, 18) = 13.78	P=0.0016 (**)	F (1, 18) = 6.589	P=0.0194 (*)
	8w	F (1, 8) = 1.098	P=0.3254	F (1, 8) = 2.700	P=0.1390	F (1, 8) = 15.95	P=0.0040 (**)
	16w	F (1, 8) = 0.0055	P=0.9430	F (1, 8) = 3.070	P=0.1179	F (1, 8) = 1.192	P=0.3067
Figure 9C							
Hepatic DIO1 activity		2-way ANOVA, post hoc: Tukey's multiple comparison test					
		Interaction		**Genotype**		**Diet**	
4w[2]		F (1, 11) = 3.310	P=0.0962	F (1, 11) = 0.2900	P=0.6010	F (1, 11) = 69.61	P<0.0001 (****)
8w		F (1, 9) = 1.400	P=0.2670	F (1, 9) = 0.5745	P=0.4679	F (1, 9) = 4.866	P=0.0548
16w		F (1, 9) = 19.21	P=0.0018 (**)	F (1, 9) = 0.4311	P=0.5279	F (1, 9) = 15.06	P=0.0037 (**)
Figure 10: Thyroid hormone status in TRβ knockout mice at RT and thermoneutrality.							
Figure 10A							

Peptide	2-way ANOVA, post hoc: Tukey's[1] or Šídák's[2] multiple comparisons test					
	Interaction		**Genotype**		**Temperature**	
TSH[1]	F (1, 19) = 6.970	P=0.0161 (*)	F (1, 19) = 302.7	P<0.0001 (****)	F (1, 19) = 0.0263	P=0.8729
Figure 10B-C						
Gene	2-way ANOVA, post hoc: Tukey's[1] or Šídák's[2] multiple comparisons test					
	Interaction		**Genotype**		**Temperature**	
TSHb[2]	F (1, 14) = 2.542	P=0.1331	F (1, 14) = 7.418	P=0.0165 (*)	F (1, 14) = 4.498	P=0.0523
Trhr1[2]	F (1, 13) = 3.683	P=0.0772	F (1, 13) = 12.84	P=0.0033 (**)	F (1, 13) = 0.6594	P=0.4314
Trh[2]	F (1, 9) = 1.250	P=0.2925	F (1, 9) = 3.629	P=0.0892	F (1, 9) = 0.1817	P=0.6799
Figure 11: Hepatic TH responsive genes in TRβ knockout mice.						
Gene		2-way ANOVA, post hoc: Tukey's[1] or Šídák's[2] multiple comparisons test				
		Interaction		**Genotype**	**Diet**	
Thrsp	4w[2]	F (1, 17) = 0.0784	P=0.7828	F (1, 17) = 0.1058	P=0.7490	F (1, 17) = 119.0	P<0.0001 (****)
	8w[2]	F (1, 9) = 0.0674	P=0.8009	F (1, 9) = 2.370	P=0.1580	F (1, 9) = 16.02	P=0.0031 (**)
	16w[2]	F (1, 9) = 0.0004	P=0.9853	F (1, 9) = 0.2613	P=0.6215	F (1, 9) = 5.286	P=0.0471 (*)
Thrα	4w	F (1, 17) = 1.304	P=0.2693	F (1, 17) = 2.228	P=0.1538	F (1, 17) = 0.1897	P=0.6686
	8w	F (1, 10) = 0.0233	P=0.8818	F (1, 10) = 1.868	P=0.2017	F (1, 10) = 0.0129	P=0.9119
	16w	F (1, 10) = 0.9985	P=0.3412	F (1, 10) = 1.873	P=0.2011	F (1, 10) = 0.0091	P=0.9257
Klf9	4w[2]	F (1, 16) = 0.7152	P=0.4102	F (1, 16) = 0.3874	P=0.5424	F (1, 16) = 10.50	P=0.0051 (**)
	8w[1]	F (1, 9) = 7.651	P=0.0219 (*)	F (1, 9) = 1.164	P=0.3087	F (1, 9) = 6.833	P=0.0281 (*)
	16w[2]	F (1, 10) = 0.072	P=0.7939	F (1, 10) = 0.0339	P=0.8576	F (1, 10) = 19.84	P=0.0012 (**)
Dio1	4w[1]	F (1, 16) = 8.257	P=0.0110 (*)	F (1, 16) = 8.701	P=0.0094 (**)	F (1, 16) = 0.1864	P=0.6717
	8w	F (1, 9) = 3.411	P=0.0978	F (1, 9) = 3.174	P=0.1085	F (1, 9) = 2.678	P=0.1361
	16w[2]	F (1, 9) = 0.4916	P=0.5010	F (1, 9) = 4.512	P=0.0626	F (1, 9) = 3.365	P=0.0998
Figure 12: Effect of MASH in TRβ overexpressing mice.						

Figure 12B			
Gene	Unpaired Student´s t-test		
	Organ	**T, df**	**P value**
Thrb1	Liver	t=11.45, df=6	<0.0001
	Kidney	t=2.250, df=5	0.0742

Figure 12C		
Gene	Unpaired Student´s t-test	
	T, df	**P value**
WPRE	t=3.402, df=7	0.0114

Figure 12E-F		
Parameter	Unpaired Student´s t-test	
	T, df	**P value**
Delta body mass	t=0.8406, df=6	0.4328
Kcal/day/BW	t=0.09796, df=7	0.9247
Fat mass	t=1.130, df=5	0.3098
Lean mass	t=2.319, df=5	0.0681
LW/BW	t=0.5876, df=7	0.5753

Figure 12G								
Test	2-way ANOVA, post hoc: Šídák's multiple comparisons test							
	Time x Geno-type		**Genotype**		**Time**		**Subject**	
GTT	F (4, 28) = 1.901	P=0.1381	F (1, 7) = 0.054	P=0.8222	F (2.358, 16.51) = 15.75	P<0.0001 (****)	F (7, 28) = 6.141	P=0.0002 (***)
ITT	F (5, 30) = 1.063	P=0.4001	F (1, 6) = 0.06227	P=0.8113	F (2.578, 15.47) = 87.33	P<0.0001 (****)	F (6, 30) = 16.50	P<0.0001 (****)

Figure 12H			
Parameter	2-way ANOVA, post hoc: Šídák's multiple comparisons test		
	Interaction	**Genotype**	**Time**

EE (kJ/12h)	F (1, 10) = 0.1383	P=0.7177	F (1, 10) = 0.7474	P=0.4076	F (1, 10) = 4.794	P=0.0534
RQ	F (1, 10) = 0.03506	P=0.8552	F (1, 10) = 0.5358	P=0.4810	F (1, 10) = 0.2437	P=0.6322

Parameter	Unpaired Student´s t-test	
	T, df	**P value**
RMR	t=0.6335, df=5	0.5542

Figure 12I

Parameter	Simple linear regression				
	Time	**F (DFn, DFd)**	**Equation**	**R^2**	**P value**
EE (kJ/day)/BW	Day	F (1, 5) = 2.163	Y = 0.2205*X + 6.037	0.3019	0.2014
	Night	F (1, 5) = 1.421	Y = 0.2746*X + 5.893	0.2213	0.2868
RMR/BW	-	F (1, 5) = 7.589	Y = 1.235*X + 4.528	0.6028	0.0401

Parameter	Unpaired Student´s t-test		
	Organ	**T, df**	**P value**
ΔNorm. Temp	BAT	t=0.6911, df=7	0.5117
	Tail	t=0.9741, df=7	0.3625

Figure 12L-N

Parameter/ Gene	Unpaired Student´s t-test	
	T, df	**P value**
SR	t=0.6941, df=6	0.5136
Serum tT3/tT4	t=1.102, df=6	0.3128
Glis2	t=1.698, df=7	0.1333
Elf3	t=0.7636, df=6	0.4741
Col1α1	t=1.346, df=5	0.2361
TNFα	t=1.695, df=5	0.1509
IL6	t=0.3682, df=7	0.7236
IL1b	t=0.6626, df=5	0.5369

Thrsp	t=1.127, df=5	0.3109
Fasn	t=0.6584, df=6	0.5347
Me1	t=1.019, df=7	0.3423
CD5L	t=0.2328, df=5	0.8251

Figure 13: Effect of pharmacological stimulation of *Thrb1* and *Dio1* in PMH

Figure 13A

Gene	One-way ANOVA, post hoc: Tukey's multiple comparison test		
Thrb1	**Treatment**	**F (DFn, DFd)**	**P value**
	T3	F (2, 7) = 0.1376	0.8738
	T3 (48h)	F (2, 8) = 2.270	0.1656
	Insulin	F (4, 18) = 0.6653	0.6242
	Insulin (48h)	F (4, 20) = 1.157	0.3589
	Corticosterone	F (2, 7) = 2.705	0.1348
	Simvastatin	F (2, 7) = 6.903	0.0221
	Unpaired Student´s t-test		
	Treatment	**T, df**	**P value**
	Sobetirome (GC-1)	t=2.183, df=6	0.0717
	Metformin	t=0.7665, df=7	0.4684
	High glucose	t=1.048, df=6	0.3350
	Fatty acids (24h)	t=0.5459, df=8	0.6000
	Fatty acids (48h)	t=3.729, df=6	0.0097

Figure 13B

Gene	One-way ANOVA, post hoc: Tukey's multiple comparison test		
Dio1	**Treatment**	**F (DFn, DFd)**	**P value**
	T3	F (2, 8) = 2.030	0.1937
	T3 (48h)	F (2, 8) = 4.832	0.0421
	Insulin	F (4, 19) = 0.4912	0.7422
	Insulin (48h)	F (4, 22) = 0.8426	0.5131
	Corticosterone	F (2, 7) = 2.962	0.1169
	Simvastatin	F (2, 8) = 2.030	0.1937
	Unpaired Student´s t-test		
	Treatment	**T, df**	**P value**
	Sobetirome (GC-1)	t=0.3885, df=6	0.7111
	Metformin	t=0.4777, df=6	0.6498
	High glucose	t=1.668, df=6	0.1464
	Fatty acids (24h)	t=1.596, df=7	0.1546
	Fatty acids (48h)	t=1.096, df=8	0.3051

Figure 14: DIO1 status in MASLD and MASH mice at different housing conditions.

Figure 14B

Gene		2-way ANOVA, post hoc: Tukey's multiple comparisons test					
		Interaction		**Time**		**Diet**	
Dio1	1-18w	F (6, 95) = 6.325	P<0.0001 (****)	F (6, 95) = 21.08	P<0.0001 (****)	F (1, 95) = 259.8	P<0.0001 (****)
		One-way ANOVA, post hoc: Tukey's multiple comparisons test					
		F (DFn, DFd)		**P value**			
	14w	F (2, 24) = 65.55		P<0.0001 (****)			
	18w	F (2, 25) = 26.56		P<0.0001 (****)			
Figure 14C							
Gene		Simple linear regression					
Dio1		**Diet**	**F (DFn, DFd)**	**Equation**	**R^2**	**P value**	
		Chow	F (1, 5) = 2.794	Y = -0.02085*X + 0.9838	0.3584	P= 0.1555	
		HFD	F (1, 5) = 16.14	Y = -0.06190*X + 2.151	0.7635	P= 0.0101 (*)	
		Differences in the lines					
		Slope		**Elevation or intercepts**			
		F (DFn, DFd)	**P value**	**F (DFn, DFd)**	**P value**		
		F (1, 10) = 4.287	0.0652	F (1,11) = 36.77	P<0.0001 (****)		
Figure 14D							
Gene		2-way ANOVA					
		Interaction		**Time**		**Diet**	
Dio1	4-16w	F (2, 18) = 1.515	P=0.2465	F (2, 18) = 0.4793	P=0.6269	F (1, 18) = 0.0003370	P=0.9856
		One-way ANOVA, post hoc: Tukey's multiple comparisons test					
		F (DFn, DFd)		**P value**			
	4w	F (2, 12) = 4.566		P=0.0335 (*)			
Figure 14E							
Parameter		2-way ANOVA, post hoc: Tukey's[1] or Šídák's[2] multiple comparisons test					

		Interaction		Time		Diet	
DIO1 activity	4-18w (Chow vs. HFD)[1]	F (3, 27) = 4.569	P=0.0103 (*)	F (3, 27) = 4.941	P=0.0073 (**)	F (1, 27) = 9.020	P=0.0057 (**)
	4w-16w (Con-trol vs CD-HFD)[2]	F (2, 16) = 3.396	P=0.0590	F (2, 16) = 1.181	P=0.3324	F (1, 16) = 3.892	P=0.0661
		One-way ANOVA, post hoc: Tukey's multiple comparisons test					
		F (DFn, DFd)		**P value**			
	4w	F (2, 9) = 16.73		P=0.0009 (***)			

Figure 14F				
Parameter		Correlation		
		Pearson r	**R^2**	**P value**
DIO1 activity/ *Dio1*	Chow	0.7648	0.5849	0.0009
	HFD	0.2380	0.05663	0.3265
	Cntrl	0.3662	0.1341	0.2980
	CD-HFD	0.1105	0.01221	0.7325

Figure 15: Role of Dio1 in MASH.			
Figure 15A			
Gene	Unpaired Student´s t-test		
	Organ	**T, df**	**P value**
Dio1	Liver	t=1.304, df=5	0.2491
	Kidney	t=1.267, df=6	0.2520

Figure 15B-E		
Parameter/ Gene	Unpaired Student´s t-test	
	T, df	**P value**
WPRE	t=3.607, df=6	0.0113

DIO1 activity	t=2.899, df=4	0.0441
Delta body mass	t=2.076, df=6	0.0832
Kcal/day/BW	t=1.748, df=6	0.1311
Fat mass	t=0.6776, df=5	0.5281
Lean mass	t=0.7417, df=5	0.4916
LW/BW	t=0.3104, df=6	0.7667

Figure 15F

Test	2-way ANOVA, post hoc: Šídák's multiple comparisons test							
	Time x Genotype		**Genotype**		**Time**		**Subject**	
GTT	F (4, 24) = 1.701	P=0.1827	F (1, 6) = 1.120	P=0.3306	F (1.852, 11.11) = 14.38	P=0.0010 (***)	F (6, 24) = 1.660	P=0.1743
ITT	F (5, 30) = 0.1738	P=0.9703	F (1, 6) = 0.7822	P=0.4105	F (1.643, 9.857) = 95.15	P<0.0001 (****)	F (6, 30) = 23.78	P<0.0001 (****)

Figure 15G

Parameter	2-way ANOVA, post hoc: Šídák's multiple comparisons test					
	Interaction		**Genotype**		**Time**	
EE (kJ/12h)	F (1, 10) = 0.001290	P=0.9721	F (1, 10) = 0.4276	P=0.5279	F (1, 10) = 6.731	P=0.0267 (*)
RQ	F (1, 10) = 0.3478	P=0.5684	F (1, 10) = 0.001775	P=0.9672	F (1, 10) = 2.051	P=0.1826

Parameter	Unpaired Student´s t-test	
	T, df	**P value**
RMR	t=0.7611, df=5	0.4809

Figure 15H

Parameter	Simple linear regression				
	Time	**F (DFn, DFd)**	**Equation**	**R^2**	**P value**
EE (kJ/day)/BW	Day	F (1, 5) = 0.7268	Y = 0.1492*X + 8.297	0.1269	0.4328
	Night	F (1, 5) = 2.270	Y = 0.5568*X - 4.222	0.3122	0.1923

RMR/BW	-	F (1, 5) = 2.378	Y = 1.230*X + 4.665	0.3223	0.1837

Parameter	Unpaired Student´s t-test		
	Organ	**T, df**	**P value**
ΔNorm. Temp	BAT	t=0.4687, df=6	0.6559
	Tail	t=1.463, df=6	0.1937

Figure 15K-N		
SR	t=1.445, df=6	0.1987
Glis2	t=1.121, df=5	0.3132
Elf3	t=2.130, df=4	0.1002
Col1α1	t=0.1876, df=5	0.8585
TNFα	t=3.588, df=4	0.0230
IL6	t=0.4059, df=5	0.7016
IL1b	t=1.329, df=4	0.2546
Thrsp	t=1.148, df=4	0.3148
Fasn	t=1.480, df=4	0.2129
Me1	t=0.04530, df=5	0.9656
CD5L	t=1.711, df=4	0.1623
Thrb1	t=1.159, df=5	0.2989
Serum tT3/tT4	t=1.446, df=5	0.2077
Hepatic T3/T4	t=3.244, df=4	0.0316
Hepatic T3	t=1.551, df=4	0.1958
Hepatic T4	t=0.5664, df=4	0.6014

Figure 16: DIO1 impact on metabolism in mice housed at 22°C.

Figure 16A

Parameter	2-way ANOVA, post hoc: Šídák's multiple comparisons test					
	Interaction		**Genotype**		**Time**	
EE (kJ/12h)	F (1, 10) = 0.9522	P=0.3522	F (1, 10) = 4.896	P=0.0513	F (1, 10) = 38.64	P<0.0001 (****)

RQ	F (1, 10) = 0.2991	P=0.5965	F (1, 10) = 1.802	P=0.2092	F (1, 10) = 0.0618	P=0.8087

Parameter	Unpaired Student´s t-test	
	T, df	**P value**
RMR	t=2.957, df=5	0.0316
Figure 16B		

Parameter	Simple linear regression				
	Time	**F (DFn, DFd)**	**Equation**	**R^2**	**P value**
EE/BW	Day	F (1, 4) = 0.6850	Y = 0.3313*X + 10.88	0.1462	0.4544
	Night	F (1, 5) = 0.2837	Y = 0.3245*X + 14.82	0.2238	0.2837
RMR/BW	-	F (1, 5) = 2.799	Y = 1.183*X + 45.37	0.3589	0.1552
Figure 16C-D					

Parameter/ Gene	Unpaired Student´s t-test	
	T, df	**P value**
Hepatic glyco-gen	t=2.561, df=4	0.0625
Muscle glyco-gen	t=0.9495, df=6	0.3790
Fgf21 (L)	t=0.5204, df=5	0.6250
Igf1 (L)	t=9.893, df=5	0.0002
Ucp1	t=0.1403, df=5	0.8939
Fgf21 (B)	t=0.9191, df=5	0.4002
Igf1R	t=1.664, df=4	0.1715
Glut2	t=2.209, df=5	0.0783
Igf1 (M)	t=1.197, df=6	0.2763
Figure 18: Effect of miR34a-5p and STAT3 pathway on DIO1 and its impact on MASH.		
Figure 18B-F		

Gene	Unpaired Student´s t-test		
	Organ	**T, df**	**P value**

miR34a-5p	Liver	t=0.6163, df=7	0.5572
	Kidney	t=0.2976, df=7	0.7746
Socs3	Liver	t=8.451, df=8	<0.0001
	Kidney	t=0.7184, df=7	0.4958
WPRE	AAV-miR34a-5p-S	t=8.337, df=10	<0.0001
	AAV-SOCS3	t=4.096, df=9	0.0027
Delta body mass	AAV-miR34a-5p-S	t=2.882, df=8	0.0205
	AAV-SOCS3	t=0.7740, df=9	0.4588
Kcal/day/BW	AAV-miR34a-5p-S	t=1.256, df=7	0.2494
	AAV-SOCS3	t=2.765, df=7	0.0279
Fat mass	AAV-miR34a-5p-S	t=0.1313, df=7	0.8992
	AAV-SOCS3	t=2.035, df=8	0.0762
Lean mass	AAV-miR34a-5p-S	t=0.1797, df=7	0.8625
	AAV-SOCS3	t=1.702, df=8	0.1272
LW/BW	AAV-miR34a-5p-S	t=0.5737, df=9	0.5802
	AAV-SOCS3	t=0.9012, df=9	0.3910

Figure 18G

Test	2-way ANOVA, post hoc: Šídák's multiple comparisons test							
	Time x Genotype		**Genotype**		**Time**		**Subject**	
GTT	F (8, 56) = 1.424	P=0.2068	F (2, 14) = 1.863	P=0.1916	F (2.752, 38.53) = 126.1	P<0.0001 (****)	F (14, 56) = 2.682	P=0.0045 (**)
ITT	F (10, 70) = 1.545	P=0.1421	F (2, 14) = 0.8149	P=0.4626	F (2.898, 40.57) = 158.7	P<0.0001 (****)	F (14, 70) = 4.371	P<0.0001 (****)

Figure 18H

Parameter	2-way ANOVA, post hoc: Šídák's multiple comparisons test			
	Transgene	**Interaction**	**Genotype**	**Time**

EE	AAV-miR34a-5p-S	F (1, 18) = 0.3355	P=0.5696	F (1, 18) = 5.426	P=0.032 (*)	F (1, 18) = 51.88	P<0.0001 (****)
	AAV-SOCS3	F (1, 16) = 1.739	P=0.2059	F (1, 16) = 0.6082	P=0.4468	F (1, 16) = 81.09	P<0.0001 (****)
RQ	AAV-miR34a-5p-S	F (1, 16) = 0.02128	P=0.8858	F (1, 16) = 3.975	P=0.0635	F (1, 16) = 12.26	P=0.0030 (**)
	AAV-SOCS3	F (1, 18) = 1.513	P=0.2345	F (1, 18) = 1.029	P=0.3238	F (1, 18) = 3.251	P=0.0882

Parameter	Unpaired Student´s t-test		
	Transgene	**T, df**	**P value**
RMR	AAV-miR34a-5p-S	t=0.9913, df=9	0.3474
	AAV-SOCS3	t=0.3458, df=9	0.7374

Figure 18I

Parameter	Simple linear regression				
	Time	**F (DFn, DFd)**	**Equation**	**R^2**	**P value**
EE/BW	Day	F (1, 14) = 0.9620	Y = 0.1242*X + 8.995	0.0643	0.3433
	Night	F (1, 14) = 0.4502	Y = -0.1071*X + 19.22	0.03115	0.5132
RMR/BW	-	F (1, 15) = 0.4860	Y = 0.7597*X + 17.30	0.0314	0.4964

Parameter	Unpaired Student´s t-test		
	Transgene	**T, df**	**P value**
ΔNorm. Temp	AAV-miR34a-5p-S (BAT)	t=0.003899, df=7	0.9970
	AAV-miR34a-5p-S (Tail)	t=0.1318, df=7	0.8989
	AAV-SOCS3 (BAT)	t=0.2881, df=8	0.7806
	AAV-SOCS3 (Tail)	t=0.7723, df=8	0.4621

Figure 18J

Parameter	Unpaired Student´s t-test		
	Transgene	**T, df**	**P value**
	AAV-miR34a-5p-S	t=1.037, df=8	0.3299

Serum ratio tT3/tT4	AAV-SOCS3	t=0.2521, df=8	0.8074
Figure 18K-L			
Parameter	Unpaired Student´s t-test		
	Transgene	**T, df**	**P value**
DIO1 activity	AAV-miR34a-5p-S	t=1.523, df=8	0.1664
	AAV-SOCS3	t=4.733, df=8	0.0015
Thrb1	AAV-miR34a-5p-S	t=3.113, df=9	0.0125
	AAV-SOCS3	t=3.100, df=8	0.0147
TRα	AAV-miR34a-5p-S	t=1.161, df=10	0.2726
	AAV-SOCS3	t=2.582, df=9	0.0296
Dio1	AAV-miR34a-5p-S	t=1.297, df=9	0.2269
	AAV-SOCS3	t=0.5320, df=8	0.6092
Thrsp	AAV-miR34a-5p-S	t=0.1076, df=9	0.9167
	AAV-SOCS3	t=0.2354, df=9	0.8192
Fasn	AAV-miR34a-5p-S	t=1.212, df=8	0.2603
	AAV-SOCS3	t=1.180, df=8	0.2720
Me1	AAV-miR34a-5p-S	t=0.4899, df=8	0.6374
	AAV-SOCS3	t=1.632, df=8	0.1412
CD5L	AAV-miR34a-5p-S	t=2.011, df=9	0.0752
	AAV-SOCS3	t=0.3703, df=10	0.7189
Figure 19: Liver damage, fibrosis, and steatosis levels in MASH mice treated with associated adenovirus.			
Figure 19A-B			
Parameter/ Gene	Unpaired Student´s t-test		
	Transgene	**T, df**	**P value**
SR	AAV-miR34a-5p-S	t=0.6168, df=8	0.5545
	AAV-SOCS3	t=0.4764, df=9	0.6451
ORO	AAV-miR34a-5p-S	t=2.703, df=8	0.0269

	AAV-SOCS3	t=2.775, df=8	0.0241
Glis2	AAV-miR34a-5p-S	t=2.108, df=8	0.0681
	AAV-SOCS3	t=2.488, df=8	0.0376
Elf3	AAV-miR34a-5p-S	t=2.488, df=8	0.0376
	AAV-SOCS3	t=1.156, df=10	0.2745
Col1α1	AAV-miR34a-5p-S	t=2.095, df=8	0.0695
	AAV-SOCS3	t=0.1720, df=9	0.8673
TGFb	AAV-miR34a-5p-S	t=1.143, df=9	0.2824
	AAV-SOCS3	t=1.168, df=8	0.2762
TNFα	AAV-miR34a-5p-S	t=2.856, df=6	0.0290
	AAV-SOCS3	t=2.819, df=6	0.0304
IL6	AAV-miR34a-5p-S	t=1.925, df=8	0.0904
	AAV-SOCS3	t=0.7918, df=8	0.4513
IL1β	AAV-miR34a-5p-S	t=1.353, df=9	0.2091
	AAV-SOCS3	t=0.3515, df=9	0.7333
IL10	AAV-miR34a-5p-S	t=2.132, df=8	0.0656
	AAV-SOCS3	t=1.951, df=9	0.0828
Cpt1α	AAV-miR34a-5p-S	t=2.404, df=8	0.0429
	AAV-SOCS3	t=2.240, df=8	0.0554
PPARα	AAV-miR34a-5p-S	t=1.614, df=9	0.1411
	AAV-SOCS3	t=1.956, df=8	0.0862
PPARγ	AAV-miR34a-5p-S	t=0.3895, df=8	0.7071
	AAV-SOCS3	t=1.395, df=8	0.2006
Crtc1	AAV-miR34a-5p-S	t=3.888, df=8	0.0046
	AAV-SOCS3	t=1.084, df=8	0.3099
Pcyt1b	AAV-miR34a-5p-S	t=0.1832, df=9	0.8587
	AAV-SOCS3	t=1.908, df=9	0.0887

Figure 20: miR34a-5p target genes.			
Gene	Unpaired Student´s t-test		
	Transgene	**T, df**	**P value**
Bcl2	AAV-miR34a-5p-S	t=0.9091, df=8	0.3899
	AAV-SOCS3	t=0.6270, df=8	0.5481
Sirt1	AAV-miR34a-5p-S	t=0.05727, df=8	0.9557
	AAV-SOCS3	t=0.4658, df=8	0.6538
Foxp1	AAV-miR34a-5p-S	t=0.7458, df=9	0.4748
	AAV-SOCS3	t=1.498, df=9	0.1684
p53	AAV-miR34a-5p-S	t=2.082, df=8	0.0709
	AAV-SOCS3	t=2.730, df=9	0.0232

Table S 2| Adult diagnostic criteria of steatotic liver diseases sub-categories. Former vs. new nomenclature in patients.

Former Nomenclature			
		EASL-EASO-EADS (232)	AASLD (194)
NAFLD	NAFL	• Hepatic steatosis: ○ >5% of hepatocytes measured by histological analysis. ○ >5.6% of hepatocytes by H-MRS or MRI. • Lack of secondary causes for hepatic fat accumulation. • Alcohol consumption daily <30g for male (M) and <20g for female (F). • Associated with metabolic risk factors/components of Metabolic Syndrome: 1. Waist circumference ⩾94/⩾80 cm for Europid men/women. 2. Arterial pressure ⩾130/85 mmHg or treated for hypertension. 3. Fasting glucose ⩾100 mg/dl (5.6 mmol/L) or treated for T2DM. 4. Serum triacylglycerols >150 mg/dl (>1.7 mmol/L). 5. HDL cholesterol <40/50 mg/dl for men/women (<1.0/<1.3 mmol/L).	• Hepatic steatosis: ○ >5% without evidence of hepatocellular injury (e.g., ballooning or fibrosis) by either histology or imaging • Lack of secondary causes for hepatic fat accumulation. • Alcohol consumption daily <42g (M) and <28g (F).
	NASH	• NAFL criteria	• NAFL criteria

		• Inflammation (steatohepatitis)
		• Hepatocyte injury (e.g., ballooning)
		• With or without fibrosis:
		  ○ Early NASH: nor or mild (F0-F1) fibrosis
		  ○ Fibrotic NASH: significant (≥F2) or advanced (≥F3) fibrosis.
		  ○ NASH-Cirrhosis (F4)
			• Inflammation (steatohepatitis)
			• Hepatocyte injury (e.g., ballooning)
			• With or without fibrosis.

New Nomenclature			
		Multi-Society Delphi Consensus 2023 (16)	
MASLD	MASLD	• Hepatic steatosis • Lack of secondary causes • Alcohol consumption daily ≤20g-30g • At least 1 out of 5 cardiometabolic criteria: 1. BMI ≥25 kg/m² [23 Asia] or WC >94 cm (M) 80 cm (F) or ethnicity adjusted equivalent. 2. Fasting serum glucose ≥5.6 mmol/L [100 mg/dl] or 2-hour post-load glucose levels ≥7.8 mmol/L [≥140 mg/dl] or HbA1c ≥5.7% [39 mmol/L] or type 2 diabetes or treatment for type 2 diabetes. 3. Blood pressure ≥130/85 mmHg OR specific antihypertensive drug treatment. 4. Plasma triglycerides ≥1.70 mmol/L [150 mg/dl] OR lipid lowering treatment. 5. Plasma HDL-cholesterol ≤1.0 mmol/L [40 mg/dl] (M) and ≤1.3 mmol/L [50 mg/dl] (F) OR lipid lowering treatment	
	MASH	• MASLD criteria • Inflammation (steatohepatitis) • Fibrosis	

Acknowledgements

Completing a PhD is a monumental task that cannot be achieved without the support and encouragement of many individuals. I am deeply grateful to those who have been with me throughout this journey.

First and foremost, I would like to express my sincere gratitude to my supervisor, Prof. Jens Mittag. His exceptional mentorship, invaluable guidance, and constant encouragement have been crucial to my success. His readiness to assist, even during late-night lab sessions, and his humor during challenging times have been a source of immense support. His trust and freedom allowed me to grow as a researcher, and his push for excellence helped me achieve the Von Basedow prize.

I am also thankful to my co-supervisor, Prof. Henriette Kirchner, for her guidance in cell culture treatment experiments and for providing crucial samples that were essential to my research. Also, thanks to Dr. Eva Wirth and Yingfu Chen for their significant contributions in measuring DIO1 enzymatic activity at the Charité Universitätsmedizin Berlin.

I extend my gratitude to the entire consortium "CRC296/Locotact" for almost four years of support, even when Covid restrictions made it difficult. The collaborative and youthful environment of my PhD colleagues, combined with the guidance and knowledge of everyone involved, created a rich and stimulating research environment.

Special recognition goes to Riccardo Dore. His encouragement and humor brought a slice of Mediterranean warmth into the lab. His expertise in statistical analysis and our in-depth scientific discussions enriched my research, leading to several fruitful collaborations.

Rebecca Oelkrug deserves special thanks for her expertise and patience with the complex calorimetry system and mouse handling. Her expert eye in details helped me to improve my figures and presentations, and her support was a beacon during challenging times. Her sweet personality and willingness to help were invaluable.

I am deeply grateful to Sarah C Senis for her unwavering support, which made settling in Germany much smoother and manageable. Her assistance in both personal and professional matters was indispensable.

A heartfelt thank you to Jan Hendric Britsemmer for his friendship and support during difficult times in the lab. His willingness to chat over coffee was a much-needed respite, and I also thank Natalie for her insights and guidance in cell data analysis.
To Julia Resch, our dedicated lab technician, thank you for your assistance with technical issues, protocols, and orderings, and for our enjoyable exchanges about series and movies.

To my friends and family back in Spain, their support from afar kept me motivated and helped me in my pursuit of this degree. Special thanks to Nuria González Castillo for her immense support, encouragement, and understanding me better than I understand myself. Your presence in my life has been a source of strength and inspiration.

Lastly, to my partner, Keno Teppris. Your support, encouragement, knowledge of productivity tools and software, and his help in reducing my mental load allowed me to focus on my PhD. Additionally, for his assistance with optimizing macro scripts for fast and accurate analysis saved me hours, if not weeks, of work.